Cranfield UNIVERSITY

Emanuele Pagone

Advanced low carbon power systems — The Advanced Zero Emissions Power plant

School of Engineering

Master of Science by Research

Cranfield UNIVERSITY

School of Engineering

Master of Science by Research Full Time

Academic year 2008-2009

Emanuele Pagone

Advanced low carbon power systems — The Advanced Zero Emissions Power plant

Supervisor: Stephen Ogaji

October 2009

Typeset in LaTeX 2_ε.

Abstract

The global warming issue is becoming more and more important in the public opinion, because its effects on everyday life of the entire mankind are starting to become appreciable. On the next (2009) December will be held in Copenhagen the fifteenth United Nations Climate Change Conference which is expected to be crucial for the future choices to deal with the anthropogenic greenhouse gases issue.

The power generation sector is one of the most important contributors to the emissions of greenhouse gases (of which the carbon dioxide is the main anthropogenic example), and it is facing in the last decades a problem that will exacerbate surely the already alarming effect on the global warming: the rapid increase of the world power demand.

For these reasons the carbon capture topic is gaining nowadays a lot of attention, especially in the industrial sector, since it will be a strategic field for the power generation in the short-medium term. In fact, it is really likely that will be introduced soon a so-called "cap and trade" system, with the trading of pollution licences related to the CO_2 emissions, as the USA president Obama has recently proposed to the Congress. This option would turn out in a completely new scenario in the power generation sector with novel, cleaner concepts being economically more attractive than the conventional ones.

This project investigates the performance of a novel thermodynamic cycle with carbon capture, called Advanced Zero Emissions Power plant (AZEP), which has been analysed in the open literature just partially and superficially up to now. Since this project is part of a bigger one in which several carbon capture novel cycles options will be compared, the main objective is to provide a flexible, modular, modern computational tool, called eAZEP, developed *from scratch*. The second objective is the evaluation of the four main layouts of the AZEP concept as a stand alone power plant, assessing their inclination to be included in an unfired combined cycle featured with an Heat Recovery Steam Generator (HRSG). A final, third objective is the development of a routine for the off-design performance calculation to be included in on old pre-existing computational tool.

The original contribution of this work to the knowledge on the topic comprises

1. the conception of two new layouts for the AZEP cycle (the Post Expansion Heat exchanger layouts);

2. the performance evaluation of the long term potential for the power plant;

3. a sensitivity analysis of the thermodynamic concept.

The best suitable arrangements of the plant layout are identified together with the main parameters which influence their performance, both for the combined cycle perspective implementation and for the stand alone option.

Thanks to the flexibility of eAZEP will be easy to consider, in a future work, a pretty wide number of alternative concepts and investigate more cycle parameters in order to broaden the conclusions obtained in this work. Moreover the combined cycle off-design new routine must be debugged and validated.

An expert is a person who has made all the mistakes that can be made in a very narrow field.

— Niels Bohr

To Marta, “my wittiest mistake”.

Acknowledgements

I would like to thank Professor Pericles Pilidis and Doctor Stephen Ogaji not only because without their help I would not be able to participate to the project described in this thesis. They made a lot more. They proved there could always be an opportunity, for a willing person, to pursue his ambitions regardless of the bureaucratic impediments or the formal restrictions. In my opinion, this is the highest expression of the meritocracy. They gave me the *hope*, something priceless. They did it allowing me to spend this wonderful year, so full of teachings, in Cranfield.

Accordingly, I am very grateful to E.ON UK for sponsoring my project and in particular to Mister Martyn Adams for his time and attention in helping me develop my work better and better. Also the support of Professors Sergio Camporeale and Bernardo Fortunato (who referenced me to Cranfield) was important and I owe them my gratitude.

I thank also Giuseppina Di Lorenzo for the huge amount of time that she invested with me in the discussion of every aspect of the project, keeping always high my motivation and my enthusiasm in the work. I am happy to acknowledge also the support of Doctor Vishal Sethi, Pablo Bellocq and Badar Al-Abri for dedicating to me their valuable attention.

For what concerns the human experience, in this last year I knew a lot of great and special people that surely influenced in some way the fulfilment of this project and, most important, enriched my soul. For this reason I would like to thank the Thermal Power MSc mates, the several researchers I met in a lot of diverse occasions, in general all my friends here on campus, but also Andrea Ghiani, Francesca Dell'Aia, Andrea Martella, Eliana Eliardo, Gianluigi Aronica, Lucia Restivo, Enzo Gregoriano, Salvatore Caracappa, Cinzia Paci, Paola Dieci, Vincenza De Nigris, Natascia Spera, Vincenzo Pintagro, Maddalena Congiu, Alessandra Cantera, Stella Grasso and Giovanni Vizzini. Thank you my friends!

Of course I thank my family for the help and the support. A special thanks to Marta for her endless patience and for her love that she always brought to me for all these months; I love you!

One last sentence is due to the reader (whoever she or he is): thanks for your attention in this work.

Cranfield, October 5, 2009 E. P.

Contents

List of Figures

Nomenclature

α	Combution gas fuel ratio
β	Bleed mass flow ratio
χ_i	Molar fraction of the i-th component of a gas mixture
η	Efficiency
η_π	Pneumatic efficiency
κ	Turbine characteristic constant for a Stodola-like choking relation
$\mathcal{A}$	Interval amplitude
$\mathcal{E}$	Numerical error
$\mathcal{F}$	Bracketing expansion interval method factor
$\mathcal{M}$	Molecular weight
$\mathcal{R}$	Universal gas constant
$\mathcal{W}$	Mechanical work (J)
ω	Oxygen transfer ratio
π	Compressor pressure ratio
ρ	Recirculated mass flow ratio
σ	MCM electric conductivity
ε	Heat exchanger efficiency
$\boldsymbol{f}$	Mass composition vector
ξ	Generic function percentage variation

A	Area
c_p	Specific heat at constant pressure
c_v	Specific heat at constant volume
f	Generic function
f'	Generic function first derivative
f_i	Mass fraction of the i-th component of a gas mixture
h	Specific enthalpy
H_l	Fuel lower heating value
j_{O_2}	Oxygen flux
L	MCM Thickness
m	Mass
n	Number of moles
N_tu	Number of Thermal Units (NTU)
P	Mechanical power
p	Pressure
R	Ideal gas constant of the gas
s	Specific entropy
T	Temperature
U	Overall heat transfer coefficient
u	Specific internal energy
V	Volume
v	Specific volume
W	Mass flow
x	Generic independent variable
$\dot{C}$	Heat capacity rate

e	Euler's number
F	Faraday constant
$\dot{Q}$	Thermal heat rate

Chapter 1

Introduction

According to the sixth EEA[1] energy and environment report of the 2008 [8], the effect of the energy production and use on the environment and the health is still one of the most important issues in Europe.

The 80% of the greenhouse gases and atmospheric pollutant are generated by the energetic sector and, in particular, the power generation from fossil fuels is still the main source of the climate change.

In the last years has been detected a gradual reduction in the pollutant emissions (including the greenhouse gases) accordingly with the aim agreed the 9 March 2007 by the European Commission called "20-20-20", that turned into a political constraint for all the European Union countries. The aforementioned aim consists in the achievement, within the 2020, of:

- the 20% of reduction in the CO_2 emissions;
- the 20% of increase in the energetic efficiency;
- the 20% of power generation from renewable resources over the total generation.

Among the main contributors to the reduction of the emissions, there are the gradual substitution of the coal with the oil and the natural gas, a more efficient production of energy and heat, a larger and larger use of renewable energies, together with the application of new technologies.

Notwithstanding this positive trend, the EEA reports that if the European countries would stick to the present policies, the energy consumption would still increase of the 26% within the 2030, confirming the fossil fuels as the main source of energy supply. Moreover, according to a recent speech of

[1] European Environment Agency.

the IEA[2] Deputy Executive Director Richard Jones, in order to keep the same trend of the productive growth of the last decades, the world would need seven times the current capacity of the Saudi Arabia until the 2030 (see http://www.iea.org/Textbase/speech/2009/Jones/appea.pdf).

On the other hand, the climate change issue generated just by the past and present consumption of fossil fuels is already an alarming problem at present, and it will be discussed very lively in the upcoming fifteenth United Nations Climate Change Conference that will be held in Copenhagen on next December (http://en.cop15.dk/).

The project presented in this work slots in the background outlined above and, particularly, its main objective is the provide a computational tool (the program eAZEP) to evaluate a novel thermodynamic cycle with carbon capture (called AZEP[3]), able to contrast the climate change generated by the fossil fuels with a reasonable penalty on the performance.

The AZEP concept would permit a significant improvement in the field of the the oxy-fuel combustion cycles (the family of concepts it belongs to) since it employs a multi-disciplinary knowledge (including, for example, advanced chemical engineering ideas) to bring its performance closer to the reference conventional power plant. Unfortunately, up to now, because of the complexity and the novelty of the concept, the AZEP cycle has been investigated in the open literature just partially and superficially.

The software eAZEP is intended to allow its user to fill this gap in the knowledge enabling her or him to consider several different layouts of the power plant with relative little effort and to evaluate the influence of its numerous characteristic parameters on the performance. This goal has been achieved to benefit the bigger project of which this one is part of.

In summary the objectives of this work are (sorted by relevance):

1. the development of eAZEP a flexible, modular, modern computational tool, written in Fortran from scratch;

2. the use of eAZEP in order to investigate the potential of the main AZEP layouts for different technological levels;

3. the development of a routine for the off-design performance calculation of the steam plant to be used for the AZEP combined cycle implementation.

The project is founded by E.ON UK as part of its commitment to the climate change issue.

[2] International Energy Agency.
[3] Advanced Zero Emissions Power Plant.

Chapter 2

Literature survey

The carbon capture and sequestration (the main framework in which the project is included) is a fairly new topic although it is becoming more and more popular for its strategic potential importance for the power generation market in the future short-medium term. In the next sections will be described increasingly in more detail the object of this project and finally will be presented in details the AZEP concept.

2.1 Carbon capture concepts for the power generation

There are several strategies that has been investigated for the CO_2 capture in the power generation field, but there is a general agreement [7, 9, 6, 3] in dividing them in three main categories:

- pre-combustion capture;
- oxy-fuel combustion;
- post-combustion capture.

The first category includes a number of processes (steam reforming, gasification, partial oxidation [7, 6]) that roughly could be described in the transformation of the fuel in a mixture of CO_2 and H_2 (with CO, sometimes), using the latter as a fuel and separating the CO_2 before the combustion with a chemical or a physical method.

The oxy-fuel principle operates the combustion in a pure (or almost pure) oxygen environment (achieving, in this way, also the advantage to avoid the production of nitrogen and sulphur oxides), and requires the recirculation

of the exhaust gas in order to dilute the reactive mixture and obtain, after the combustion, an acceptable temperature [9]. In all these concepts the flue gas is basically constituted by steam and carbon dioxide, so it is simple to separate the steam by condensation [7]. There are several options to carry out the oxy-fuel combustion, they will be described in the next section.

The post-combustion processes are the most mature: they exploit physical or chemical techniques in order to capture the CO_2 from the exhaust gas of a conventional combustion. The main problem here is the low concentration of the carbon dioxide that requires the use of large and expensive devices [7] affecting remarkably also the thermodynamic performance of the power plant because of the pressure loss through them [9]. The aforementioned techniques vary from the chemical absorption (the most popular choice), physical absorption or adsorption and the use of solid chemicals [7, 9] till the application of membranes or distillation processes [3].

All the described strategies are energy demanding and require also, in many cases, a significant aggravation for the capital costs of the power plant. In fact the pre-combustion processes reduce the heating value of the fuel, the oxy-fuel approach requires efforts for the oxygen production and the post-combustion option involves energy also for the regeneration of the chemicals, used in the most popular choice [3].

2.2 The oxy-fuel cycles

The oxygen-fuel combustion has been applied to the glass melting and the steel and aluminium industry [6] but, to the knowledge of the author, there is no industrial application of this concept for what concerns the power generation sector. The options available in this field are several and comprise (among others less important) [3]

- the semi-closed cycle (also known as the "oxy-fuel combined cycle");
- the Chemical Looping Combustion cycle;
- the electrochemical reactions in fuel cells;
- the concept object of our project: the AZEP cycle.

The common feature of them is the composition of the exhaust gas that is mainly made up of steam and carbon dioxide.

The semi-closed cycle concept (Figure 2.1) shows several similarities with the conventional combined cycle: the heat of the exhaust gas is released in a Heat Recovery Steam Generator after the combustion process, but the

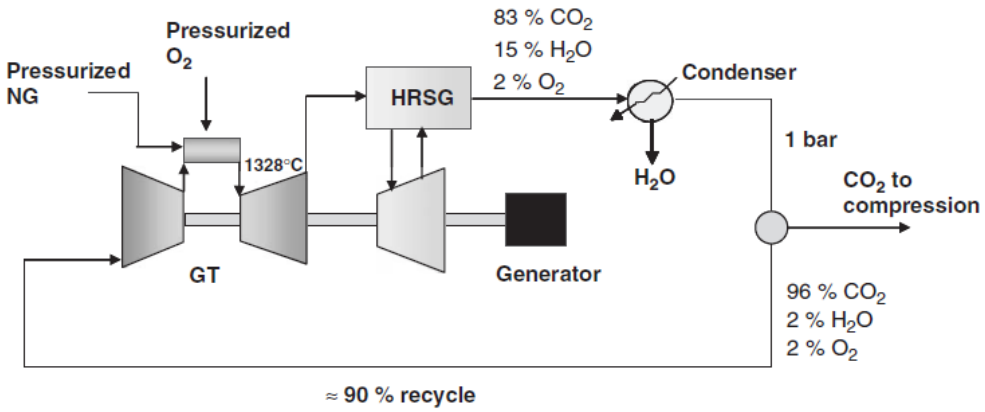

Figure 2.1. A simple process flow diagram of the "oxy-fuel combined cycle" concept [1].

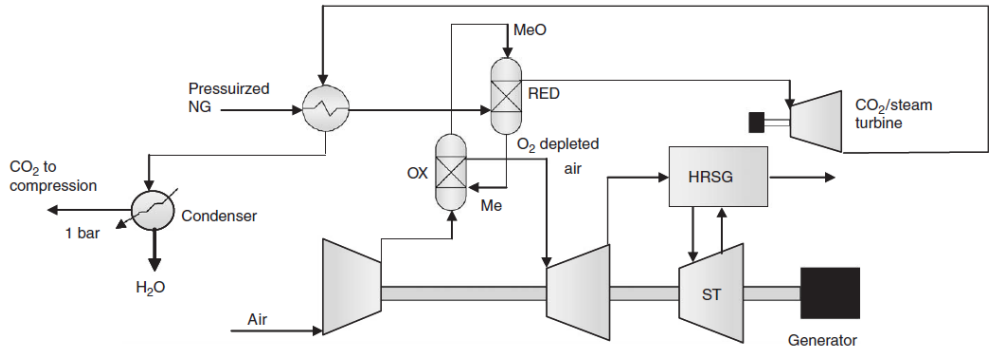

Figure 2.2. Process flow diagram of the Chemical Looping Combustion cycle [1].

reaction with the fuel is carried out with pure oxygen. As shown in the figure, there is a remarkable quantity (about the 90%) of flue gas recirculated at the inlet of the compressor, in order to lower the combustor outlet temperature to an acceptable value.

The oxygen supplied for the reaction is produced in a dedicated device (the Air Separation Unit) with a cryogenic process that results in a loss of electrical efficiency of about 10% [7]. Moreover there are studies on chemical cycles for the oxygen generation [9].

In the Chemical Looping Combustion concept (Figure 2.2), the oxy-fuel process is carried out by an oxygen carrier (a metal oxide) that circulates between two reactors, one for the oxidation and the other for the reduction. The reactors environment is kept as close as possible to the thermodynamic equilibrium [1].

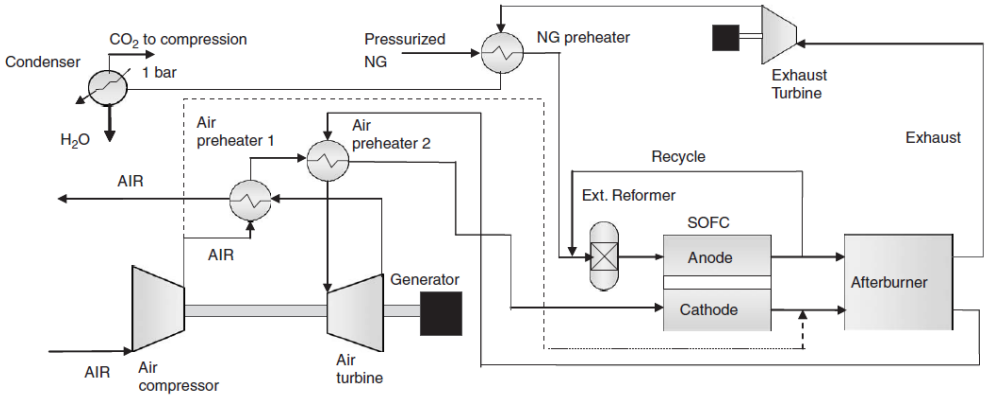

Figure 2.3. Integration of a Solid Oxide Fuel Cell (SOFC) with a gas turbine (simplified process flow diagram) [1].

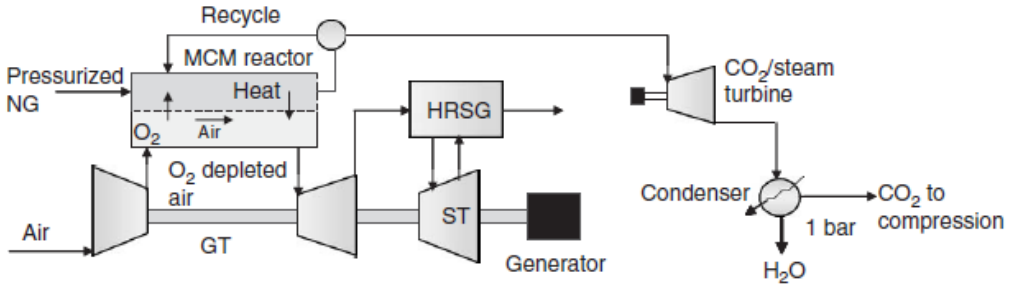

Figure 2.4. A simple process flow diagram of the Advanced Zero Emissions Power plant concept [1].

In another oxy-fuel option (Figure 2.3), a Solid Oxide Fuel Cell can operate the reaction of the air previously compressed and pre-heated with fuel, exploiting just its oxygen. It is important that the anode and cathode flows are not mixing in order to have just steam and carbon dioxide in the exhaust mixture. An afterburner is needed (as well as a stream of air bled from the compressor) to complete the oxidation of the fuel, that is just partially carried out in the fuel cell [1].

Finally, the Advanced Zero Emissions Power plant (AZEP) will be discussed thoroughly in the next section, anyway a very brief and simple description will be given here. The cycle (Figure 2.4) adopts a special membrane to substitute a conventional combustor; so the new device operates the separation of the oxygen from the air, the combustion of the fuel with pure oxygen and, finally, transfers the heat of combustion to the oxygen-depleted air.

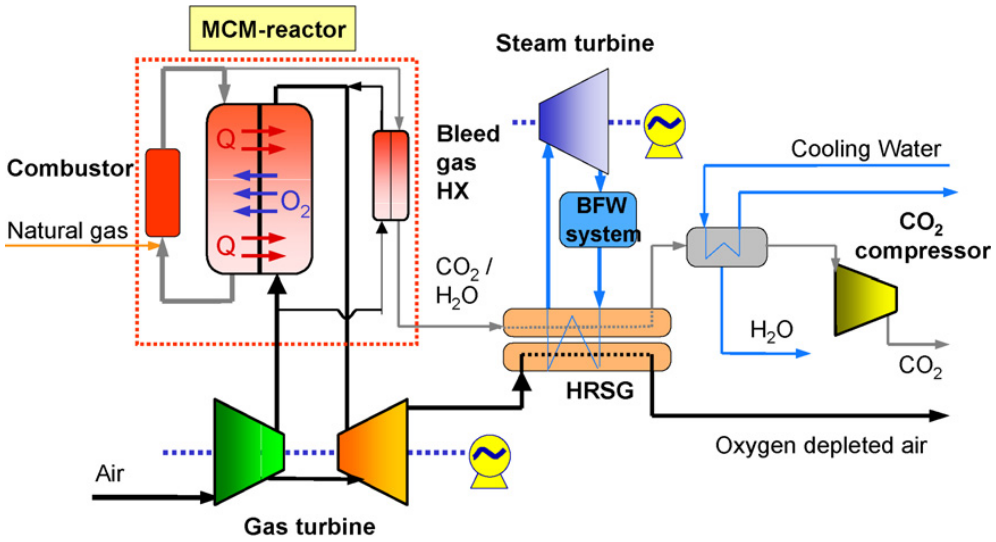

Figure 2.5. The process flow diagram of the AZEP cycle basic concept [2].

2.3 The Advanced Zero Emissions Power plant

The AZEP cycle is one of the most promising oxy-fuel concepts and, although there are several studies that investigated its potential, at the moment, there is no extensive knowledge on its application and its key parameters that affects significantly its performance.

In the last section the basic idea of this novel cycle is showed, so now will be presented a more comprehensive process flow sheet (Figure 2.5) in which the membrane is sketched in more detail. As represented, the "membrane reactor" comprises a Mixed Conductive Membrane together with a combustor and a Bleed gas Heat Exchanger (sometimes referred to the acronym BHX). As detailed in the Figure 2.6, the central device of the membrane reactor is actually made up of three parts: a Low and High Temperature Heat Exchanger (respectively LTHX and HTHX) and the membrane itself that performs at the same time the oxygen mass transfer and the heat exchange.

The insertion of the LTHX and the HTHX, respectively before and after the membrane is necessary to keep its temperature as constant as possible at the optimal value for the oxygen transport. Basically the higher is the temperature of the membrane, the higher is the mass of the oxygen depleted from the compressed air, as will be shown in Equation (3.54), so in theory would be desirable to boost it as much as possible also to reduce the exchange area [10]. Unfortunately the aforementioned temperature is limited to about 1200 °C by the degradation of the device and the HTHX is necessary to reduce the difference between the combustor outlet temperature of a conventional power

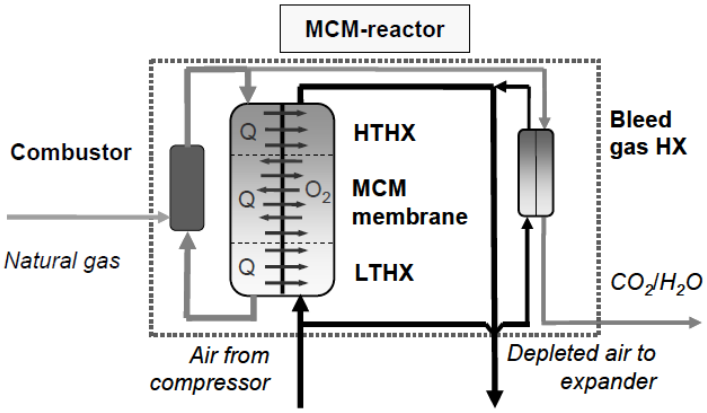

Figure 2.6. A detailed view of the membrane reactor [3].

plant and the turbine inlet temperature of the AZEP cycle [10, 11, 1, 3, 5, 6, 7]. This limitation turns out in the constitutional disadvantage of the AZEP concept versus the reference thermodynamic cycle.

Moreover comparing Figure 2.4 to Figure 2.5, could be observed that in the second diagram the stream of flue gas is conveyed to the Heat Recovery Steam Generator instead of being expanded in a CO_2/H_2O turbine (first diagram). The two figures represent different implementations of the AZEP cycle: the concept with the flue gas turbine is stated to be better performing than the other, but it requires the development of a novel kind of gas turbine working with a significantly different mixture of gas than the conventional nitrogen-based air turbines [7, 5]. Moreover, a CO_2/H_2O turbine is not available at the moment on the market and its development would require great efforts in terms of time and money. So the scheme of Figure 2.5 could be more interesting in the short term, even if it achieves reduced performance.

Another popular option often considered alongside the "standard" AZEP cycle, is the modification of the layout with the insertion of a conventional afterburner before the expansion of the oxygen-depleted stream (Figure 2.7). In fact, the air at the outlet of the membrane still retains a quantity of oxygen capable to react with additional fuel, increasing the turbine inlet temperature and reaching values close to the conventional case. In this way the performance of the power plant are more similar to the reference one but the payback is the incapability to capture *all* the generated CO_2. For this reason this concept is usually called "AZEP 85%" since the plant is designed to capture just the 85% of the carbon dioxide originated in the energy conversion process [3, 1].

The Bleed gas Heat Exchanger is adopted to increase slightly the inlet temperature at the turbine of the oxygen-depleted air stream, but mainly to

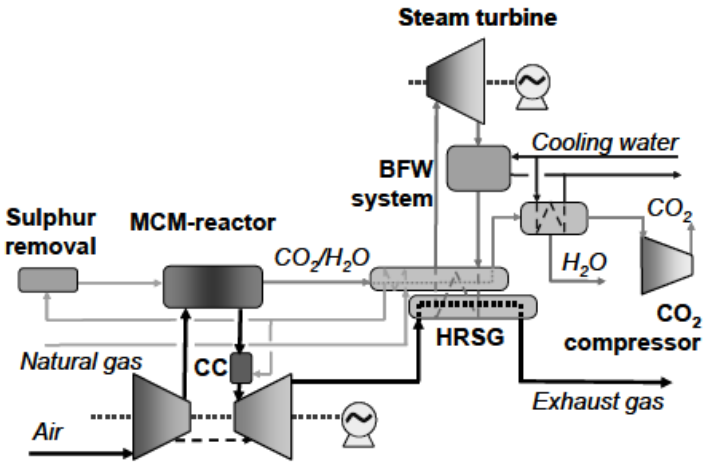

Figure 2.7. The alternative AZEP layout with a conventional afterburner before the expansion of the oxygen-deplated air flow [3].

reduce the temperature of the flue gas that could be unacceptable for the Heat Recovery Steam Generator or (less likely) for the CO_2/H_2O turbine.

The literature values available prescribe that about the 10% of the bleed flow is conveyed to the BHX, a range of 40%–50% of the oxygen present in the air is, on the whole, transferred to the oxy-fuel combustor in the membrane (with a concentration of about 10% of O_2 at the combustor inlet) and about the 90% of the flue gas is recirculated via the High Temperature Heat Exchanger to the membrane and then to the combustor [10].

Some investigations are present in the literature about the performance of the AZEP cycle, but usually they are not extensive and not completely explanatory about the computational assumptions.

A first study [11] reports a penalty of the 4.5 points for the thermal efficiency of a 50 MW combined cycle plant, according to the AZEP 100% layout, and less than 3.0 points for the AZEP 85%; there are no specifications about the bottoming cycle characteristic parameters. It is also considered a 400 MW combined cycle computation, where the reference engine is a Siemens V94.3A plant. It results in a higher reduction in the efficiency (compared to the smaller size case) that is 4.5 percentage points for the AZEP 85% concept and it is not specified in the 100% CO_2 capture case. The concentration of the NO_x in the oxygen-depleted stream is claimed to be lower than 1 ppm in volume in the AZEP 100% layout.

All the computations assume that the flue gas goes to the Heat Recovery Steam Generator *without* any CO_2/H_2O turbine and that the compression of the CO_2 for the storage is included in the overall balance. Other useful

assumptions reported in the paper are the plant pressure ratio of about 18, approximately 10% of oxygen concentration in the recirculation flow, the pressure difference over the membrane below 0.5 bar, about 10% of the flue gas conveyed to the Bleed gas Heat Exchanger, the outlet temperature of the oxygen-depleted air from the High Temperature Heat Exchanger that is about 1200 °C and the specification that the CO_2 is first compressed from the flue gas pressure, liquefied and then pumped to 100 bar.

Other investigations [1] report a thermal efficiency of 50% for the AZEP 100% and 53% for the AZEP 85% with the reference engine, GE9351FA, giving 57%. The bottoming cycle modelled is a triple pressure steam plant with reheat where the pressure levels are 111, 27 and 4 bar and it is supposed to have a turbine able to expand the oxy-fuel combustion exhaust gas with a polytropic efficiency of the 87%. The authors do not specify the output power but includes in the performance computation the CO_2 preparation for the storage, operated by four inter-cooled stages of compression to 200 bar.

In another paper [3] is investigated again the effect of the power plant size on the performance, while comparing the conventional combined cycle and the AZEP one without CO_2/H_2O turbine. A 50 MW plant is referred to the conventional Siemens SGT800 gas turbine coupled with a dual pressure steam cycle (80 bar and 510 °C for the high pressure level). The AZEP 100% has 4.6 points of reduction in the thermal efficiency, while the AZEP 85% (with a turbine inlet temperature of 1327 °C) results in less than three percentage points of penalty. The reference plant for the 400 MW is a Siemens SGT5-4000F engine with a triple pressure Heat Recovery Steam Generator with reheat of about 130, 30, 5 bar and 560, 545, 240 °C. The AZEP 100% gives a too low exhaust gas temperature for the triple pressure bottoming cycle, so it is used the dual pressure reference cycle of the 50 MW case; it turns out in a reduction of more than eight points on the efficiency percentage; the AZEP 85%, instead, shows a penalty of about 4%. The power output reduction is about a quarter of the reference case in the AZEP 100% and, respectively, 10 and 100 MW for the 50 and 400 MW for the AZEP 85%.

A similar study [5] was carried out in comparison with a conventional Siemens V94.3A combined cycle with an efficiency of 57.9% and considers again the AZEP layout without the CO_2/H_2O turbine. For what concerns the 100% case (with a turbine inlet temperature of 1200 °C) the efficiency drops of 8.3 percentage points, instead in the AZEP 85%, the efficiency is claimed to be 53.4%.

Although other interesting investigations could be referenced [12, 13, 6] the common problem faced when browsing the literature data on this topic, is the lack of specification for some computational assumption and (most important) the effect that the main cycle parameters determine to the performance and

the extent of application of a certain AZEP cycle. In fact, must be observed (and this could appear even more clearly looking at the process flow diagram of Figure 3.1) that the choice to adopt or not a CO_2/H_2O turbine and also the advantage in inserting the Bleed gas Heat Exchanger are driven by cycle parameters as the recirculated flue gas pressure, or the mass flow bled from the compressor. Consequently, also the application of a specified AZEP cycle is affected by these parameters that, in the literature, not only are not considered in a sensitivity analysis, but are always completely neglected.

In the scope of this project will be carried out with eAZEP a sensitivity analysis (in analogy with what is usually done for the conventional power plants) in order to investigate the capability of the different AZEP layout arrangements for the power generation purposes.

Chapter 3

Methods

3.1 The physical model

The Process Flow Diagram of the modelled power plant (Figure 3.1) shows the logical representation that eAZEP has of the different layouts that could be considered. The single-shaft engine is made up of 35 stations (34 represent air/gas mixtures plus 1 for the fuel mixture) of which just 25 are showed in the PFD. The remaining stations not present in the picture concerns the carbon dioxide compression and pumping process for storage purposes; in particular there is a condenser that eliminates the steam present in the flue gas, four inter-cooled stages of compression up to the CO_2 critical pressure, one last cooler that makes the carbon dioxide liquid and a final pumping station to the storage pressure.

For every station eAZEP figures five flow quantities:

1. the mass flow W;
2. the pressure p;
3. the temperature T;
4. the specific enthalpy h;
5. the composition $\boldsymbol{f}$.

Since the composition is a vector with five components (at least for the air and the gas stations; of two components for the fuel), see Section 3.1.1 at page 21, there are nine scalar quantities describing each air/gas station and six quantities for the fuel. This turns out in a system of roughly[1] $34 \cdot 9 + 6 = 312$

[1] Actually not all the stations quantities could be strictly considered unknowns as, for instance, the inlet conditions at station 1.

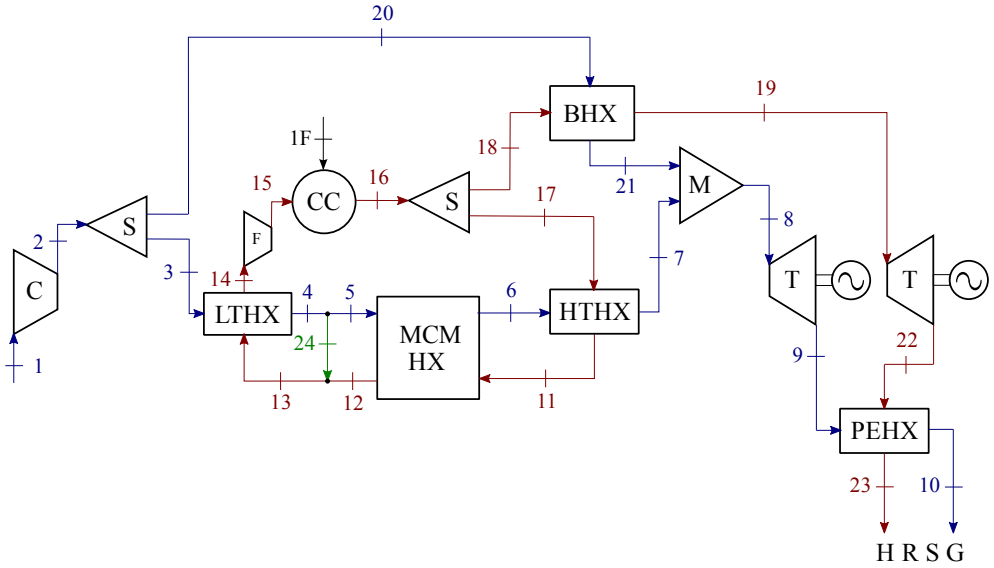

Figure 3.1. The process flow diagram of the AZEP cycle.

scalar unknowns for the same number of equations, in order to solve the complete model of the AZEP cycle.

Actually Figure 3.1 includes all the layouts that, at the moment, eAZEP can represent and none of them will use all the components drawn in the figure. There are four possible layouts to be considered.

Simple Bleed gas Heat exchanger layout: the Post Expansion Heat exchanger (PEHX) is not present in the layout (eAZEP will simply bypass it on both the streams) as well as the flue gas turbine between stations 19 and 22.

Bleed gas Heat exchanger layout with flue gas turbine: the Post Expansion Heat exchanger (PEHX) is bypassed again but the turbine is present.

Simple Post Expansion Heat exchanger layout: this is an original contribution of this work. At the knowledge of the author there are no studies about this arrangement which looks very attractive, especially for combined cycle purposes (see Section 4). In this option the is no mass flow bled at the outlet of the compressor (there is no stream at

station 20) and the flue gas turbine and the Bleed gas Heat exchanger are skipped. This means that there is no actual mixing at the inlet of the air turbine, since the mass flow at station 21 is zero.

This layout was conceived observing that for some combinations of the operating parameters, the temperature at the inlet of the air turbine is lowered and *not* increased by the adiabatic mixing between stations 7 and 21. So the PEHX layout idea is to keep the stream at the inlet of the air turbine equal to station 7 and to cool the flue gas with an heat exchanger after the turbine expansion. If a lower pressure of the streams in the heat exchangers is slightly detrimental for the heat exchange coefficient [14], on the other hand the device works at remarkable lower temperatures that makes it very cheaper.

Post Expansion Heat exchanger layout with flue gas turbine: this option avoids to bypass the flue gas turbine in the PEHX arrangement described before.

The kind of streams that go through the power plant could be classified according to the composition in:

Air stations: describe the behaviour of the standard or oxygen depleted air (the blue lines);

Exhaust gas stations: the result of the oxy-fuel combustion (mainly carbon dioxide and steam) and their mixture with oxygen (red lines);

Fuel station: the black line at the inlet of the combustion chamber.

Now will be described in details the physical model adopted for each component of the power plant, starting from the model of the operating fluids.

3.1.1 Operating fluids

Gas behaviour

All the operating fluids are mixtures of *perfect gases*; this means that they behave according to the *ideal gas law*

$$p\,v = R\,T \tag{3.1}$$

The gas constant R of each of them is

$$R = \frac{\mathcal{R}}{\mathcal{M}} \tag{3.2}$$

where $\mathcal{R} = 8314.3\,{}^{\mathrm{J}}/_{\mathrm{kmol\,K}}$ is the ideal gas constant and $\mathcal{M}$ is the molecular weight of the compound.

Moreover the specific heat of each gas is not considered constant, but depends just on the temperature

$$\begin{cases} c_p = c_p(T) = {}^{\mathrm{d}h}/_{\mathrm{d}T} \\ c_v = c_v(T) = {}^{\mathrm{d}u}/_{\mathrm{d}T} \end{cases} \tag{3.3}$$

so, in order to obtain the finite expression of the specific enthalpy and the specific internal energy, will be necessary to transform the previous equations

$$\begin{cases} \mathrm{d}h = c_p(T)\,\mathrm{d}T \\ \mathrm{d}u = c_v(T)\,\mathrm{d}T \end{cases}$$

thus

$$\begin{cases} h(T) = \displaystyle\int_{T_\mathrm{r}}^{T} c_p(T)\,\mathrm{d}T + h_\mathrm{r} \\ u(T) = \displaystyle\int_{T_\mathrm{r}}^{T} c_v(T)\,\mathrm{d}T + u_\mathrm{r} \end{cases} \tag{3.4}$$

where the subscript "r" indicates an arbitrary reference state where $u_\mathrm{r} = u(T_\mathrm{r})$ e $h_\mathrm{r} = h(T_\mathrm{r})$.

In this work will be used just the specific enthalpy (not the internal energy) and the reference enthalpy h_r is assumed to be the enthalpy of formation of the compound at the standard state[2] $h_\mathrm{r} \equiv h_\mathrm{f}^0$. The *enthalpy of formation* of a chemical compound is defined as the heat that must be supplied (if it is positive) or removed (if negative) in a stoichiometric reaction starting from the constituent elements in their natural forms. Thus, the standard enthalpy of formation of stable compounds at the standard state is zero, as for example the oxygen and nitrogen in the molecular form (O_2 and N_2).

Therefore the specific enthalpy can be broken up in two components:

$$h(T) = h_\mathrm{s}(T) + h_\mathrm{f}^0 \tag{3.5}$$

where $h(T)$ is the *total enthalpy* (or, simply, enthalpy) and $h_\mathrm{s}(T)$ is the l'*sensible enthalpy*, that is the amount of the total enthalpy dependant on the temperature.

While performing the energy balance of a component, it is necessary to consider the enthalpy of formation every time that the chemical composition of the working fluid is changing across the component, or when a substance

[2] $T_0 = 298.15\,\mathrm{K}$ and $p_0 = 1\,\mathrm{atm} = 101.325\,\mathrm{kPa}$.

is changing its phase. Examples of the first case are the combustion chamber and the membrane of the power plant studied in this work; the second case could be observed in a humidification tower, for example.

Differently, in the devices where the fluid composition and phase state are constant, since the enthalpy of formation is a constant that can be neglected, it is easier to evaluate just the variations in the sensible enthalpy (equal to zero at the standard state).

The program is able to figure both the total enthalpy and the sensible one, simply setting a logical variable (see page 21 for details).

Mixtures of gas

In order to calculate the properties of the working fluid it is necessary to deal with mixtures of gas, so must be known its composition and the values of the properties for every gas that constitutes the mixture. Will be supposed that the gases behave as described in the previous subsection, and that they are in thermodynamic equilibrium.

In order to describe the composition of a given mixture of gas made up of N components, there are two options.

Gravimetric analysis: it is based on the mass of each component; it specifies the *mass fraction* of each gas f_i according to this definition:

$$f_i = \frac{m_i}{\sum_{i=1}^{N} m_i} = \frac{m_i}{m_{\text{tot}}} \tag{3.6}$$

where m_i is the mass of each component and m_{tot} is the total mass of the mixture.

Molar analysis: it indicates the number of moles of each component, specifying the *molar fractions*, χ_i:

$$\chi_i = \frac{n_i}{\sum_{i=1}^{N} n_i} = \frac{n_i}{n_{\text{tot}}} \tag{3.7}$$

where n_i is the number of moles of each component and n_{tot} is the total number of moles[3].

[3]It is possible, with a bit of basic algebra, obtain f_i from χ_i and vice versa.

The average molecular weight of the mixture, $\mathcal{M}_\mathrm{m} = {}^{m_\mathrm{tot}}/_{n_\mathrm{tot}}$, can be evaluated from the mass fractions, with this formula

$$\mathcal{M}_\mathrm{m} = \frac{1}{\sum_{i=1}^{N} \frac{f_i}{\mathcal{M}_i}} \tag{3.8}$$

while the average ideal gas constant could be obtained with the following equation

$$R_\mathrm{m} = \frac{\mathcal{R}}{\mathcal{M}_\mathrm{m}} \tag{3.9}$$

It is necessary to distinguish between extensive and intensive properties in order to evaluate them for the gaseous mixture.

Extensive properties: the mixture value is obtained simply adding up the values for each component; it is particularly useful for the calculation of the mass and the volume:

$$m_\mathrm{tot} = \sum_{i=1}^{N} m_i \qquad V_\mathrm{tot} = \sum_{i=1}^{N} V_i$$

Intensive properties: in this case must be performed the weighted mean of the quantities, where the weights are the mass fractions (if the property is referred to the unit of mass) or the molar fractions (if the property is referred to the single mole of mixture).

For example, the software will perform the following computation in order to figure the specific enthalpy of the air (h_a), starting from the mass composition (f_i) and the enthalpy of the components (h_i):

$$h_\mathrm{a} = \sum_{i=1}^{N} f_i \, h_i \tag{3.10}$$

Although the pressure is an intensive quantity, the previous rule does not apply directly. Since the mixture is made up of ideal gases, the *Dalton law* applies: the pressure of the mixture is the sum of the pressures that each constituent gas would have in the same conditions of temperature and volume of the mixture, if it would be alone. That is, for the air:

$$p_\mathrm{a} = \sum_{i=1}^{N} p_i(T_\mathrm{a}, V_\mathrm{a}) \tag{3.11}$$

Moreover since for both the constituent gas and the mixture, the ideal gas law applies — Equation (3.1) — it is possible to obtain the pressure as $p = {}^{n\mathcal{R}T}/_{V}$, in order to express conveniently the pressure ratio between the component and the mixture; for the air: ${}^{p_i}/_{p_\mathrm{a}}$. Applying the law (3.11):

$$\frac{p_i}{p_\mathrm{a}} = \frac{{}^{n_i \cancel{\mathcal{R}} \cancel{T_\mathrm{a}}}/{\cancel{V_\mathrm{a}}}}{{}^{n_\mathrm{a} \cancel{\mathcal{R}} \cancel{T_\mathrm{a}}}/{\cancel{V_\mathrm{a}}}} = \frac{n_i}{n_\mathrm{a}} = \chi_i$$

that is

$$p_i = \chi_i \, p_\mathrm{a} \tag{3.12}$$

where $\chi_i \, p_\mathrm{a}$ is called *partial pressure* (coinciding with the component pressure p_i for an ideal gas).

Since the computer program does not deal with molar fractions explicitly (all the specific quantities figured are referred to the unit of mass), the expression used directly by the computational code can be easily derived

$$p_i = \frac{\dfrac{f_i}{\mathcal{M}_i}}{\displaystyle\sum_{i=1}^{N} \frac{f_i}{\mathcal{M}_i}} \, p_\mathrm{a} \tag{3.13}$$

where only the mass fractions appear.

A number of the previous equations are referred to the air but, obviously, they are still valid for every mixture of ideal gas (as the fuel or the exhausted gas).

Polynomial expression of the thermodynamic properties

A polynomial can express the specific heat at constant pressure as a function of the temperature for every gas constituting the mixture of the working fluid. The model selected for the implementation was developed by the NASA [15]:

$$\frac{c_{p,i}(T)}{R_i} = \frac{a_{1,i}}{T^2} + \frac{a_{2,i}}{T^2} + a_{3,i} + a_{4,i} \, T + a_{5,i} \, T^2 + a_{6,i} \, T^3 + a_{7,i} \, T^4 \tag{3.14}$$

The specific enthalpy as a function of the temperature in a polynomial form, can be obtained starting from the previous expression and integrating the equation $\mathrm{d}h_i = c_{p,i} \, \mathrm{d}T$:

$$\begin{aligned} \frac{h_i(T)}{R_i} = -\frac{a_{1,i}}{T} + a_{2,i} \ln T + a_{3,i} \, T + a_{4,i} \frac{T^2}{2} + a_{5,i} \frac{T^3}{3} + a_{6,i} \frac{T^4}{4} + \\ + a_{7,i} \frac{T^5}{5} + b_{1,i} \end{aligned} \tag{3.15}$$

where $b_{1,i}$ is an integration constant.

> The coefficients are taken from the NASA Glenn Research Center database that comprises more than 2000 chemical species divided among gases, liquids, solids and ions [15]. Those values were determined applying a least squares regression analysis on experimental data or using thermodynamic functions that include, at the same time, the specific heat at constant pressure, the entropy and the enthalpy. A previous version of this model (declared obsolescent in the 1994) had two coefficients less in every polynomial.
>
> This database has been massively used in a computer program called *Chemical Equilibrium with Applications* (CEA), now available on the NASA website[4] as a new version called CEAgui; the compounds coefficients used in the model of this work were extracted exactly from the CEAgui.

For the substances constituting the working fluid (Ar, CO_2, N_2, O_2, $H_2O_{(g)}$, CH_4) the coefficients are given for temperature ranges[5]: from 200 K to 1000 K, from 1000 K to 6000 K and (just for some species, but of no use for the model of this work) from 6000 K to 20 000 K.

It is useful to observe that the Equations (3.14) and (3.15) are equally applicable if referred to both the mass fractions and the molar units since the coefficients are non-dimensional quantities and — thanks to the Equation (3.2) — the following equalities stands:

$$\frac{c_{p,i}}{R_i} = \frac{\hat{c}_{p,i}}{\mathcal{R}} \qquad \text{and} \qquad \frac{h_i}{R_i} = \frac{\hat{h}_i}{\mathcal{R}}$$

where $\hat{c}_{p,i}$ and $\hat{h}_i$ are the same quantities at the left-hand side, but referred to the unit of kilomole.

The output of the Equation (3.15) is the total enthalpy, the sum of the sensible enthalpy and the formation enthalpy — see Equation (3.5). For the thermodynamic transformations with constant enthalpy of formation (see page 16 for details), could be evaluated just the variations of the sensible enthalpy in order to avoid round-off errors; in fact the enthalpy of formation is often remarkably bigger than the sensible enthalpy associated with the temperature change. Moreover in this way it is pursued another advantage in

[4] http://www.grc.nasa.gov/WWW/CEAWeb/ceaHome.htm.

[5] The integration constant $b_{1,i}$, present in the formula of the specific enthalpy, is obtained exactly imposing the continuity of the integrated function at the common bounds of these intervals.

debugging the program: we can check the convergence to obviously wrong values just with "a glance".

In order to evaluate *just* the sensible enthalpy it is necessary to call the function that figures the enthalpy (`h_air`) setting the logical variable `total` to `.FALSE.`, then the Equation (3.15) will be modified in the following way

$$h_{i,\mathrm{s}}(T) = R_i \left(-\frac{a_{1,i}}{T} + a_{2,i} \ln T + a_{3,i} T + a_{4,i} \frac{T^2}{2} + a_{5,i} \frac{T^3}{3} + a_{6,i} \frac{T^4}{4} + a_{7,i} \frac{T^5}{5} + b_{1,i} \right) - \frac{\hat{h}^0_{\mathrm{f},i}}{\mathcal{M}_i} \tag{3.16}$$

Mixtures composition

The composition of the ambient air flowing across the stations 1, 2, 3, 4, 17 and 18 (see Figure 3.1) is described by a vector of five components $\boldsymbol{f}_\mathrm{a}$, according to the gravimetric analysis:

$$\boldsymbol{f}_\mathrm{a} = \left\{ f_\mathrm{Ar}, f_{\mathrm{CO_2}}, f_{\mathrm{N_2}}, f_{\mathrm{O_2}}, f_{\mathrm{H_2O}} \right\} \tag{3.17}$$

Although the program is able to take into account the effect of humidity, the ambient air will be considered as dry ($f_{\mathrm{H_2O}} = 0$), while the other components of the vector are listed in the Table 3.1.

Table 3.1. The mass fractions of the dry ambient air constituents (five significant digits) [16].

Compound	**Mass fraction** (f_i)
Ar	0.01282600
CO_2	0.00045584
N_2	0.75527000
O_2	0.23145000

For what concerns the fuel (natural gas), its composition vector $\boldsymbol{f}_\mathrm{f}$ comprises two components

$$\boldsymbol{f}_\mathrm{f} = \left\{ f_{\mathrm{CH_4}}, f_{\mathrm{N_2}} \right\} \tag{3.18}$$

with the following mass fractions

Compound	**Mass fraction** (f_i)
CH_4	0.9292
N_2	0.0708

In reality the natural gas is made up of several components (mainly hydrocarbons) where the methane is anyway the most abundant. The aforementioned mass composition has been obtained from the balance between the methane and inert gas (the nitrogen) in order to match the average calorific value of the commercial natural gas [16].

In the plant layout there are two components that change the composition of the flows in a *not* straightforward way:

- a *mixer* before the station 7 (as shown in Figure 3.1);
- the *membrane* in which takes place the extraction of the oxygen from one side and its injection in the other (see Figure 3.6).

In both cases, supposing to know all the quantities at the inlet stations, in order to determine the composition at the outlet, we construct the output vector $\boldsymbol{f}_{\text{out}}$ component by component, applying the following formula for every constituent gas:

$$f^i_{\text{out}} = \frac{f^i_{\text{in}} W_{\text{in}} + f^i_{\text{m\e}} W_{\text{m\e}}}{W_{\text{in}} + W_{\text{m\e}}} \tag{3.19}$$

where the subscript m\e stands for "mixed or extracted". This means that the formula is valid in the algebraic sense and thus the mass flow will have the positive sign if mixed (stations 7 and 9, for the flue gas side of the membrane) or negative (station 9 for the air side of the MCM).

Of course the procedure shown above could be applicable for the injection or extraction of every component of the gas mixture (for example to take into account the humidity of the air), but it will not be used in any other case.

3.1.2 Power plant components

Will be now described the elements that, assembled, constitute the power plant. Their different disposition determines the layouts available of which just the most interesting and promising sub set will be considered. For every component is supposed to know the inlet station and some parameters specified case by case.

Compressors

The eAZEP compressors (Figure 3.2) are turbomachineries which have the pressure ratio π, the polytropic η_{y}, and the mechanical efficiency η_{m} defined. The thermodynamic transformation of the working fluid is considered *adiabatic* because the heat rate leaking from the machinery to the surroundings is negligible compared to the compression work.

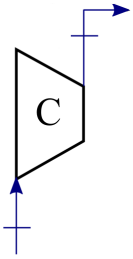

Figure 3.2. A generic process flow diagram for the eAZEP compressors.

Since there are no mass flow variations, neither composition changes, results

$$W_{\text{out}} = W_{\text{in}} \tag{3.20}$$

$$\boldsymbol{f}_{\text{out}} = \boldsymbol{f}_{\text{in}} \tag{3.21}$$

and, obviously (from the definition of the pressure ratio)

$$p_{\text{out}} = \pi\, p_{\text{in}} \tag{3.22}$$

In order to determine the final temperature T_{out} is necessary to take into account the variation of the specific heat at constant pressure with the temperature, according to the implemented model of the working fluids. Considering this aspect, can be proofed (see Appendix A) that the equation describing the compression of an ideal gas in which appears the polytropic efficiency is

$$\eta_{\text{y,c}}\,(s_{\text{out}} - s_{\text{in}}) = \mathcal{R}\,\ln\left(\frac{p_{\text{out}}}{p_{\text{in}}}\right) \tag{3.23}$$

Since the entropy is a function of the temperature, must be found the temperature T_{out} which gives the s_{out} able to satisfy the last equality. Must be observed that before to start the root finding process to calculate T_{out}, must be evaluated the average gas constant $\mathcal{R}$ from the composition vector (see Section 3.1.1)

$$\mathcal{R} = R_{\text{gas}}(\boldsymbol{f}_{\text{in}}) \tag{3.24}$$

Then it is straightforward to calculate the outlet enthalpy and the compressor work:

$$h_{\text{out}} = h_{\text{gas}}(T_{\text{out}}, \boldsymbol{f}_{\text{out}}) \tag{3.25}$$

$$P_{\text{c}} = \frac{W_{\text{in}}}{\eta_{\text{m}}}\,(h_{\text{out}} - h_{\text{in}}) \tag{3.26}$$

Turbines

The solving procedure for a generic turbine (Figure 3.3) is very similar to the previous, thus the expansion is considered adiabatic with negligible variation of the kinetic energy and the gravitational energy between the inlet and the outlet. The main difference compared to the compressor case is that is supposed to be known the outlet pressure of the turbine (this substitutes the need to know the pressure ratio as a parameter). Furthermore the turbine element contains also the electric generator efficiency η_{el}, as additional parameter compared to the compressor.

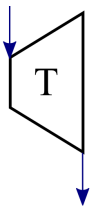

Figure 3.3. A generic process flow diagram for the eAZEP turbines.

Thus, the mass flow and the composition are constant along the machinery

$$W_{\mathrm{out}} = W_{\mathrm{in}} \tag{3.27}$$

$$\boldsymbol{f}_{\mathrm{out}} = \boldsymbol{f}_{\mathrm{in}} \tag{3.28}$$

and also the average gas constant is simply figured

$$\mathcal{R} = R_{\mathrm{gas}}(\boldsymbol{f}_{\mathrm{in}}) \tag{3.29}$$

For the determination of the final temperature T_{out}, the equation describing the thermodynamic process is very similar to the compressor one (see Appendix A)

$$\frac{(s_{\mathrm{in}} - s_{\mathrm{out}})}{\eta_{\mathrm{y,t}}} = \mathcal{R} \ln\left(\frac{p_{\mathrm{in}}}{p_{\mathrm{out}}}\right) \tag{3.30}$$

and so s_{out} brings the required T_{out}.

Finally the outlet enthalpy and the turbine work are calculated:

$$h_{\mathrm{out}} = h_{\mathrm{gas}}(T_{\mathrm{out}}, \boldsymbol{f}_{\mathrm{out}}) \tag{3.31}$$

$$P_{\mathrm{t}} = \eta_{\mathrm{m}}\, \eta_{\mathrm{el}}\, W_{\mathrm{in}}\, (h_{\mathrm{in}} - h_{\mathrm{out}}) \tag{3.32}$$

Heat exchangers

The design criterion for the eAZEP heat exchangers (Figure 3.4) is based on the ε-N_{tu} method [17, 18], considering all them as perfect counter-current devices.

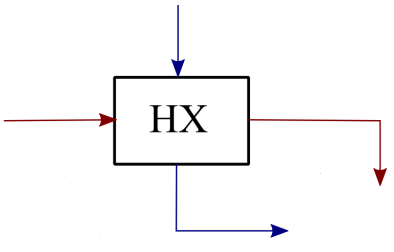

Figure 3.4. A generic process flow diagram for the eAZEP heat exchangers.

First of all the mass flow and the composition, which are constant, are calculated at the output both on the cold and on the hot side

$$W_{\text{out,c}} = W_{\text{in,c}} \tag{3.33}$$
$$W_{\text{out,h}} = W_{\text{in,h}} \tag{3.34}$$
$$\boldsymbol{f}_{\text{out,c}} = \boldsymbol{f}_{\text{in,c}} \tag{3.35}$$
$$\boldsymbol{f}_{\text{out,h}} = \boldsymbol{f}_{\text{in,h}} \tag{3.36}$$

Then since the pneumatic efficiencies on both sides are known ($\eta_{\pi,\text{c}}$ and $\eta_{\pi,\text{h}}$), the output pressures reads

$$p_{\text{out,c}} = \eta_{\pi,\text{c}}\, p_{\text{in,c}} \tag{3.37}$$
$$p_{\text{out,h}} = \eta_{\pi,\text{h}}\, p_{\text{in,h}} \tag{3.38}$$

In this way is now possible to estimate the overall heat transfer coefficient U which is dependent on the pressure of the low pressure side (almost always the flue gas side). In fact for a gas-gas heat exchanger, U can be estimated starting from the pressure of the cold and hot side; in particular U spans between 100 to 300 $^{\text{W}}/_{\text{m}^2\,\text{K}}$ according to the low pressure side increasing from 1 to 20 bar [14]. Thus is possible to determine U starting from the averaged lower pressure side value (almost always the hot side), with a linear interpolation. Must be clarified that the program checks first which side has the lower average pressure and then it figures the overall heat transfer coefficient.

Then it is well-known from the heat transfer fundamentals that the fluid with the lower heat capacity rate, experience the larger variation of temperature in an heat exchanger. The ε-N_{tu} method is based also on this observation, so it is necessary to set the fluid with the minimum and the maximum heat capacity rate, $\dot{C}_{\text{min}}$ and $\dot{C}_{\text{max}}$. Unfortunately $\dot{C}$ depends on the temperature

$$\dot{C} = W\, c_p(T, \boldsymbol{f}) \tag{3.39}$$

that is changing along the device (the specific heat at constant pressure c_p is changing) and, since T_{out} is unknown, in turn, the goes for the outlet value of c_p as well as for the corresponding heat capacity rate. Thus the real $\dot{C}$ value is replaced with an estimated one $\tilde{C}$ evaluated on the span of a ΔT_{hx} (usually 30 K), considering that generally the variation with the temperature of the c_p is not very considerable over a span of tens kelvin of difference. Then

$$\tilde{C}_{\text{out,c}} = C_{\text{gas}}(W_{\text{out,c}}, T_{\text{in,c}} - \Delta T_{\text{hx}}, \boldsymbol{f}_{\text{out,c}}) \tag{3.40}$$

$$\tilde{C}_{\text{out,h}} = C_{\text{gas}}(W_{\text{out,h}}, T_{\text{in,h}} + \Delta T_{\text{hx}}, \boldsymbol{f}_{\text{out,h}}) \tag{3.41}$$

so that

$$\tilde{C}_{\text{c}} = \frac{\dot{C}_{\text{in,c}} + \tilde{C}_{\text{out,c}}}{2} \tag{3.42}$$

$$\tilde{C}_{\text{h}} = \frac{\dot{C}_{\text{in,h}} + \tilde{C}_{\text{out,h}}}{2} \tag{3.43}$$

making possible the assignment of the $\dot{C}_{\text{min}}$ and $\dot{C}_{\text{max}}$, although on an approximated basis.

It is possible to evaluate the ideal thermal heat rate $\dot{Q}_{\text{id}}$

$$\dot{Q}_{\text{id}} = W_{\text{min}} \left[h_{\text{air}}(T_{\text{in,h}}, f_{\text{min1}}) - h_{\text{air}}(T_{\text{in,c}}, f_{\text{min2}}) \right] \tag{3.44}$$

based on the following case analysis:

- if $\dot{C}_{\text{c}} = \dot{C}_{\text{max}}$ then
  - $\text{min1} = \text{in}, \text{h}$
  - $\text{min2} = \text{out}, \text{h}$;
- if $\dot{C}_{\text{h}} = \dot{C}_{\text{max}}$ then
  - $\text{min1} = \text{out}, \text{c}$
  - $\text{min2} = \text{in}, \text{c}$.

Starting from the design point number of thermal units N_{tu}, the heat exchange area A is easily figured:

$$A = \frac{N_{\text{tu}}\, \dot{C}_{\text{max}}}{U} \tag{3.45}$$

as well as the efficiency of the device ε [17, 18, 14]

$$\varepsilon = \frac{1 - \exp\left[-(1 - \dot{C}_{\text{min}}/\dot{C}_{\text{max}})\, N_{\text{tu}}\right]}{1 - (\dot{C}_{\text{min}}/\dot{C}_{\text{max}})\, \exp\left[-(1 - \dot{C}_{\text{min}}/\dot{C}_{\text{max}})\, N_{\text{tu}}\right]} \tag{3.46}$$

There are two limiting cases

- for $\dot{C}_{\min}/\dot{C}_{\max} = 1$ the previous equation is indeterminate, applying L'Hôpital's rule results [17, 18]

$$\varepsilon = \frac{N_{\text{tu}}}{N_{\text{tu}} + 1} \tag{3.47}$$

- for $\dot{C}_{\min}/\dot{C}_{\max} = 0$ the efficiency formula reads

$$\varepsilon = 1 - \mathrm{e}^{-N_{\text{tu}}} \tag{3.48}$$

As will be shown in the next section, the Mixed Conductive Membrane follows a slightly different calculation process while evaluating the area and the number of thermal units, for its behaviour as an heat exchanger; the efficiency formula will be applied in the same way.

The output specific enthalpies are then figured

$$h_{\text{out,c}} = \frac{W_{\text{in,c}}\, h_{\text{in,c}} + \varepsilon\, \dot{Q}_{\text{id}}}{W_{\text{out,c}}} \tag{3.49}$$

$$h_{\text{out,h}} = \frac{W_{\text{in,h}}\, h_{\text{in,h}} - \varepsilon\, \dot{Q}_{\text{id}}}{W_{\text{out,h}}} \tag{3.50}$$

with the corresponding temperatures

$$T_{\text{out,c}} = T_{\text{gas}}(h_{\text{out,c}}) \tag{3.51}$$

$$T_{\text{out,h}} = T_{\text{gas}}(h_{\text{out,h}}) \tag{3.52}$$

The membrane

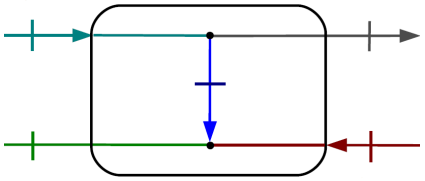

Figure 3.5. The *theoretical* Mixed Conductive Membrane process flow diagram.

The Mixed Conductive Membrane is the most important and complicated device of the power plant. It performs the extraction of the oxygen (the

light blue line in Figure 3.5) from the compressed air flow (dark blue and grey line) transferring it to an almost oxygen-free gas stream (the red line). The compressed air stream will be called *feed flow* while the flue gas stream *permeate flow*. The peculiarity of this device is that, *at the same time* of the mass transfer, takes place the counter-current heat exchange between the two flows, turning out in a remarkable increase of the model complexity. The outcome of the previous observations is that the quantities describing the streams crossing the membrane are all varying continuously along it, then the conventional design criteria are, in principle, inapplicable to this component.

In order to take into account the complex thermodynamic transformations of the device, it is considered consistent with the overall accuracy of the power plant model the application of the *superimposition principle*: the corresponding process flow diagram is shown in Figure 3.6. Applying the superimposition principle, the membrane process is divided into two sub-processes: an adiabatic transfer of oxygen from the feed flow to the permeate flow and the heat exchange.

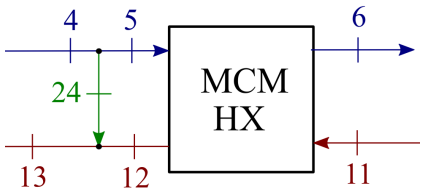

Figure 3.6. The eAZEP Mixed Conductive Membrane process flow diagram.

For what concerns the calculation of the device, it is actually the sum of the heat exchanger (Section 3.1.2, Page 24) plus the mixer solving procedures (Section 3.1.2, Page 31). For this reason, the reader is invited to bear on the corresponding sub-process section. Here will be outlined just the additional calculations required.

Should be observed that the membrane surface A_{mcm} must satisfy, at the same time, the mass transfer and the heat transfer constraint. Thus the number of thermal units for the MCM $N_{\mathrm{tu,mcm}}$ is not a design parameter, but it is determined by the equation that drives the mass transfer through the membrane. It is the Nernst-Einstein formula, a simple case of integration of the Wagner equation [19, 20, 21]:

$$j_{\mathrm{O}_2} = \frac{\sigma\,\mathcal{R}\,T}{4\,L\,n^2\,\mathrm{F}^2}\,\ln\frac{p^{\mathrm{F}}_{\mathrm{O}_2}}{p^{\mathrm{P}}_{\mathrm{O}_2}} \tag{3.53}$$

where[6]

[6] Although all the quantities are expressed in SI units of measure, the author prefer to

j_{O_2} is the oxygen flux ($^{mol}/_{m^2\,s}$);

σ is the membrane *electric* conductivity ($^{S}/_{m}$);

$\mathcal{R}$ is the ideal gas constant ($^{J}/_{mol\,K}$);

T is the membrane *absolute* temperature (K);

L is the membrane thickness (m);

n is the valency number of the element permeated (in this case we deal with oxygen, then, $n = 2$) (0);

F is the Faraday constant ($^{mol}/_{C}$);

$p^{F}_{O_2}$ is the partial pressure of the oxygen on the *feed* side (Pa);

$p^{P}_{O_2}$ is the partial pressure of the oxygen on the *permeate* side (Pa).

Since the oxygen mass flow W_{24} in $^{kg}/_{s}$ (instead of the oxygen flux) is needed explicitly, the previous equation is modified accordingly (substituting also $n = 2$)

$$W_{24} = \frac{\sigma\,\mathcal{R}\,T}{16\,L\,F^2}\,\ln\frac{p^{F}_{O_2}}{p^{P}_{O_2}}\,A_{mcm}\,\mathcal{M}_{O_2} \tag{3.54}$$

where A_{mcm} is the overall permeation area and $\mathcal{M}_{O_2}$ is the molecular weight of the oxygen.

The quantities T, $p^{F}_{O_2}$, $p^{P}_{O_2}$ are not constant along the membrane but they are varying continuously, so it is impossible to apply the last expression directly. In order to simplify the calculation procedure of the device and to keep the demand of the computational resources at the same order of magnitude of the other components of the power plant, a *lumped approach* for the model of the membrane has been adopted. This means that the following quantities are considered constant and equal to their average value:

$$\begin{aligned} \hat{T} &= \frac{T_4 + T_6 + T_{11} + T_{13}}{4} \\ \hat{p}^{F}_{O_2} &= \frac{p^{(4)}_{O_2} + p^{(6)}_{O_2}}{2} \\ \hat{p}^{P}_{O_2} &= \frac{p^{(11)}_{O_2} + p^{(13)}_{O_2}}{2} \end{aligned} \tag{3.55}$$

indicate them explicitly.

Must be noticed that the oxygen partial pressure is evaluated starting from the flow composition (known once the design-point value of W_{24} is set). Consequently, substituting in the Equation (3.54) the approximations (3.55), the final formula actually implemented for the membrane calculation is obtained:

$$W_{24} = \frac{\sigma \mathcal{R} \hat{T}}{16 L \mathrm{F}^2} \ln \frac{\hat{p}^{\mathrm{F}}_{\mathrm{O}_2}}{\hat{p}^{\mathrm{P}}_{\mathrm{O}_2}} A_{\mathrm{mcm}} \mathcal{M}_{\mathrm{O}_2} \tag{3.56}$$

The oxygen mass flow to extract is a cycle design parameter, so the overall heat exchange area (coinciding with the permeation area) A_{mcm} can be determined from the last equation. Then $N_{\mathrm{tu,mcm}}$ can be obtained from the values of U_{mcm}, A_{mcm} and $\dot{C}_{\mathrm{min,mcm}}$

$$N_{\mathrm{tu,mcm}} = \frac{U_{\mathrm{mcm}} A_{\mathrm{mcm}}}{\dot{C}_{\mathrm{min,mcm}}} \tag{3.57}$$

In this way the calculation can proceed according to the description given in the Section 3.1.2 at Page 24 with the evaluation of the efficiency of the membrane $\varepsilon_{\mathrm{mcm}}$ as heat exchanger.

Splitters

The splitters (Figure 3.7) divide a main flow into two streams of the *same composition* according to a ratio specified as a component parameter. This parameter is the outlet mass flow of the first output station W_{split}.

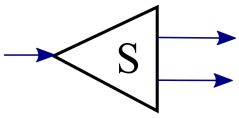

Figure 3.7. A generic process flow diagram for the eAZEP splitters.

Then the mathematical model is quite simple. First of all the program checks if W_{split} is greater than the inlet mass flow and, if so, prompts an error. If everything is right, the procedure sets the outlet mass flows

$$W_{\mathrm{out1}} = W_{\mathrm{split}} \tag{3.58}$$

$$W_{\mathrm{out2}} = W_{\mathrm{in}} - W_{\mathrm{split}} \tag{3.59}$$

It is possible also to specify a pneumatic efficiency for the process on each side ($\eta_{\pi 1}$ and $\eta_{\pi 2}$)

$$p_{\mathrm{out1}} = \eta_{\pi 1} p_{\mathrm{in}} \tag{3.60}$$

$$p_{\mathrm{out2}} = \eta_{\pi 2} p_{\mathrm{in}} \tag{3.61}$$

The assignment of the remaining quantities (temperature, specific enthalpy, composition) is banal

$$T_{\text{out1}} = T_{\text{in}} \tag{3.62}$$
$$T_{\text{out2}} = T_{\text{in}} \tag{3.63}$$
$$h_{\text{out1}} = h_{\text{in}} \tag{3.64}$$
$$h_{\text{out2}} = h_{\text{in}} \tag{3.65}$$
$$\boldsymbol{f}_{\text{out1}} = \boldsymbol{f}_{\text{in}} \tag{3.66}$$
$$\boldsymbol{f}_{\text{out2}} = \boldsymbol{f}_{\text{in}} \tag{3.67}$$

Mixers

The eAZEP mixers (Figure 3.8) model the adiabatic mixing of two flows.

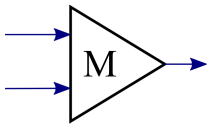

Figure 3.8. A generic process flow diagram for the eAZEP mixers.

The solving process starts with the evaluation of the outlet mass flow

$$W_{\text{out}} = W_{\text{in1}} + W_{\text{in2}} \tag{3.68}$$

The output pressure is the weighted average of the inlet pressures (where the weights are the mass flows) since considering the momentum equation was considered unnecessarily too accurate for the overall degree of accuracy of the plant model

$$p_{\text{out}} = \frac{W_{\text{in1}}\, p_{\text{in1}} + W_{\text{in2}}\, p_{\text{in2}}}{W_{\text{out}}} \tag{3.69}$$

The outlet composition, instead, implements Equation (3.19)

$$\boldsymbol{f}_{\text{out}} = \frac{\boldsymbol{f}_{\text{in1}}\, W_{\text{in1}} + \boldsymbol{f}_{\text{in2}}\, W_{\text{in2}}}{W_{\text{out}}} \tag{3.70}$$

The exit specific enthalpy reads

$$h_{\text{out}} = \frac{W_{\text{in1}}\, h_{\text{in1}} + W_{\text{in2}}\, h_{\text{in2}}}{W_{\text{out}}} \tag{3.71}$$

while the outlet temperature is obtained from the enthalpy just figured

$$T_{\text{out}} = T_{\text{gas}}(h_{\text{out}}) \tag{3.72}$$

Combustors

The combustor device (Figure 3.9) is the heat input device for the power plant. It is modeled as an adiabatic and perfect reactor (there are no unburned compounds at the outlet) since nowadays the industrial state-of-the-art guarantee heat leakages and combustion losses (due to incomplete chemical reactions) lower than the 1% of the heat rate introduced into the device.

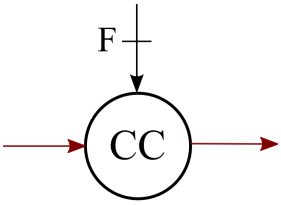

Figure 3.9. A generic process flow diagram for the eAZEP combustors.

The outlet temperature is a design parameter and its choice is driven by combustion stability reasons. In fact, the composition of the typical AZEP combustor inlet gas mixture increases the ignition delay and reduces the flame speed, turning out in a remarkable reduction in the reactivity of the oxygen-gas mixture [10, 22]. In order to contrast this issue, a suitable combustor outlet temperature must be set.

It is supposed that the fuel (natural gas) is always available at a sufficient pressure for the injection in the combustion chamber (usually some extra kilopascals more than the reactor pressure are enough). Must be noticed that the potential correction of this assumption would be marginal since it would include the work of an auxiliary compressor for the fuel. Instead, for what concerns the thermodynamic properties of the fuel, as shown in Section 3.1.1, they are not dependent on the pressure.

The first outlet quantity evaluated is the final pressure from the pneumatic efficiency of the device $\eta_{\pi,\mathrm{cc}}$

$$p_{\mathrm{out}} = \eta_{\pi,\mathrm{cc}}\, p_{\mathrm{in}} \tag{3.73}$$

Then, since both the inlet fuel temperature T_{f} and its composition vector $\boldsymbol{f}_{\mathrm{f}}$ are known as input parameters, also the fuel specific enthalpy h_{f} has been figured at the program initialization (see Section 3.3.5)

$$h_{\mathrm{f}} = h_{\mathrm{gas}}(T_{\mathrm{f}}, \boldsymbol{f}_{\mathrm{f}}) \tag{3.74}$$

The combustion involves only the methane (in the natural gas) and the oxygen (in the inlet gas mixture) according to this basic chemical reaction

$$\mathrm{CH_4} + 2\,\mathrm{O_2} \longrightarrow 2\,\mathrm{H_2O} + \mathrm{CO_2} \tag{3.75}$$

determining at the outlet a deep variation of the composition for the working fluid. This vector $\boldsymbol{f}_{\text{out}}$ is dependent on the inlet compositions $\boldsymbol{f}_{\text{in}}$, on the fuel composition $\boldsymbol{f}_{\text{f}}$ and on the gas fuel ratio α defined as follows

$$\alpha = \frac{W_{\text{in}}}{W_{\text{f}}} \tag{3.76}$$

Can be proofed (see Appendix B) that the outlet composition vector $\boldsymbol{f}_{\text{out}}$ has this expression

$$\begin{cases} f_{\text{Ar}}^{\text{out}} = f_{\text{Ar}}^{\text{in}} \dfrac{\alpha}{\alpha+1} \\ f_{\text{CO}_2}^{\text{out}} = f_{\text{CO}_2}^{\text{in}} \dfrac{\alpha}{\alpha+1} + \dfrac{\mathcal{M}_{\text{CO}_2}}{\mathcal{M}_{\text{CH}_4}} \dfrac{f_{\text{CH}_4}^{\text{f}}}{\alpha+1} \\ f_{\text{O}_2}^{\text{out}} = f_{\text{O}_2}^{\text{in}} \dfrac{\alpha-\alpha_s}{\alpha+1} \\ f_{\text{N}_2}^{\text{out}} = f_{\text{N}_2}^{\text{in}} \dfrac{\alpha}{\alpha+1} + \dfrac{f_{\text{N}_2}^{\text{f}}}{\alpha+1} \\ f_{\text{H}_2\text{O}}^{\text{out}} = f_{\text{H}_2\text{O}}^{\text{in}} \dfrac{\alpha}{\alpha+1} + \dfrac{\mathcal{M}_{\text{H}_2\text{O}}}{\mathcal{M}_{\text{CH}_4}} \dfrac{2\, f_{\text{CH}_4}^{\text{f}}}{\alpha+1} \end{cases} \tag{3.77}$$

under the hypothesis of the Section 3.1.1 about the components of the gas mixture for the inlet flow $\boldsymbol{f}_{\text{in}}$ and the fuel $\boldsymbol{f}_{\text{f}}$. In the last set of equalities there is the stoichiometric gas fuel ratio α_{s} that, for the reaction (3.75), is

$$\alpha_{\text{s}} = \frac{2\, f_{\text{CH}_4}^{\text{f}}}{f_{\text{O}_2}^{\text{in}}} \frac{\mathcal{M}_{\text{O}_2}}{\mathcal{M}_{\text{CH}_4}} \tag{3.78}$$

However, although $\boldsymbol{f}_{\text{in}}$ is known, α and the output vector $\boldsymbol{f}_{\text{out}}$ can be determined just solving a system of equations including the previous (3.77), the device energy balance where α is given explicitly

$$\frac{\alpha+1}{\alpha}\, h_{\text{out}} = h_{\text{in}} + \frac{h_{\text{f}}}{\alpha} \tag{3.79}$$

and the output enthalpy

$$h_{\text{out}} = h_{\text{gas}}(T_{\text{out}}, \boldsymbol{f}_{\text{out}}) \tag{3.80}$$

remembering that T_{out} is a cycle input parameter. It is interesting to observe that in the energy balance there is no explicit reference to the fuel calorific value because the *total* specific enthalpies are considered. If, instead, the same

energetic balance would be expressed with the use of the sensible enthalpies h_{s}, it would be

$$W_{\mathrm{out}}\, h_{\mathrm{out,s}} = W_{\mathrm{in}}\, h_{\mathrm{in,s}} + W_{\mathrm{f}} \left(h_{\mathrm{f,s}} + H_{\mathrm{l}}\right) \tag{3.81}$$

where H_{l} is the lower heating value of the fuel derived exactly from the enthalpy of formation of the reactants and supposing that the water vapour generated by the chemical reaction would not condense.

Thanks to the heating value definition (or, equally, to the concept of enthalpy of formation), the heat input $\dot{Q}_{\mathrm{in}}$ is evaluated calculating the enthalpies at standard conditions (see Section 3.1.1)

$$\dot{Q}_{\mathrm{in}} = W_{\mathrm{in}}\, h_{\mathrm{in}}(T_0, \boldsymbol{f}_{\mathrm{in}}) + W_{\mathrm{f}}\, h_{\mathrm{f}}(T_0, \boldsymbol{f}_{\mathrm{f}}) - W_{\mathrm{out}}\, h_{\mathrm{out}}(T_0, \boldsymbol{f}_{\mathrm{out}}) \tag{3.82}$$

Since were obtained $\boldsymbol{f}_{\mathrm{out}}$, h_{out}, α and α_{s} with the solution of the previous system of equations, then it is possible to figure the fuel mass flow

$$W_{\mathrm{f}} = \frac{W_{\mathrm{in}}}{\alpha} \tag{3.83}$$

and the output mass flow

$$W_{\mathrm{out}} = W_{\mathrm{in}} + W_{\mathrm{f}} \tag{3.84}$$

The `bypass` components

This component is used just to skip a certain device in the plant layout. It has just one input and one output station, this means that must be applied two times (for each stream) if a component that involve four stations (like, for instance, an heat exchanger) has to be skipped. Mathematically the bypass element simply equals the output quantities to the input one; it is considered useless to analytically specify each trivial equality.

3.2 Solving strategy

The performance evaluation of the power plant will require the solution of the equations that describe the behaviour of its components, that is a *system* of equations to solve just in a numerical way, since most of them are *non-linear*. In this case the solving strategies are basically two:

1. methods based on the iterative *sequential* substitution of the unknowns;
2. methods based on the *simultaneous* root finding (they are an extension, in the multi-dimensional case, of the Newton-Raphson method).

Each of the two has advantages and disadvantages. The sequential iteration allows to follow the fluid transformations along its path through the plant (useful feature during the debugging), requires less computational resources and a smaller number of starting guess for the root.

On the contrary, the simultaneous root finding allows a modular setting-up of the program simply assembling, in any order, the equations of the system. This makes remarkably easier to edit the model, simply including or erasing equations; on the other hand, however, it requires more computational resources and a guess of the root reasonably good in order to avoid the divergence of the method.

In this work a sequential iterative process has been chosen, so the several possible implementations of this method will be described in the following sections.

3.2.1 Iterative sequential methods

Given a system of non-linear equations described by the arrays of the functions $\boldsymbol{f} = \{f_1, f_2, \ldots, f_n\}$ and the unknowns $\boldsymbol{x} = \{x_1, x_2, \ldots, x_n\}$

$$\begin{cases} f_1(x_1, x_2, \ldots, x_n) = 0 \\ f_2(x_1, x_2, \ldots, x_n) = 0 \\ \vdots \\ f_n(x_1, x_2, \ldots, x_n) = 0 \end{cases}$$

it is always possible to give every equation explicitly for an unknown

$$\begin{cases} x_1 = F_1(x_1, x_2, \ldots, x_n) \\ x_2 = F_2(x_1, x_2, \ldots, x_n) \\ \vdots \\ x_n = F_n(x_1, x_2, \ldots, x_n) \end{cases} \tag{3.85}$$

Then a guess of the root $\boldsymbol{x^{(1)}}$ can be substituted in the system (3.85), yelding to a new approximation of the solution $\boldsymbol{x^{(2)}}$ that will be introduced again in the array $\boldsymbol{F} = \{F_1, F_2, \ldots, F_n\}$ for the next iteration. So, obtained the solution at the k iteration, the solution at the $k+1$ step is:

$$\begin{cases} x_1^{k+1} = F_1(x_1^k, x_2^k, \ldots, x_n^k) \\ x_2^{k+1} = F_2(x_1^k, x_2^k, \ldots, x_n^k) \\ \vdots \\ x_n^{k+1} = F_n(x_1^k, x_2^k, \ldots, x_n^k) \end{cases} \tag{3.86}$$

This way to proceed is called the *Jacobi method* (because of the analogy with the solving algorithm for linear systems of equations that brings the same name).

If it is used the *Gauss-Seidel method*, instead, at the iteration $k+1$ will be:

$$\begin{cases} x_1^{k+1} = F_1(x_1^k, x_2^k, \ldots, x_n^k) \\ x_2^{k+1} = F_2(x_1^{k+1}, x_2^k, \ldots, x_n^k) \\ \qquad\qquad \vdots \\ x_n^{k+1} = F_n(x_1^{k+1}, x_2^{k+1}, \ldots, x_n^k) \end{cases} \tag{3.87}$$

that is, the components of the unknown array already figured during the iteration $k+1$, are immediately used to determine the remaining ones. Can be proofed that both methods converge, if the starting guess $\boldsymbol{x}^{(1)}$ is close enough to the root of the system.

Although in general is necessary to provide an array of guesses, in several cases the modelling of thermodynamic cycles requires to specify just a few components x_i of the entire array $\boldsymbol{x}^{(1)}$. In these cases, in fact, the plant layout is arranged as a "chain" of components where the equations of an element can be solved starting from the solution of the preceding component. In these cases is possible to reduce remarkably the number of the guesses required, at the price of solving the system of equations following the working fluid path along the power plant. This last aspect is definitely a loss of flexibility, but provides also a big advantage for the debugging of the algorithm (especially for very complicated layout like the AZEP one).

Moreover this approach has the other advantage to allow the algorithm designer to choose conveniently the quantities to guess, in order to give a good estimate on the values and, eventually, turning out in an higher probability to drive to convergence the solving process. Of course, choosing this approach requires to apply compulsorily the Gauss-Seidel method.

3.2.2 non-linear one-dimensional root finding

The choice of the iterative sequential method, moves the non-linear root finding problem from the multi-dimensional case to the one-dimensional scenario; this helps remarkably the convergence of the solving process. This advantage is explained by the fact that for a one-dimensional equation

$$f(x) = 0$$

it is possible to "trap" one or more roots between two values x_a and x_b such that

$$f(x_a)\, f(x_b) < 0 \tag{3.88}$$

This approach, known as *bracketing*, prevents the solving strategy from failure. Unfortunately there is no general method to bracket the root for a generic function, but there are two main techniques always valid.

Bracketing strategies

One possibility is to set two starting values x_a, x_b and, first of all, to check if the bracketing condition is satisfied. If not ($f(x_a)\, f(x_b) \geq 0$), the searching interval will be expanded. Will be called x_ζ the generic bound to "move", where ζ will coincide with a or b according to the point where the function will take its smaller absolute value.

The process must be repeated until the condition (3.88) results satisfied. Thus, considering the generic iteration i and detected the x_ζ^i, the interval expansion is obtained starting from x_ζ^i plus the product of a factor $\mathcal{F}$ times the range amplitude $\mathcal{A}$:

$$x_\zeta^{i+1} = x_\zeta^i + \mathcal{F} \cdot \mathcal{A} \tag{3.89}$$

The aforementioned amplitude $\mathcal{A}$ depends on ζ

- if $\zeta = a$, then $\mathcal{A} = x_b - x_a$;
- if $\zeta = b$, then $\mathcal{A} = x_a - x_b$;

while $\mathcal{F}$ is determined as a function of the percentage deviation ξ that the function experience in the last interval extension of the bound x_ζ:

$$\xi = \frac{f(\mu^i) - f(\mu^{i-1})}{f(\mu^i)} \cdot 100 \tag{3.90}$$

where

$$\begin{aligned} \mu &= x_a \quad \text{if} \quad \zeta = a \\ \mu &= x_b \quad \text{if} \quad \zeta = b \end{aligned}$$

Finally, must be applied the following case analysis:

- if $\xi \in \Big[0\%, 50\%\Big]$, then $\mathcal{F} = 3$;
- if $\xi \in \Big]50\%, 150\%\Big]$, then $\mathcal{F} = 1.6$;
- if $\xi > 150\%$, then $\mathcal{F} = 0.5$.

Since the ξ definition includes informations obtained in the previous iteration (μ^{i-1}), for the first application of the algorithm with each bound it is set $\mathcal{F} = 1.6$.

The procedure must be repeated, considering the new bounds, until the condition (3.88) is satisfied (so the bracketing strategy is successful) or if the maximum number of iterations allowed is exceeded (in the case of this work, fifty).

Alternatively, it is possible to search for roots *inside* the interval with bounds x_a and x_b. The starting range is divided in an increasing number of equal parts, checking for each of them if the condition (3.88) results true. Following this approach, it is possible to find more than one root in the starting interval; if so, the program lists every range containing a root and prompts the user to choose one. Also this iterative process keeps running until one or more roots are found or the starting interval is divided in the maximum number of subintervals described (in this case fifty).

The computational program combines both the described bracketing strategies, using the other when the first fails (see Section 3.3.2).

The Brent method

When an interval that contains a root is detected, there are several methods to find the solution[7]. These strategies differ for the speed and the robustness to reach the solution.

Generally, the non-linear root finding methods that ensure convergence proceed slowly (for example, the bisection method), while the strategies that quickly pounce on the solution could equally diverge suddenly (it is the case of the Newton-Raphson algorithm), if special countermeasures are not implemented to avoid their failure.

The solving strategy chosen in this work, ascribed to Richard Brent, has become very popular since it conjugates a higher convergence speed than the simple bisection method (called *super-linear convergence*), with the certainty to obtain the desired solution. Brent, in the first half of the Seventies, improved a method conceived by Theodorus Dekker in the previous decade.

The Dekker method This algorithm requires, of course, the root bracketing between two bounds a_0, b_0 and, for each iteration i, three points are considered:

b_i : the guess of the root for the function f in the current iteration (that is, the the bound where the function takes the smaller absolute value);

[7]For an overview of the main methods that will be referenced also later, please see the Chapter 9 of the Volume 1 in [4].

a_i : the other bound of the interval containing the root;

b_{i-1} : b_i of the previous iteration.

The method proceeds considering two candidates to replace one of the bounds in the next iteration:

- $s = b_i - \dfrac{b_i - b_{i-1}}{f(b_i) - f(b_{i-1})} f(b_i)\,,$ according to the secant method;
- $m = \dfrac{a_i + b_i}{2}\,,$ according to the bisection method.

If the s value is between b_i and m, it becomes the new b_i ($b_{i+1} = s$), otherwise the midpoint m is chosen ($b_{i+1} = m$).

Then must be choose the value of a_{i+1} for the next iteration. If $f(a_i)$ and $f(b_{i+1})$ take opposite sign, the same point is confirmed $a_{i+1} = a_i$, otherwise $f(b_{i+1})$ and $f(b_i)$ will have opposite sign, so it is set $a_{i+1} = b_i$. Finally must be decided in which point (between a_{i+1} e b_{i+1}) the function takes the value closer to the x-axis: if $|f(a_{i+1})| < |f(b_{i+1})|$, the values of a_{i+1} and b_{i+1} will be swapped.

The Dekker method owns some very good properties.

- It is a robust algorithm: since it exploits the root bracketing, the new point determined for the next iteration can not go out of the interval where the solution is included; moreover it shrinks the interval range more and more.
- It avoids that the simple application of the secant method moves the next calculation point far from the bound with lower absolute value on the y-axis. In this way it avoids that the convergence process moves away from the zone where the function is going to reach zero. If this danger is detected, the algorithm takes a bisection step.
- It benefits from the quick convergence rate of the secant method when it is proceeding in the "right" direction.

The example in Figure 3.10 shows a case when a "traditional" method (as, for instance, the secant or the false position) would require a lot more iterations to find the root than the Dekker method that, instead, would use some bisection steps to speed up the process. Please note that in the case of the secant algorithm application, the process would even diverge.

These cases are usually related to discontinuities or to functions that shows important non-linearities in the proximity of the root. In fact, both the

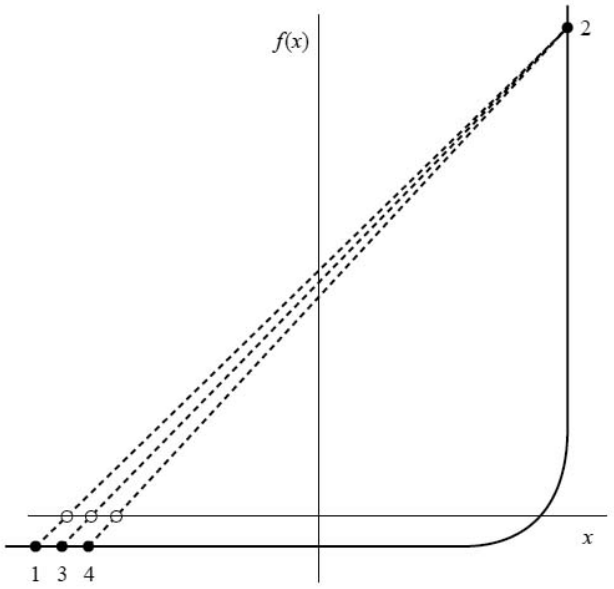

Figure 3.10. Example where the Dekker method is much more efficient than the secant or the false position to find the root [4].

secant and the false position methods perform a linear interpolation between two points of the function (different in each method). When the hypothesis of the linear behaviour is not satisfied, the algorithm lose efficiency.

Thus the Dekker method is very valuable, however there are some cases in which even a so sophisticated strategy could result not very efficient. An example (taken from http://en.wikipedia.org/wiki/Brent_method) is given by the function $f(x) = (x+3)(x-1)^2$, if it is desired to find the root $x = -3$ starting from a bracketing interval wider than $[-3, 1]$ (Figure 3.11).

Brent's modifications Brent noticed that functions with sharp fluctuations of the second derivative in the proximity of the root (like in Figure 3.11) can trick the Dekker algorythm, moving the point b_i of an arbitrary quantity and, then, converging slowly. In order to avoid this problem, he thought to add a test about the speed of the converging process for the linear interpolation steps. If this convergence is not quick enough, a bisection step is taken.

Before to describe in more detail this aspect, must be outlined that Brent improved further also Dekker's interpolation method. He substituted the *linear* interpolation (that requires two points to determine the line that approximates the function) with a *quadratic* interpolation (that requires three points to determine a parabola able to describe with a smaller error even sharp slope variations). This improvement enhance slightly the efficiency of

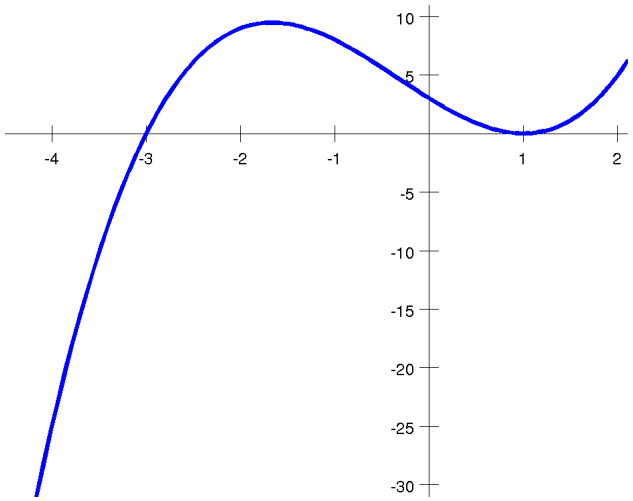

Figure 3.11. Example in which the Dekker method requires more iterations than Brent's one (source: http://en.wikipedia.org/wiki/Brent_method).

the algorithm.

Considered three points a, b, and c, with the corresponding values taken by the function $f(a)$, $f(b)$, and $f(c)$, they can be interpolated by a parabola, that is a quadratic function of x. The next point of the root finding algorithm will be the value of x where the parabola intersects the x-axis. Unfortunately the curve may not cross at all the axis: in fact, a quadratic function not necessarily has real roots[8].

Thus, to obtain a function that intersects always the x-axis, it is necessary to interpolate the aforementioned three points with a parabola in y, namely perform an *inverse quadratic interpolation*. In this way it is obtained a curve $P(y)$ that is the quadratic interpolation of $f^{-1}(x)$ and provides the next point for the iterative process in $y = 0$ ($x = P(0)$).

According to this point of view, the point s obtained by the inverse quadratic interpolation, is determined with the following

$$s = b + \frac{P}{Q} \tag{3.91}$$

where, substituting the terms

$$R = \frac{f(b)}{f(c)}, \quad S = \frac{f(b)}{f(a)}, \quad T = \frac{f(a)}{f(c)}, \tag{3.92}$$

[8]In other cases, this could be considered as an advantage since an algorithm, known as Müller's method, uses exactly the complex roots of a quadratic function to approximate the complex zeros of a given $f(x)$ [4, 23].

results

$$\begin{aligned} P &= S\left[T\left(R-T\right)\left(c-b\right)-\left(1-R\right)\left(b-a\right)\right], \\ Q &= \left(T-1\right)\left(R-1\right)\left(S-1\right). \end{aligned} \tag{3.93}$$

Must be clarified that b is the counterpart of b_i for the Dekker algorythm, c corresponds to a_i and a stands for the aforementioned b_{i-1}.

Basically b is the guess of the root and P/Q is a correction. The quadratic interpolation is very effective just when the function behaves regularly, while it gives a completely wrong estimate of the root when Q is close to zero. The Brent method guards against this danger checking where the interpolation would bring the working point before to accept it. Then the condition set by Dekker is substituted by other two:

1. the correction P/Q must provide a result between b and c (the bounds that contain the root);

2. the convergence rate of the method must be quick enough; quantitatively:

$$2\,P < \min\Big(3\,m\,Q - \left|\mathcal{T}\cdot Q\right|, \left|\left(b-a\right)Q\right|\Big) \tag{3.94}$$

with

$$\mathcal{T} = 2\,\mathcal{E}_{\mathrm{m}}\left|b\right| + \frac{\mathcal{E}_{\max}}{2} \tag{3.95}$$

where $\mathcal{E}_{\mathrm{m}}$ is the machine precision[9] and $\mathcal{E}_{\max}$ is the maximum error allowed for the solution.

If both the conditions are not satisfied, a bisection step is taken. Please note that for the first iteration (when just two points are available instead of the usual three) and when $a = c$, is not possible to determine the parabola of the inverse quadratic interpolation, so the secant method is used. Finally, the root finding process is however stopped if the solution is not reached in the maximum number of iterations allowed (in this case one hundred).

For what concerns the efficiency of the method, must be observed that the main "quality leap" offered by the Brent version compared to the Dekker one, is the second additional condition to satisfy, while it is less sensitive the positive contribution of the inverse quadratic interpolation instead of the linear one.

[9]This quantity is easily implemented in a portable fashion (once for every machine), thanks to the intrinsic function `EPSILON` included in the Fortran 90 standard.

Comparison with other root finding methods Although the Brent method is the most popular root finding algorithm, there are other valuable alternatives that could be considered. In this excerpt it will be briefly compared to two good competitors: the Newton-Raphson and the Ridders method.

The Newton-Raphson algorithm is maybe the most famous root finding strategy for non-linear equations, but requires the knowledge of the function first derivative in the point of application. If the derivative is known, the Newton-Raphson method performs the best convergence rate possible: the exact number of decimal digits doubles at every iteration; this behaviour is called *quadratic convergence*.

Its picking is not prevented by the global convergence difficulties that characterise it, in fact they are overtaken simply including the algorithm in a bracketing strategy. The problem for the adoption of the Newton-Raphson strategy is the knowledge of the first derivative of the function that is being solved. In some cases it is analytically complicated or computationally very expensive to obtain the derivative, so may seem a smart walkaround to approximate it with the finite difference quotient of the function between the point considered and another one very close to it

$$f'(x) \approx \frac{f(x + \mathrm{d}x) - f(x)}{\mathrm{d}x}$$

This way to proceed is not advisable at least for two reasons [4].

1. For each iteration two function evaluations are performed then, *at best*, the rate of convergence would be $\sqrt{2}$. This value is lower than the convergence rate of the secant method that, can be proofed, is equal to the golden ratio [4].

2. The choice of $\mathrm{d}x$ is critical: if it is too small, it will be cancelled by the round-off error, instead if it is too big the convergence rate results simply linear, equal to the one obtained without updating the starting value of $f'(x)$.

   About this last observation must be noticed that, for several functions, the first derivative converges to the machine precision before the $f(x)$, so it is completely useless to update its value in the following iterations. In this cases the convergence rate is just linear and then the advantage of the Newton-Raphson method compared to the other ones results reduced [4].

Then, if the goal is to implement a root finding algorithm working with a wide variety of equations (like in the case of this work), the Newton-Raphson

method must be excluded, unless one wants to provide for every function to resolve the analytic expression of the first derivative. On the other hand, for specific cases, could be affordable to use the Newton-Raphson method. In this work the routine that extracts the n-th root of a floating point number (Section 3.3.5), applies implicitly the Newton-Raphson strategy with the analytic derivative.

Another valuable competitor of the Brent method is the Ridders one (more details in [4]). The big advantage of the latter is the simple implementation: the entire algorithm is based on a single formula able to provide the next guess of the root. The output of the Ridders formula has excellent properties: it is surely included in the bracketing interval, the convergence rate is super-linear and can generally deal with functions with sharp slope variations.

Unfortunately there are cases when the Brent method is more robust and/or efficient than the Ridders one, but the payback (as previously shown) is a remarkable increase of complexity.

Convergence criterion The iterative process must be stopped when the guess is close enough to the root. When setting a convergence criterion must be kept in mind that floating point numbers are represented in computers by a fixed number of binary digits. This means that although a function can analytically intersects the x-axis, the value figured by a computer would never reach exactly zero, whatever floating point value of x would be considered. So it is important to decide which is the acceptable accuracy of the solution: if, for instance, a convergence below the absolute value of 10^{-6} is sensible for a root in the proximity of 1, it is surely impossible to be satisfied if the root is close to 10^{26} [4].

Thus would be considerate to set case by case the accuracy required for the solution; it could be chosen according to the physical process modeled by the function to solve. As easily deducible, this way to proceed is not practical if the aim is to put the solver in a black box. So one way out is to consider a convergence criterion based on an non-dimensional, relative error. This procedure works very well almost in every circumstance but when the root is close to the value zero. Since for several physical and thermodynamic quantities is improbable (and sometimes impossible) to reach zero, in engineering applications the convergence criterion is usually based on an non-dimensional error.

For this work, this choice has been pursued to test the convergence of the system of equations, while was not applicable to the Brent method since, in that case, the convergence was tested satisfying the condition

$$|m_i| \leq \mathcal{T} \tag{3.96}$$

where the term $\mathcal{T}$ is defined, Equation (3.95), from an accuracy based on absolute terms $\mathcal{E}_{\max}$. So, considering that all the variables in eAZEP have fifteen significant figures, $\mathcal{E}_{\max}$ was set to 10^{-9}.

3.2.3 eAZEP solving sequence

In this section will be described in details how eAZEP proceeds during the execution of the calculation routine. Before the actual start of the solving procedure, there is an initialization where the input file parameters are read and assigned to the corresponding cycle component or variable, the composition of pure oxygen is assigned to the station 24 and are set the flags handling the plant layout of the cycle and the output file printing.

Then the pressure ratio of the flue gas recirculation compressor is initially set starting from the pneumatic efficiencies η_π on the flue gas recirculation path

$$\pi_{\text{flue}} = \frac{1}{\eta_{\pi,\text{cc}} \cdot \eta_{\pi,17} \cdot \eta^{\text{h}}_{\pi,\text{HTHX}} \cdot \eta^{\text{P}}_{\pi,\text{mcm}} \cdot \eta^{\text{h}}_{\pi,\text{LTHX}}} \tag{3.97}$$

where

$\eta_{\pi,17}$ is the pneumatic efficiency for the splitting of the stream at station 17;

$\eta^{\text{h}}_{\pi,\text{HTHX}}$ is the pneumatic efficiency on the hot side through the HTHX;

$\eta^{\text{P}}_{\pi,\text{MCM}}$ is the pneumatic efficiency of the Mixed Conductive Membrane on the permeate side;

$\eta^{\text{h}}_{\pi,\text{LTHX}}$ is the pneumatic efficiency on the hot side through the LTHX.

The only pressure loss not considered yet is the one derived by the mixing of the oxygen with the permeate flow, Equation (3.69); it will be determined later since it depends also on the mass flow W_{12} which is it still unknown.

The fuel station is completely assigned except for the mass flow which will be determined in the combustor solving subroutine. Then the program checks a set of conditions.

- If the final CO_2 storage pressure is higher than its critical one, if not the carbon dioxide would not be stored as a liquid.
- If the flag of the PEHX layout is on and if so sets a bypass for the BHX.
- If the flue gas turbine flag is on and the pressure on the permeate side is set as lower than 10 atm prompts an error stopping the execution of the program.

The next step of eAZEP is the assignment of the ambient conditions (specified in the input file) to the station 1; the mass flow W_1 is set as the engine inlet mass flow (specified in the input file). By the ambient conditions is also figured the theoretical quantity of the oxygen removable from the air $W_{O_2}^{th}$

$$W_{O_2}^{th} = W_1 \, f_{O_2}^{(1)} \tag{3.98}$$

and then the actual mass flow of oxygen transferred, obtained from an input factor ω

$$W_{24} = \omega \, W_{O_2}^{th} \tag{3.99}$$

Then are assigned the remaining quantities depending on the other input parameters

- p_{11} as the specified permeate side pressure;
- T_{16} as the specified Combustor Outlet Temperature;
- W_{11} as the specified fraction of the engine inlet mass flow.

The main compressor and the bleed splitter routines are then called, delivering the values for station 2 and the compressor work[10] P_c the former, the stations 3 and 20 the latter. The air turbine exit pressure p_9 is assigned with different expressions according to the layout considered.

- Bleed Heat exchanger layouts

$$p_9 = \frac{p_{amb}}{\eta_{\pi,HRSG}} \tag{3.100}$$

- Post Expansion Heat exchanger layouts

$$p_9 = \frac{p_{amb}}{\eta_{\pi,HRSG} \, \eta_{\pi,PEHX}^{c}} \tag{3.101}$$

where p_{amb} is the ambient pressure, $\eta_{\pi,HRSG}$ is the pneumatic efficiency of the HRSG and $\eta_{\pi,PEHX}^{c}$ is the pneumatic efficiency of the PEHX on the cold side[11].

There are three imbricated loops in the eAZEP solving sequence:

[10] Following a widespread ambiguous tradition, also in this work sometimes will be used the term "work" when referred to the mechanical power (measure in watts) which characterise a turbomachinery.

[11] Actually the PEHX cold and hot side are not precisely defined (especially when is present the flue gas turbine) because in some conditions could happen that the air stream is hotter than the flue gas one. Although this situation is quite infrequent, must be remembered this clarification that does not affect anything in the calculation process.

- the *outer* loop is based on T_{11};
- the *intermediate* loop on $\boldsymbol{f}_{11}$ (actually five parallel *scalar* loops);
- the *inner* loop on T_4.

The three corresponding quantities are initially guessed. From their values, eAZEP figures some derived quantities used just in the first iteration; they are

- the remaining quantities of station 4

$$W_4 = W_3 \tag{3.102}$$
$$p_4 = \eta^{\mathrm{c}}_{\pi,\mathrm{LTHX}}\, p_3 \tag{3.103}$$
$$\boldsymbol{f}_4 = \boldsymbol{f}_3 \tag{3.104}$$
$$h_4 = h_{\mathrm{gas}}(T_4, \boldsymbol{f}_4) \tag{3.105}$$

- the specific enthalpy at station 11

$$h_{11} = h_{\mathrm{gas}}(T_{11}, \boldsymbol{f}_{11}) \tag{3.106}$$

- the mass flow, the pressure and the composition at station 5

$$W_5 = W_4 - W_{24} \tag{3.107}$$
$$p_5 = p_4 \tag{3.108}$$
$$\boldsymbol{f}_5 = \frac{\boldsymbol{f}_4\, W_4 + \boldsymbol{f}_{24}\, W_{24}}{W_5} \tag{3.109}$$

Should be observed that the last formula is the application of Equation (3.19).

Then the average oxygen partial pressure on the feed side of the Mixed Conductive Membrane $\hat{p}^{\mathrm{F}}_{\mathrm{O}_2}$ is figured applying the second formula in (3.55). Now starts the iterative process: the outer loop starts and immediately after (without any additional calculation), starts the intermediate loop. Because it is based on the vector composition $\boldsymbol{f}_{11}$ it is possible to figure the average oxygen partial pressure on the permeate side of the MCM $\hat{p}^{\mathrm{P}}_{\mathrm{O}_2}$ applying the third formula in (3.55). Then eAZEP checks that $\hat{p}^{\mathrm{P}}_{\mathrm{O}_2} \leq \hat{p}^{\mathrm{F}}_{\mathrm{O}_2}$ and if not prompts and error and stops the execution of the program.

Now starts the inner loop (based on T_4): the station 5 is completely figured, the temperature and the specific enthalpy were missing

$$T_5 = T_4 \tag{3.110}$$
$$h_5 = h_{\mathrm{gas}}(T_5, \boldsymbol{f}_5) \tag{3.111}$$

In this way the routine that treats the Mixed Conductive Membrane as an heat exchanger is called returning the stations 6 and 12 and its characteristic parameters: the overall area, the Number of Thermal Units and the heat transfer efficiency. Then the temperature and the specific enthalpy of the station 24 are figured, the first from the first formula in (3.55) and the second with the usual expression

$$h_{24} = h_{\text{gas}}(T_{24}, \boldsymbol{f}_{24}) \tag{3.112}$$

in this way is now possible to obtain the conditions at station 13 with the adiabatic mixing of the oxygen (station 24) with the flue gas stream (station 12). The inner loop is closed calling the LTHX routine that returns characteristic parameters of the heat exchanger (area, Number of Thermal Units and heat transfer efficiency) and the output stations: the number 14 and 4. So the new value of T_4 is used to restart the loop until it converges.

Once the inner loop is closed is possible to now the actual value of the pressure ratio for the flue gas recirculation compressor partially set by Equation (3.97). Now is possible to add also the pressure loss due to the adiabatic mixing of the oxygen which was previously figured. Then is possible to call the routine describing the thermodynamic transformations of the recirculation compressor obtaining the conditions in the outlet station 15 and the work absorbed by it $P^{\text{c}}_{\text{flue}}$.

Solving the combustion chamber routine is possible to close the intermediate loop based on the composition of the flue gas $\boldsymbol{f}_{11}$ equal to $\boldsymbol{f}_{16}$. In fact the solving routine of the combustion chamber gives

- the conditions at station 16;
- the gas fuel ratio α and, in turn, the fuel mass flow W_{f};
- the stoichiometric gas fuel ratio α_{s};
- the input heat rate $\dot{Q}_{\text{in}}$

Before to iterate again with the new value of $\boldsymbol{f}_{11}$, the specific enthalpy at station 11 is updated

$$h_{11} = h_{\text{gas}}(T_{11}, \boldsymbol{f}_{11}) \tag{3.113}$$

Then eAZEP is able to figure the mass flow to spill from the flue gas recirculation "ring" W_{18} in order to keep constant W_{11} at its design value

$$W_{18} = W_{24} + W_{\text{f}} \tag{3.114}$$

According to this information the splitter routine is called returning the conditions at station 18 and 17. Then even the last loop is closed calling the

heat exchanger routine referred to the HTHX. The result of this last action is the calculation of the heat exchange area, the Number of Thermal Units and the heat exchange efficiency of the HTHX with the values of the quantities of station 11 and station 7.

When even the T_{11} converges starts the procedure to follow the correct path for the different AZEP layouts. If the PEHX flag is on, eAZEP skips the BHX on both the streams (air and flue gas), otherwise it calls of course the BHX routine. In both cases the stations 19 and 21 are completely known and, just in the second case, are figured the design point parameters of the Bleed Heat exchanger. Then the mixer and the air turbine routine are called one after the other resolving the stations 8 and 9, respectively, and providing the power output of the turbine P_{t}.

When the flue gas turbine flag is on, the program, at this point, figures the outlet pressure of the turbine differently if the PEHX is present or not

$$p_{22} = \frac{p_{\mathrm{amb}}}{\eta_{\pi,\mathrm{HRSG}}} \tag{3.115}$$

$$p_{22} = \frac{p_{\mathrm{amb}}}{\eta_{\pi,\mathrm{HRSG}}\,\eta^{\mathrm{h}}_{\pi,\mathrm{PEHX}}} \tag{3.116}$$

where the first equation refers to the BHX layout and the second to the PEHX one[12]. Then the flue gas turbine routine is called returning the conditions at station 22 and the power output $P^{\mathrm{t}}_{\mathrm{flue}}$ of the expander. Now is possible to figure the *provisional* power output P_o of the plant (not including the compression and pumping energetic expense yet) which reads in this case

$$P_{\mathrm{o}} = P_{\mathrm{t}} + P^{\mathrm{t}}_{\mathrm{flue}} - P_{\mathrm{c}} - P^{\mathrm{c}}_{\mathrm{flue}} \tag{3.117}$$

If the flue gas turbine flag is off, the corresponding component is skipped setting the station 22 equal to the station 19 and figuring the *provisional* power output

$$P_{\mathrm{o}} = P_{\mathrm{t}} - P_{\mathrm{c}} - P^{\mathrm{c}}_{\mathrm{flue}} \tag{3.118}$$

Then is the presence of the PEHX that must be checked. If eAZEP detects it, runs the corresponding routine which returns the values for stations 10 and 23 and the design usual parameters of the heat exchanger. If not, the component is bypassed with both the streams.

Here starts the CO_2 compression processes for the storage. The station 25 describes the flue gas at the end of the condensation at the cooler design

[12] Again, in the pneumatic efficiency of the PEHX is considered the hot stream the flue gas one, as in the majority of the cases happens. Anyway can seldom happen that is not so, in that case the soundness of the calculation is not affected but it is just a nomenclature issue.

point temperature T_{cooler} (the process is supposed to be capable to eliminate all the steam in the flue gas)

$$W_{25} = W_{23} - W_{23}\, f_{\text{H}_2\text{O}}^{(23)} \tag{3.119}$$

$$p_{25} = p_{23}\, \eta_{\pi,\text{cooler}} \tag{3.120}$$

$$T_{25} = T_{\text{cooler}} \tag{3.121}$$

$$\boldsymbol{f}_{25} = \frac{W_{23}\, \boldsymbol{f}_{23} - W_{23}\, f_{\text{H}_2\text{O}}^{(23)}}{W_{25}} \tag{3.122}$$

$$h_{25} = h_{\text{gas}}(T_{25}, \boldsymbol{f}_{25}) \tag{3.123}$$

Then the pressure ratio for each of the four inter-cooled stages of compression π_{ic}^{i} is figured distributing equally the overall pressure ratio

$$\pi_{\text{ic}}^{i} = \sqrt[4]{\frac{p_{\text{CO}_2}^{\text{cr}}}{p_{25}}} \tag{3.124}$$

where $p_{\text{CO}_2}^{\text{cr}}$ is the critical pressure of the carbon dioxide. Each of the π_{ic}^{i} is raised to take into account the pneumatic efficiency of the inter-coolers $\eta_{\pi,\text{cooler}}^{i}$. In this way eAZEP calls four times, alternatively, the compressor stage routine and the cooler one (where the gas achieve again the cooling design point temperature) describing the compression process till the critical temperature. With the last cooling process (at the critical pressure), the carbon dioxide becomes liquid and the small fractions of oxygen and nitrogen still present in the flue gas are expelled. Thus since station 32 is the outlet of the fourth (and last) compressor stage, at the end of the last cooling process (station 33) the quantities are figured as follows

$$W_{33} = W_{32} - (W_{32}\, f_{\text{O}_2}^{(32)} + W_{32}\, f_{\text{N}_2}^{(32)}) \tag{3.125}$$

$$p_{33} = p_{32}\, \eta_{\pi,\text{cooler}} \tag{3.126}$$

$$T_{33} = T_{\text{cooler}} \tag{3.127}$$

$$\boldsymbol{f}_{33} = \frac{W_{32}\, \boldsymbol{f}_{32} - (W_{32}\, f_{\text{O}_2}^{(32)} + W_{32}\, f_{\text{N}_2}^{(32)})}{W_{25}} \tag{3.128}$$

$$h_{33} = h_{\text{gas}}(T_{33}, \boldsymbol{f}_{33}) \tag{3.129}$$

The final pumping process to the storage pressure (specified as an input parameter), is simulated calling the corresponding routine which gives the final conditions at station 34 and the power required to carry out the pumping.

In this way the overall power output can be finally assessed taking into account also the power required for the compression stages and the final

pumping. Then the overall thermal efficiency of the power plant η_o is given as

$$\eta_o = \frac{P_o}{\dot{Q}_{in}} \tag{3.130}$$

3.3 Code analysis

The eAZEP code is written according to the standard Fortran 95 (with just a few enhancements derived from the 2003 one) and comprises five modules

1. the `therm_air` module;
2. the `nonlin_eq` module;
3. the `cycle_param` module;
4. the `components` module;
5. the `cycle` module.

Each of them is stored in a different file and often contains several module procedures. The main routine of the program clears the sceen, sets a few variables that handles the output of eAZEP, and then calls just two routines of the module `cycle`: `initialize` and `DP_main`; they will be described later in detail. In particular `DP_main` manages the entire calculation process.

3.3.1 The `therm_air` module

This module contains

- a library of thermodynamic routines;
- the thermodynamic quantities used throughout the program (the molecular weights of the gases, the enthalpies of formation, the universal gas constant, the polynomial coefficients for the perfect gas model);
- the definition of the derived data type `air` and `fuel` that describe the gas stations and the fuel station;
- the parameter that sets the desired precision for the floating point variables in the program (by the intrinsic function `SELECTED_REAL_KIND`).

The derived data type `air` and `fuel` comprise five variables (Page 14).

1. `T`: the absolute temperature;

2. `p`: the pressure;
3. `W`: the mass flow;
4. `h`: the specific enthalpy;
5. `f`: the composition *vector*, it is the only variable that distinguish the `air` to the `fuel` since they can have a different number of elements (components).

There are eleven module procedures in `therm_air`.

1. `molar_frac_air` (function): it simply returns the `i`-th component molar fraction, provided the *vectorial mass* composition `f` of a gas comprising the same compounds (or part of them) present in the air.
2. `p_part` (function): it returns the partial pressure of the `i`-th component for a gas mixture of composition `f` at the bulk pressure `ptot`. The evaluation is based on the assumption that the Dalton law is valid for the mixture, Equation (3.12). It is the implementation of Equation (3.13) with the use of the function `molar_frac_air`.
3. `R_calc` (function): provides the average ideal gas constant starting from the composition *vector* `f`, Equation (3.9).
4. `cp_air` (function): it performs the evaluation of the specific heat at constant pressure c_p for a mixture of perfect gas according to the model presented in the Section 3.1.1. The input variables are the temperature of the mixture `T` and the composition *vector* `f`.
5. `heat_capacity_rate` (function): starting from the mass flow `W`, the temperature `T`, and the composition *vector* `f`, it performs the heat capacity rate evaluation $\dot{C}$ calling the function `cp_air`. See Equation (3.39).
6. `hair` (function): figures the specific enthalpy of a generic mixure of gas (see Section 3.1.1) provided the temperature `T` and the composition *vector* `f`. It contains a flag `total` (a logical variable) that allows the user to switch the output from the sensible enthalpy to the total one (see Page 21).
7. `sair` (function): it provides the specific entropy of a generic mixture of gas starting from the temperature `T` and the composition *vector* `f`, exploiting the same theory of Section 3.1.1, from where its expression is derived.

8. `hfuel` (function): it is very similar to `hair`, but with the difference that the composition vector `ff`, relative to the fuel, not necessarily would have the same number of components as gaseous compounds.

9. `sfuel` (function): it is the counterpart of `sair` for the fuel, that can have a different number of gaseous components.

10. `fgas` (subroutine): it determines the chemical composition after the combustion with natural gas (see Section 3.1.2). The input variables are the inlet composition vectors of the gas `fa` and the fuel `ff`, and the gas fuel ratio `alfa`. It returns the flue gas composition at the outlet of the combustor `fg` and the stoichiometric gas fuel ratio `alfas`.

11. `mix_split_gas` (function): returns the output composition after the mixing or the extraction of a mass flow `W_mix_split` of composition `f_mix_split`, from the inlet mass flow `W_in` of composition `f_in`. It is the implementation of the Equation (3.19).

3.3.2 The `nonlin_eq` module

This module contains the eAZEP numerical solver that implements the algorithms showed in Section 3.2.2. It contains four main module procedures and two internal subroutine arranged in the following way:

- `solve`;
- `search_root`:
  - `find_factor`;
- `multiple_roots`:
  - `isolate_roots`;
- `brent`;

where the routine `solve` manages the two bracketing strategies (the subroutines `search_root` and `multiple_roots`) together with the root finding function `brent`. The `search_root` procedure implements the bracketing strategy of the interval expansion, while `multiple_roots` implements the one that scans the internal part of the interval.

The function `solve` requires seven input arguments (six mandatory and one optional).

`f:` is the function expressed in the canonical form and dependent from *just one* variable, $f(x) = 0$;

`x1 and x2:` are the bounds setting the interval where the root (or more than one) must lie to be acceptable;

`unk:` is a string containing the symbol of the unknown quantity;

`um:` again a string containing the unit of measure of the unknown quantity;

`show:` it is a logical variable that allows to print on the screen the intermediate results while the program is root finding (could be useful to activate it during the debugging);

`xhp:` it is the optional argument that, if present, is the starting point for the root finding.

The function `solve`, first of all, checks if `xhp` is present. If so, it calls `search_root` and, if any bracketing interval is found, then it calls `multiple_roots`. The subroutine `search_root`, in this case, starts testing the bracketing condition from the neighbourhood of `xhp` and expands the searching interval or until the achievement of the maximum number of iterations allowed, or when the interval bounds coincides with the limits `x1` and `x2`.

The `multiple_roots` procedure, as said, looks inside the interval between `x1` and `x2` checking the bracketing condition. If even this attempt fails (maximum number of subintervals exceeded), the solver makes two last attempts: tests if the condition (3.88) for the two bounds `x1` and `x2` is satisfied and calls `search_root` starting from `x1` and `x2` midpoint instead from `xhp`.

If `xhp` is not present, the first step is the testing of the bracketing condition between `x1` and `x2`. If not so, `multiple_roots` is called; if it fails, the last attempt is to call `search_root` starting from the midpoint of `x1` and `x2`.

Of course, if a bracketing interval is detected, the subroutines `search_root` or `multiple_roots`, call the function `brent` sending to it the bracketing interval in order to find the root. As said in Section 3.2.2, if `multiple_roots` finds more than one interval, the user is prompted to select one.

If after all these attempts, no root is found, the solver prints on the screen a message where it specifies which quantity generated the error and stops the execution of the program.

3.3.3 The `cycle_param` module

This module contains all the parameters that influence the power plant behaviour:

- all the input file variables;
- the stations array;
- the flags that allow to change the layout of the power plant and manage the output of the calculation results;
- a few output quantities not included in the components derived data types.

Although very simple, the `cycle_param` module is very important to share informations between the `components` and `cycle` modules, exploiting the Fortran 90 "use association" feature.

3.3.4 The `components` module

This module defines

- the derived data types for every component in eAZEP;
- a pointer for each derived data type;
- a library of procedures that describe their behaviour;

The derived data types are seven.

1. `compressor` (pointer `compr`): indicates a compressor turbomachinery. It comprises seven variables.
   (a) `sn_in` (input): the inlet station number;
   (b) `sn_out` (output): the outlet station number;
   (c) `R` (output): the average gas constant for the working fluid;
   (d) `pr` (input): the pressure ratio;
   (e) `eta_y` (input): the polytropic efficiency;
   (f) `eta_m` (input): the mechanical efficiency;
   (g) `power` (output): the power absorbed.
2. `turbine` (pointer `turb`): it is a turbomachinery expander where the final pressure is supposed to be known and stored in the outlet station variable. It is made up by seven variables too.
   (a) `sn_in` (input): the inlet station number;
   (b) `sn_out` (output): the outlet station number;

(c) `R` (output): the average gas constant for the working fluid;

(d) `eta_y` (input): the polytropic efficiency;

(e) `eta_m` (input): the mechanical efficiency;

(f) `eta_el` (input): the electric generator efficiency, if present;

(g) `power` (output): the power output.

3. `heat_exchanger` (pointer `hx`): describes an heat exchanger with 12 variables.

   (a) `name` (input): the name of the heat exchanger;

   (b) `sn_C_in` (input): the inlet cold stream station number;

   (c) `sn_C_out` (output): the outlet cold stream station number;

   (d) `sn_H_in` (input): the inlet heat stream station number;

   (e) `sn_H_out` (output): the outlet heat stream station number;

   (f) `eta_pi_c` (input): the pneumatic efficiency for the cold side;

   (g) `eta_pi_h` (input): the pneumatic efficiency for the hot side;

   (h) `U` (output): the overall heat transfer coefficient;

   (i) `A` (output): the heat transfer area;

   (j) `NTU` (input): the number of thermal units for the device.

   (k) `eps` (output): the efficiency of the heat transfer;

   (l) `show` (input): a flag to handle the printing on the screen of additional informations.

4. `splitter` (pointer `split`): indicates a splitter like it was presented in Section 3.1.2. It comprises six variables.

   (a) `sn_in` (input): the inlet station number;

   (b) `sn_out1` (output): the first outlet station number;

   (c) `sn_out2` (output): the second outlet station number;

   (d) `eta_pi1` (input): the pneumatic efficiency for the first stream;

   (e) `eta_pi1` (input): the pneumatic efficiency for the second stream;

   (f) `W_split1` (input): the outlet mass flow for the first stream.

5. `mixer` (pointer `mix`): a component that adiabatically mix two streams. It is described by four elements:

(a) `sn_in1` (input): the first inlet station number;

(b) `sn_in2` (input): the second inlet station number;

(c) `sn_out` (output): the outlet station number;

(d) `show` (input): a flag to handle the printing on the screen of additional informations.

6. `combustor` (pointer `cc`): it has seven variables:

   (a) `sn_in` (input): the inlet station number;

   (b) `sn_fuel` (input): the fuel station number;

   (c) `sn_out` (output): the outlet station number;

   (d) `eta_pi` (input): the pneumatic efficiency;

   (e) `Q_in` (output): the heat input;

   (f) `gas_fuel_ratio` (output): the gas fuel ratio of the combustion process;

   (g) `gfr_stoich` (output): the stoichiometric gas fuel ratio.

7. `bypass` (pointer `skip`): simply comprises two variables:

   (a) `sn_in` (input): the inlet station number;

   (b) `sn_out` (output): the outlet station number;

The pointers are necessary in order to call dynamically (via the targets defined in the module `cycle`) the same component routines for all the devices of the power plant of the same kind. For example the same subroutine `DP_compressor` is called for the main compressor of the cycle, for the flue gas recirculation compressor and for every compression stage of the carbon dioxide before the storage. This will be achieved pointing `compr` to the target corresponding to each of these devices.

The twelve routines that prescribe the behaviour of the devices are the direct implementation of the thermodynamic model described in detail in Section 3.1. Since also their names are self-explanatory, they will be just listed with their reference section.

1. `DP_compressor`, subroutine (Section 3.1.2, Page 22);

2. `DP_compr_Tout`, function;

3. `DP_turbine`, subroutine (Section 3.1.2, Page 24);

4. `DP_turbine_Tout`, function;

5. `DP_heat_exchangers`, subroutine (Section 3.1.2, Page 24);
6. `overall_heat_transf_coef`, function;
7. `DP_mcm`, subroutine (Section 3.1.2, Page 27);
8. `DP_mcm_diff`, function;
9. `DP_splitter`, subroutine (Section 3.1.2, Page 30);
10. `DP_mixer`, subroutine (Section 3.1.2, Page 31);
11. `T_hair`, function (this routine is called both by `DP_heat_exchangers` and `DP_mixer`);
12. `DP_combustor`, subroutine (Section 3.1.2, Page 32);
13. `DP_comb_balance`, function;
14. `skip_component`, subroutine (Section 3.1.2, Page 34).

About the six functions `DP_compr_Tout`, `DP_turbine_Tout`, `DP_mcm_diff`, `DP_comb_balance`, `overall_heat_transf_coef`, `T_hair`, it is interesting to explain why they are not incorporated inside the corresponding component subroutine. In order to exploit the advantage to have the non-linear equations solver in a black box, it is necessary to provide to it the equation in the canonical form ($f(x) = 0$) as a function with just *one argument*, the unknown (see Section 3.3.2).

Unfortunately all the non-linear equations that comprise the eAZEP model are not only dependent on the unknown, but also on quantities calculated just at run time, so it is necessary to pass them to the function to be solved during the execution of the program. This action can not be performed with the usual scheme with actual and dummy arguments and the call of the routine, because the function would be no more dependent on a single argument. Moreover it is not possible to set a number of arguments for the function resolved by `solve` because they would change from case to case.

The solution to this problem is to pass all the other variables but the unknown with the "use association", namely including in the same scoping unit (a module) all the variables needed and the function to solve itself.

3.3.5 The `cycle` module

This module contains the core routine of the calculation process. Analytically in the `cycle` module

- are defined the 23 target components that represent all the eAZEP devices and other auxiliary variables;
- there are five module procedures that manage the solving process from an high level point of view.

Amongst the variables, the most important are the 23 components that will be grouped according to their kind.

- Kind `compressor`:
  - `main_compr`, the main engine compressor;
  - `fan`, the flue gas recirculation compressor;
  - `CO2_compr1`, `CO2_compr2`, `CO2_compr3`, `CO2_compr4`, the four CO_2 compressor stages.
- Kind `splitter`:
  - `bleed_splitter`, the splitter at the outlet of the main compressor;
  - `flue_gas_splitter`, the splitter at the outlet of the combustion chamber.
- Kind `heat_exchanger`:
  - `mcm`, the Mixed Conductive Membrane modeled as a pure heat exchanger;
  - `lthx`, the Low Temperature Heat Exchanger;
  - `hthx`, the High Temperature Heat Exchanger;
  - `bhx`, the Bleed Heat Exchanger;
  - `pehx`, the Post Expansion Heat Exchanger.
- Kind `combustor`: just one component, `combustion_chamber`.
- Kind `mixer`:
  - `O2_mix`, the mixer that takes into account the adiabatic mixing of the oxygen with the permeate flow in the Mixed Conductive Membrane;
  - `inlet_turb_mix`, the mixer at the inlet of the air turbine.
- Kind `turbine`:
  - `main_turb`, the air turbine;

  - `flue_turb`, the flue gas turbine.

- Kind `bypass`:
  - `bhx_air`, the bypass of the Bleed Heat Exchanger for the air flow;
  - `bhx_flue`, the bypass of the Bleed Heat Exchanger for the flue gas flow;
  - `flue_turb_skip`, the bypass of the flue gas turbine;
  - `pehx_air`, the bypass of the Post Expansion Heat Exchanger for the air flow;
  - `pehx_flue`, the bypass of the Post Expansion Heat Exchanger for the flue gas flow.

The five module procedures are described below.

1. `initialize`: this subroutine
   - reads all the 56 input file parameters (from `cycle_param.txt`);
   - defines all the component variables listed above in order to arrange them in the correct layout of the power plant and stores the cycle parameters into them;
   - sets the initial values for the flags of the different layouts and the output file printing;
   - sets the fuel station variables (except the mass flow, still unknown) and the oxygen station composition.
2. `DP_main`: the subroutine implements the cycle solving sequence described in details in Section 3.2.3.
3. `nth_root`: it is an ancillary function that returns the n-th root of a floating point variable. It implements[13] the Newton-Raphson method (Section 3.2.2) to increase the performance of the the program. The routine is necessary to determine the equally distributed pressure ratio of the inter-cooled CO_2 compression for storage purposes (Section 3.2.3).
4. `output_file`: this subroutine creates an output file containing
   - the layout chosen for the power plant calculation;
   - the performance results;
   - all the stations values;
   - a list of the computational assumptions.

[13] See http://en.wikipedia.org/wiki/Nth_root_algorithm for details.

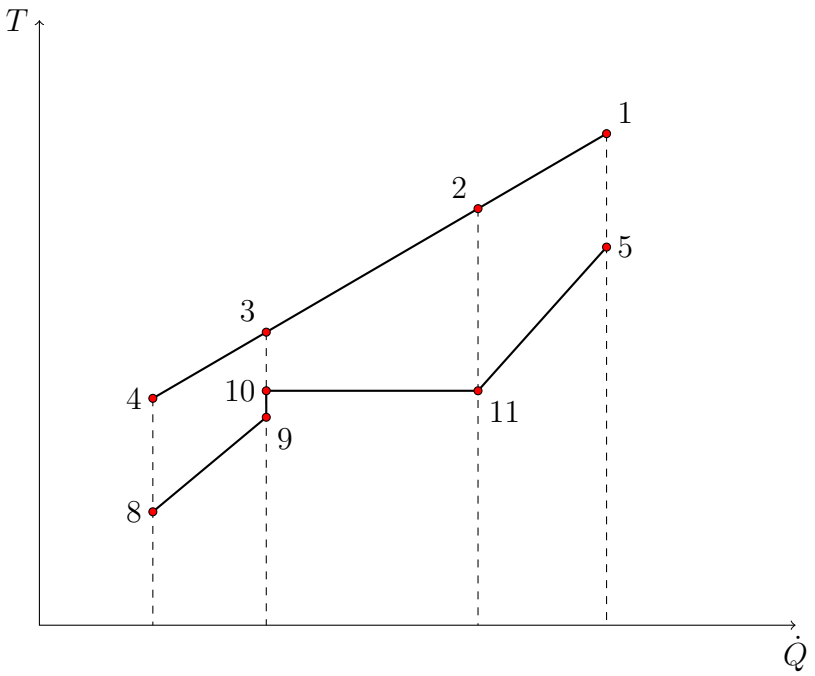

Figure 3.12. Heat transfer diagram of the single pressure HRSG module.

It prints an output file for every successful calculation run.

5. `center`: this simple ancillary function permits to centre a given string on a generic 80 columns output device (a printer, the console, an output file).

3.4 Steam plant off-design model

As additional contribution of this project to the main one investigating several low carbon concepts for power generation, the off-design core routine of an unfired steam plant — provided with an Heat Recovery Steam Generator (HRSG) — has been re-wrote from scratch. The new routine has the aim to improve the robustness of the algorithm at part-load. Since this steam plant model is the bottoming part of the AZEP cycle, another objective is to ease the interfacing between the topping and bottoming codes.

Now will be described the algorithm developed and implemented for a *single* level pressure HRSG since more complicated layouts (multi-pressure HRSG with reheat) could be modularly constructed gathering several single pressure modules [24].

The exhaust gas (see Figure 3.12) release heat starting from the inlet of

the HRSG (station 1) to the stack (station 4), while the feed water (station 8) first increases its temperature, changes phase turning into steam (station 10 to 11), and finally (station 5) achieves the steam turbine inlet temperature[14].

The algorithm adopts an iterative sequential strategy (see Section 3.2) using the same root finding solver for the solution of the one-dimensional non-linear equations (Section 3.3.2). The solving strategy comprises three iterative loops arranged in a main one and two inner cycles; the iterations of the former are counted with the *Roman* numerals while the latter use the *Arabic* numerals.

Since the success of the solving strategy is remarkably dependent on the starting point, the initial guess is always based on temperature assumptions that are more easily predictable. The initialization of the procedure begins guessing T_5 and T_{11} starting from T_1 (an input quantity); these assumptions are made just once at the start of the algorithm

$$\begin{aligned} T_5^{(1)} &= T_1 - \Delta T_{\text{guess},5} \\ T_{11}^{(\text{I})} &= T_5^{(1)} - \Delta T_{\text{guess},11} \end{aligned} \tag{3.131}$$

where $\Delta T_{\text{guess},5}$ and $\Delta T_{\text{guess},11}$ are two parameters suitably chosen. Please note that since T_5 is denoted with the Arabic numeral, it is going to be "corrected" in one of the *inner* loops, while T_{11} will be processed in a similar way in the *main* loop.

The iterative solution procedure starts with the evaluation of the temperature and the specific enthalpy at the inlet of the evaporator (respectively $T_{10}^{(\text{I})}$ and $h_{10}^{(\text{I})}$) since the former is equal to $T_{11}^{(\text{I})}$ (the substance is changing its phase) and the latter is just dependent on the temperature (the conditions at station 11 are on the saturation curve of the liquid):

$$T_{10}^{(\text{I})} = T_{11}^{(\text{I})} \tag{3.132}$$

$$h_{10}^{(\text{I})} = h_{\text{sat}}(T_{10}^{(\text{I})}) \tag{3.133}$$

Moreover, again from the $T_{11}^{(\text{I})}$ and the saturation conditions, it is possible to know the pressure of the steam throughout the HRSG $p_5^{(\text{I})}$ and the specific enthalpy $h_{11}^{(\text{I})}$

$$p_5^{(\text{I})} = p_{\text{sat}}(T_{11}^{(\text{I})}) \tag{3.134}$$

$$h_{11}^{(\text{I})} = h_{\text{sat}}(T_{11}^{(\text{I})}) \tag{3.135}$$

[14]Further details about the thermodynamic processes in a combined cycle HRSG, could be found in [25].

The first imbricated loop (governed by T_5) starts with the evaluation of the specific enthalpy $h_5^{(1)}$ and the mass of steam flowing through the plant $W_s^{(1)}$; the first is based on the knowledge of $T_5^{(1)}$ and $p_5^{(I)}$, the second is related with a Stodola-like choking relation at the steam turbine inlet [24]:

$$h_5^{(1)} = h_{\text{steam}}(T_5^{(1)}, p_5^{(I)}) \tag{3.136}$$

$$W_s^{(1)} = \frac{p_5^{(I)}\,\kappa\,A_{\text{in}}}{\sqrt{T_5^{(1)}}} \tag{3.137}$$

where κ is a characteristic constant and A_{in} is the turbine inlet area; both the variables are known from the design point performance calculation.

In order to close the first inner loop, we need to resolve the equations describing the superheater behaviour. So from its energy balance, it is possible to figure the enthalpy of the flue gas h_2

$$W_g \left(h_1 - h_2^{(1)}\right) = W_s^{(1)} \left(h_5^{(1)} - h_{11}^{(I)}\right)$$

thus

$$h_2^{(1)} = h_1 - \frac{W_s^{(1)}}{W_g} \left(h_5^{(1)} - h_{11}^{(I)}\right) \tag{3.138}$$

and then the corresponding temperature $T_2^{(1)}$

$$T_2^{(1)} = T_{\text{gas}}(h_2^{(1)}) \tag{3.139}$$

From the design criterion of the superheater (based on the logarithmic mean temperature difference $\Delta T_{\text{lm,sh}}$) $T_5^{(2)}$ is obtained

$$W_g \left(h_1 - h_2^{(1)}\right) = U_{\text{sh}}\,A_{\text{sh}}\,\Delta T_{\text{lm,sh}}$$

$$\Delta T_{\text{lm,sh}} = \frac{\left(T_1 - T_5^{(2)}\right) - \left(T_2^{(1)} - T_{11}^{(I)}\right)}{\ln \frac{T_1 - T_5^{(2)}}{T_2^{(1)} - T_{11}^{(I)}}} \tag{3.140}$$

Then it is possible to start the second iteration from the Equation (3.136), where $h_5^{(2)}$ is calculated from $T_5^{(2)}$.

At the end of the convergence process for this first inner loop, the program figures: $W_s^{(I)}$, $T_2^{(I)}$, $h_2^{(I)}$, $T_5^{(I)}$, $h_5^{(I)}$. Subsequently the steam turbine and the condenser routine are called, returning the values of $T_8^{(I)}$ and $h_8^{(I)}$. Before to

start the second imbricated loop, it is necessary to guess the starting value of T_9, namely $T_9^{(1)}$, and its corresponding specific enthalpy $h_9^{(1)}$

$$T_9^{(1)} = T_{10}^{(\mathrm{I})} - \Delta T_{\mathrm{guess},9} \tag{3.141}$$

$$h_9^{(1)} = h_{\mathrm{water}}(T_9^{(1)}, p_5^{(\mathrm{I})}) \tag{3.142}$$

The second loop starts with the energetic balance of the evaporator useful to determine $h_3^{(1)}$

$$W_{\mathrm{g}} \left(h_2^{(\mathrm{I})} - h_3^{(1)}\right) = W_{\mathrm{s}}^{(\mathrm{I})} \left(h_{11}^{(\mathrm{I})} - h_9^{(1)}\right)$$

that yields to

$$h_3^{(1)} = h_2^{(\mathrm{I})} - \frac{W_{\mathrm{s}}^{(\mathrm{I})}}{W_{\mathrm{g}}} \left(h_{11}^{(\mathrm{I})} - h_9^{(1)}\right) \tag{3.143}$$

Once obtained straightforwardly $T_3^{(1)}$

$$T_3^{(1)} = T_{\mathrm{gas}}(h_3^{(1)}) \tag{3.144}$$

it is possible to determine $T_4^{(1)}$ utilising the logarithmic difference temperature formula in the economizer

$$W_{\mathrm{s}}^{(\mathrm{I})} \left(h_9^{(1)} - h_8^{(\mathrm{I})}\right) = U_{\mathrm{eco}}\, A_{\mathrm{eco}}\, \Delta T_{\mathrm{lm,eco}}$$

$$\Delta T_{\mathrm{lm,eco}} = \frac{\left(T_3^{(1)} - T_9^{(1)}\right) - \left(T_4^{(1)} - T_8^{(\mathrm{I})}\right)}{\ln \frac{T_3^{(1)} - T_9^{(1)}}{T_4^{(1)} - T_8^{(\mathrm{I})}}} \tag{3.145}$$

and, then, the corresponding $h_4^{(1)}$

$$h_4^{(1)} = h_{\mathrm{gas}}(T_4^{(1)}) \tag{3.146}$$

The energy balance of the economizer

$$W_{\mathrm{g}} \left(h_3^{(1)} - h_4^{(1)}\right) = W_{\mathrm{s}}^{(\mathrm{I})} \left(h_9^{(2)} - h_8^{(\mathrm{I})}\right)$$

allows to close the second inner loop with the determination of $h_9^{(2)}$

$$h_9^{(2)} = h_8^{(\mathrm{I})} + \frac{W_{\mathrm{g}}}{W_{\mathrm{s}}^{(\mathrm{I})}} \left(h_3^{(1)} - h_4^{(1)}\right) \tag{3.147}$$

Then the program checks if there is steaming in the economizer, comparing the $h_9^{(2)}$ with the $h_{10}^{(\mathrm{I})}$, and showing a warning if so. If the convergence is

not reached, the iterative procedure starts again from the Equation (3.143), otherwise $T_9^{(\mathrm{I})}$ is determined from the $h_9^{(\mathrm{I})}$

$$T_9^{(\mathrm{I})} = T_{\mathrm{gas}}(h_9^{(\mathrm{I})}) \tag{3.148}$$

and the *other* output variables are: $T_9^{(\mathrm{I})}$, $h_3^{(\mathrm{I})}$, $T_4^{(\mathrm{I})}$, $h_4^{(\mathrm{I})}$.

In order to close the main loop, the program use the last equation available calculating the $T_{11}^{(\mathrm{II})}$ from the logarithmic mean difference temperature equation for the evaporator

$$\begin{aligned} W_{\mathrm{g}} \left(h_2^{(\mathrm{I})} - h_3^{(\mathrm{I})}\right) &= U_{\mathrm{ev}}\, A_{\mathrm{ev}}\, \Delta T_{\mathrm{lm,ev}} \\ \Delta T_{\mathrm{lm,ev}} &= \frac{\left(T_2^{(1)} - T_{11}^{(\mathrm{II})}\right) - \left(T_3^{(\mathrm{I})} - T_9^{(\mathrm{I})}\right)}{\ln \frac{T_2^{(1)} - T_{11}^{(\mathrm{II})}}{T_3^{(\mathrm{I})} - T_9^{(\mathrm{I})}}} \end{aligned} \tag{3.149}$$

Thus the iterative process goes back to Equation (3.132) substituting the new $T_{11}^{(\mathrm{II})}$ value. The last operations performed after the solution of the entire set of equations are the determination of the heat rate transferred in the heat exchangers (namely in the superheater $\dot{Q}_{\mathrm{su}}$, in the evaporator $\dot{Q}_{\mathrm{ev}}$ and in the economizer $\dot{Q}_{\mathrm{eco}}$)

$$\begin{aligned} \dot{Q}_{\mathrm{su}} &= W_{\mathrm{g}}\ (h_1 - h_2) \\ \dot{Q}_{\mathrm{ev}} &= W_{\mathrm{g}}\ (h_2 - h_3) \\ \dot{Q}_{\mathrm{eco}} &= W_{\mathrm{g}}\ (h_3 - h_4) \end{aligned} \tag{3.150}$$

and the test for the steaming at the economizer outlet

$$h_9 < h_{10} \tag{3.151}$$

Chapter 4

Results and discussion

In this chapter are showed the results aimed to investigate the sensitivity of the AZEP cycle in the regards of its (many) parameters utilising eAZEP. Thanks to the flexibility of the software, it is possible to consider up to four layouts (see Section 3.1), all with *complete* carbon dioxide capture:

1. the Bleed Heat Exchanger (BHX) layout *without* the flue gas turbine;
2. the Post Expansion Heat Exchanger (PEHX) layout *without* the flue gas turbine;
3. the Bleed Heat Exchanger (BHX) layout with the flue gas turbine;
4. the Post Expansion Heat Exchanger (PEHX) layout with the flue gas turbine.

Among the several output quantities to consider in the study, are chosen the four most important according to the opinion of the author. The quantities are

1. the overall thermal efficiency η_o — Equation (3.130);
2. the overall power output P_o — see Section 3.2.3;
3. the exhaust gas temperature on the flue gas side — the temperature at stations 19, 22, or 23 of Figure 3.1;
4. the Mixed Conductive Membrane average temperature — defined in the first of the Equations (3.55).

The reason for the picking of the last two variables is, respectively, the need to assess the AZEP capability to be integrated in a combined cycle arrangement and the critical role that the temperature plays in the lifing of the membrane (the most expensive and characteristic component of the power plant).

Without any doubt it would have been very interesting to present and comment also the results about other quantities. An example is the oxygen mass fraction present in the flue gas (deriving from the excess of oxygen in the combustive mixture, compared to the stoichiometric quantity) because it overloads unnecessarily the CO_2 compression process; or the exhaust temperature on the air side, in order to assess more completely the integration attitude of the AZEP to fit in a combined cycle arrangement. Several other examples can be presented, but the limited amount of time available for the research project required to make choices driven by the relevance.

4.1 Computational assumptions

The reference engine chosen to carry out the study is a single-shaft land-based gas turbine with similar features to the GE9FA and the Siemens V94.3A. This choice is due to the previous literature studies that considered mainly these two engine as reference; moreover the two power plants are not so different in terms of characteristic parameters. Although this work is focused on the study of the AZEP cycle alone and *not* on the combined cycle arrangement (as did in the literature studies), the choice of this engine has been done mostly to support the main "Advanced Low Carbon Power Systems" project on its further steps.

The performance data of the reference power plant are summarized in Table 4.1. They are calculated using the same routines of the eAZEP components, considering a simple gas turbine cycle *without* blade cooling and intake pressure loss.

The AZEP parameters that remain constant throughout the study (besides the quantities derived from the reference engine) are listed, instead, in Table 4.2. Must be pointed out that the conductivity and the thickness of the Mixed Conductive Membrane active material, were directly chosen from the open literature, since they belong to a different field where the author does not have the same "sensitivity" that allowed him to choose the other quantities. Nonetheless there is a pretty broad agreement [26, 27, 2, 21] on the values that should be used for these critical parameters of the AZEP cycle. Moreover, again by the literature [26, 10], has been suggested an higher pneumatic efficiency of the membrane (compared to the other heat exchangers) since the current state-of-the-art for these devices is based on ceramic monolith

Table 4.1. Reference engine data.

Parameter	**Value**
Inlet mass flow	640 $^{kg}/_{s}$
Pressure ratio	17
Combustor outlet temperature	1570 K
Combustion chamber pneumatic efficiency	0.99
Compressor polytropic efficiency	0.84
Turbine polytropic efficiency	0.88
Compressor and turbine mechanical efficiency	0.998
Electric generator efficiency	0.98
Turbine outlet temperature	874.12 K
Overall LHV thermal efficiency	37.04%
Power output	256.12 MW

structures with high surface-to-volume ratio and low Reynolds flow numbers. The values of the Number of Thermal Units for the heat exchangers were suggested, as well, from literature data [14].

4.2 Sensitivity analysis

When considering the effect of an AZEP parameter on its performance, it is useful to investigate at the same time the effect of the sweep gas pressure. In fact, in many cases, the pressure of the flue gas recirculation "ring" affects remarkably the performance of the power plant and decides also if would be possible to add or not a flue gas turbine in the plant layout. For this reason, for each parameter considered, has been undertaken a study keeping the Mixed Conductive Membrane inlet pressure on the permeate side equal to the outlet pressure of the main compressor. This approach traces out, basically, the usual investigations carried out in the open literature.

Another possibility is to keep the permeate side pressure close to the atmospheric value. At the knowledge of the author, this possibility has always been discarded in the literature study most probably because of its difficult industrial implementation in the short-medium term. The main issue in this case is the mechanical stability of the Mixed Conductive Membrane materials that could be remarkably compromised by the mechanical loading caused by the high pressure ratio between the feed and the permeate side (to broaden the matter there is a study in [27]; see also for a less detailed description [2]).

Keeping in mind that this additional study is purely theoretic (for the

Table 4.2. AZEP parameters kept constant for the parametric study.

Parameter	Value
Flue gas intercooler exit temperature (for CO_2 storage)	300 K
CO_2 storage pressure	100 atm
Heat exchangers pneumatic efficiency (both sides)	0.98
Flue gas intercooler pneumatic efficiency	0.98
MCM pneumatic efficiency (both sides)	0.99
HRSG pneumatic efficiency	0.96
Number of Thermal Units (all heat exchangers)	3
Flue gas recirculation compressor polytropic efficiency	0.83
Flue gas recirculation compressor mechanical efficiency	0.99
Flue gas turbine polytropic efficiency	0.86
Flue gas compressor and turbine mechanical efficiency	0.998
CO_2 pump overall efficiency	0.85
MCM active material conductivity	$10\,^{S}/_{m}$
MCM active material thickness	30 µm

present state-of-the-art of the Mixed Conductive Membranes technology), it appeared interesting to investigate also the long-term potential of the AZEP technology which turned out to be very promising.

Since the pressure of the permeate side of the membrane is kept at 1.1 atm (just to avoid parts of the power plant working at lower pressure than the ambient because of the pressure losses), the flue gas turbine options are not applicable to this case.

4.2.1 Main compressor pressure ratio effect

The main compressor pressure ratio is the parameter which more than any other is strictly correlated to the flue gas side pressure of the power plant. The linkage between the two quantities is mainly the Nernst-Einstein formula — Equation (3.53) — which affects the Mixed Conductive Membrane behaviour (see Section 3.1.2).

Permeate side pressure equal to the compressor outlet pressure

The trend of the thermal efficiency for the four layouts follows the reference cycle one (Figure 4.1), showing an optimum pressure ratio in agreement with the basic theory of the gas turbines. The optimal value is lower for less performing layouts (without flue gas turbine), exacerbating their inferiority

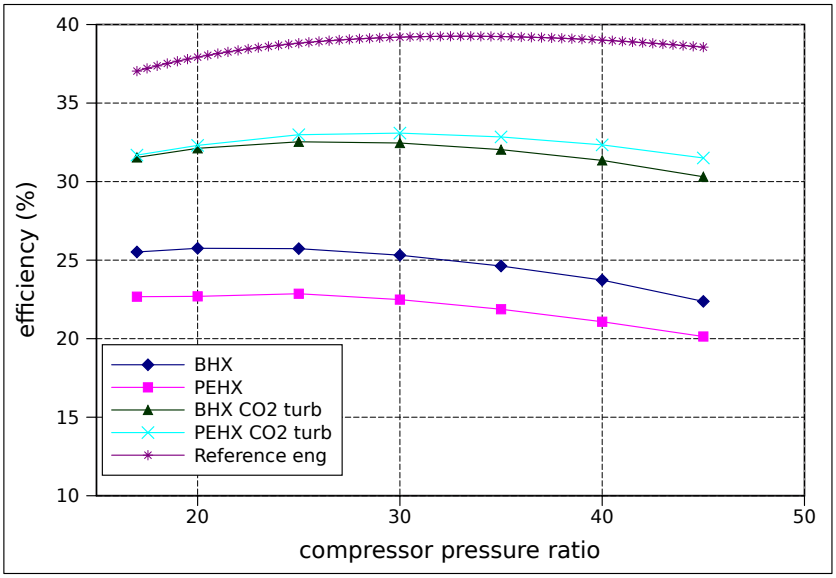

Figure 4.1. AZEP overall thermal efficiencies as a function of the main compressor pressure ratio, with the reference engine performance.

at high pressure ratio. In the study of the overall power output (Figure 4.2), again the AZEP cycles resemble the behaviour of the reference engine but in this case there is no relative worsening with the increase of the pressure ratio: the power output curves are simply shifted on the y-axis.

Both the graphs show that the insertion of the flue gas turbine reduces remarkably the gap between the base case and the AZEP even halving it, and it is more beneficial for the PEHX that profit by the more rational scheme where after the expansion of *both* the streams, they equalize their temperature. This last aspect is also very important in evaluating the best layout for the AZEP combined cycle arrangement where the inlet HRSG temperature is very important.

In that regard, leaving out the depleted air stream temperature that is always similar to the reference engine exhaust temperature, and looking at the flue gas temperatures (Figure 4.3) results evident that again the best choice is the PEHX arrangement with the flue gas turbine, while the simple BHX layout shows temperatures unacceptably high. Moreover the BHX option shows an opposite trend, compared to the other options, because the particular arrangement of its layout connects "directly" the flue gas combustor outlet temperature with the increasing compressor outlet temperature (see Figure 3.1). About the simple PEHX layout must be said that could be considered very interesting its slightly higher exhaust temperature than the conventional one, since it could be exploited by the most advanced HRSG

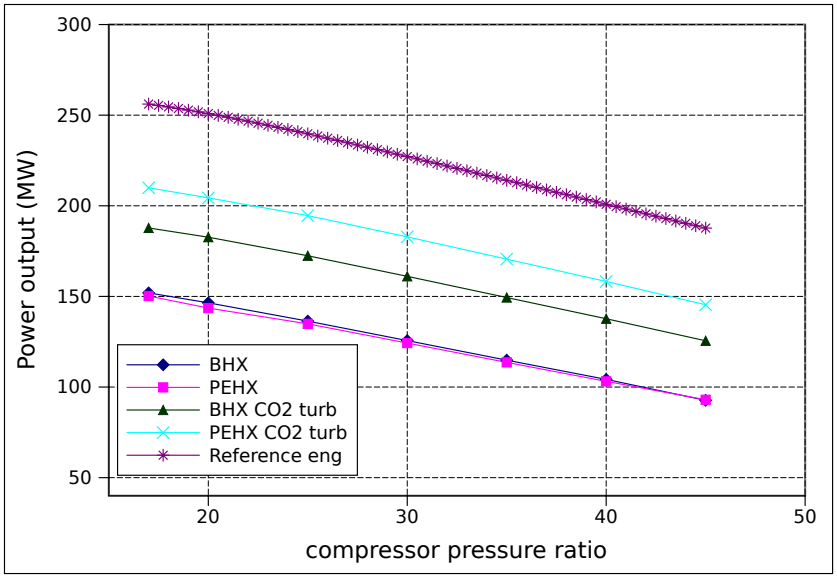

Figure 4.2. Power output of the eAZEP layouts for different values of the main compressor pressure ratio, compared with the reference case data.

and steam turbine technology for the bottoming cycle.

Another very important variable to check is the temperature of the membrane that, if too high, reduces rapidly the life of this very expensive device (see Section 2.3). Unfortunately (Figure 4.4), just the PEHX layouts comply with the temperature constraint of 1473 K and not for every value of the pressure ratio. Must be said, however, that when the aforementioned condition is not respected, the values of the pressure ratio are absolutely not tipical of a land-based gas turbine to be coupled with an HRSG. Moreover the almost complete superimposition of the curves for the layouts with or without the flue gas turbine, shows how the membrane temperature is almost "protected" from external perturbations by the heat exchangers that surrounds it (Section 2.3).

All the results showed since now were obtained with a recirculated flue gas mass flow of about 596 $^{kg}/_{s}$ and varying the percentage of the oxygen depleted between the 28% and the 41% of the theoretical amount removable from the compressed air. The quantity is variable because with the increase of the pressure ratio, the area required to transfer a certain amount of oxygen increase as well and, in some cases, it achieves unacceptable values (a limit of 1000 m^2 was set in eAZEP). There is also a lower limit for the oxygen fraction transferred due to the stoichiometric quantity required to reach the combustor outlet temperature.

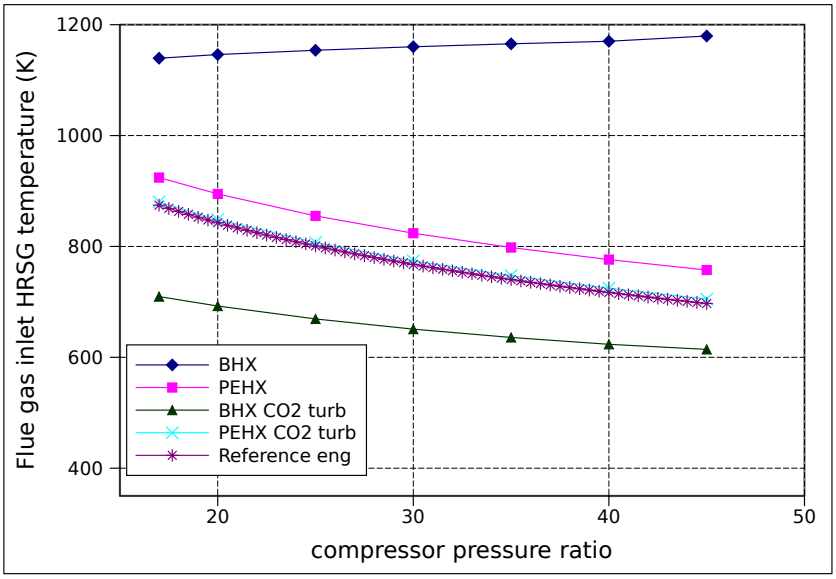

Figure 4.3. Flue gas HRSG inlet temperature for the AZEP cycles and the reference engine as a function of the main compressor pressure ratio.

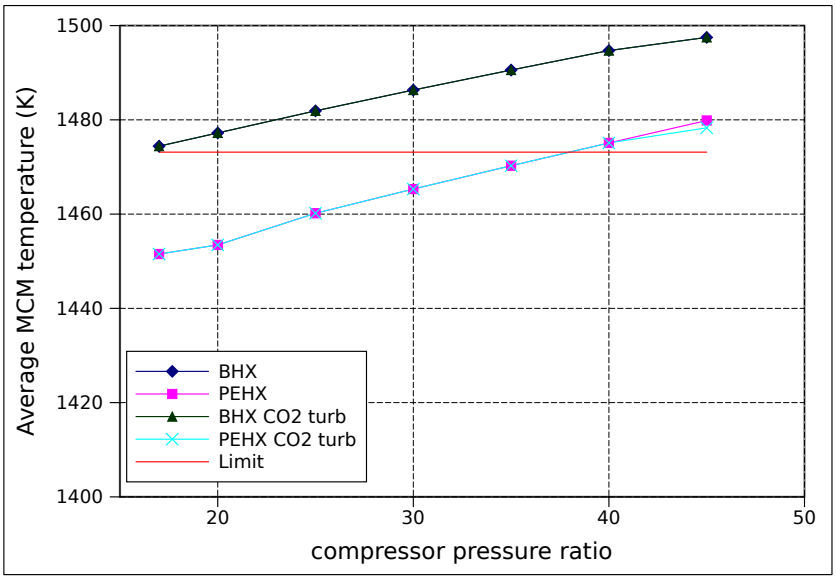

Figure 4.4. Average temperature of the MCM for the eAZEP layouts compared to its limit of 1200 °C [5, 6, 7], when the main compressor pressure ratio is increasing.

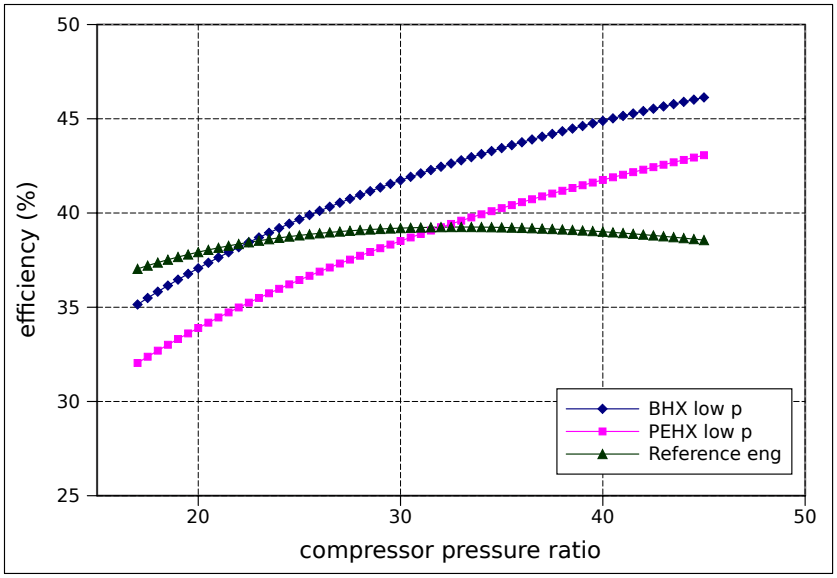

Figure 4.5. AZEP overall thermal efficiencies as a function of the main compressor pressure ratio, with the reference engine data, keeping the permeate side pressure almost atmospheric.

Low constant permeate side pressure

For the study that keeps the flue gas side pressure constant (and close to the ambient value), has been considered the depletion of the 50% of the theoretical amount of oxygen removable and the same flue gas mass flow of the previous study (about 596 $^{kg}/_{s}$). The efficiency and the power output results are very interesting (Figures 4.5 and 4.6).

Although at the reference engine pressure ratio π the efficiency of the AZEP cycle is lower than the base case, the BHX layout equals at $\pi = 22.5$ the conventional power plant and exceeds clearly the 45% (46.13% exactly) at pressure ratio 45. The trend is similar for the PEHX layout which equals the reference engine at $\pi = 32$ and shows the maximum efficiency (43.07%) at the maximum pressure ratio. As usual, the PEHX option is less performing than the BHX one.

In the power output chart is even more definite the advantage of the AZEP cycle upon the reference engine. The rapid decline of the base engine performance contrasts with the AZEP constant increase which achieves almost the 340 MW for the BHX layout at the maximum pressure ratio; this value is almost the double (187.69 MW) of the corresponding power output for the reference power plant.

Analysing also in this case the exhaust flue gas temperature directed to

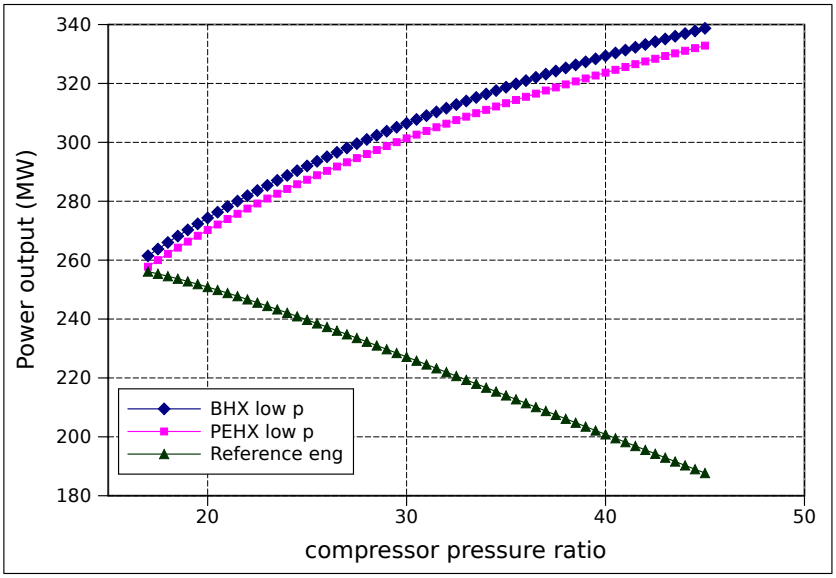

Figure 4.6. Power output of the eAZEP layouts for increasing values of the main compressor pressure ratio and at constant atmospheric pressure on the permeate side. The results are compared with the reference case data.

the HRSG inlet (Figure 4.7) and the temperature of the Mixed Conductive Membrane (Figure 4.8), the observations to point out are not different from the ones expressed for the previous study. The values of the flue gas HRSG inlet temperature and the membrane average temperature, confirm the superiority of the PEHX solution and show how already for main compressor pressure ratios higher than 18.5, the temperature of the MCM exceeds the suggested limit for the BHX layout. Consistently, also the flue gas exhaust temperature assumes unacceptable values for the direct delivery of the stream to the HRSG.

4.2.2 Combustor outlet temperature effect

This study investigates the range between 1400 and 1600 K of the flue gas temperature at the outlet of the combustor (also referenced as COT — Combustor Outlet Temperature). With the increase of the COT required, the fraction of the oxygen mass flow extracted over the theoretical one is increased accordingly, in order to avoid the achievement of a gas fuel ratio value lower than stoichiometric. This expedient is not necessary in the low permeate side

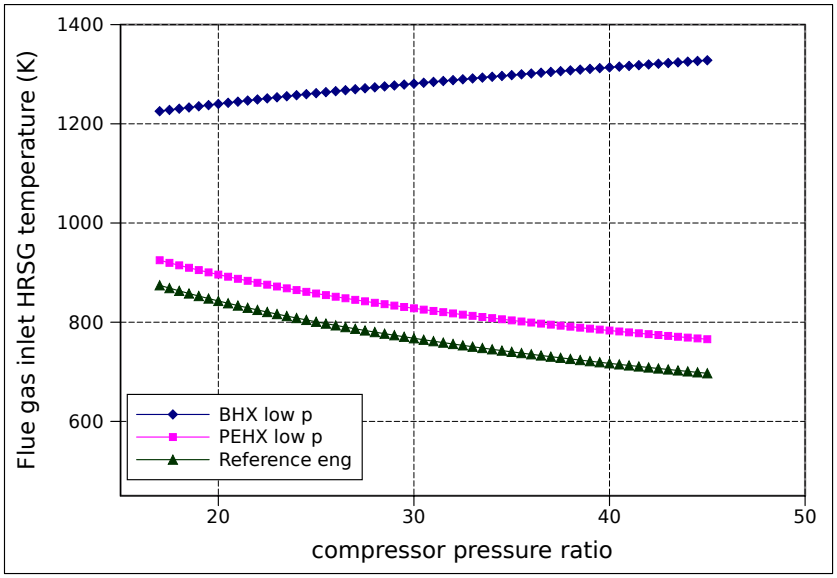

Figure 4.7. Flue gas HRSG inlet temperature for the AZEP cycles and the reference power plant as a function of the main compressor pressure ratio. The pressure on the permeate side is kept constant and almost at ambient pressure.

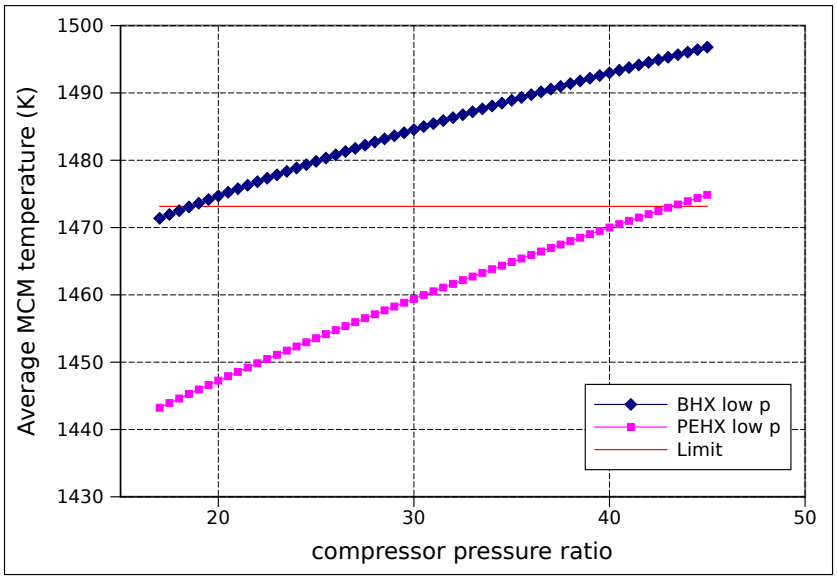

Figure 4.8. Average temperature of the MCM in the eAZEP layouts compared to the limit of 1200 °C [5, 6, 7], when the main compressor pressure ratio is increasing and the permeate side pressure of the power plant is constant, equal to the atmospheric pressure.

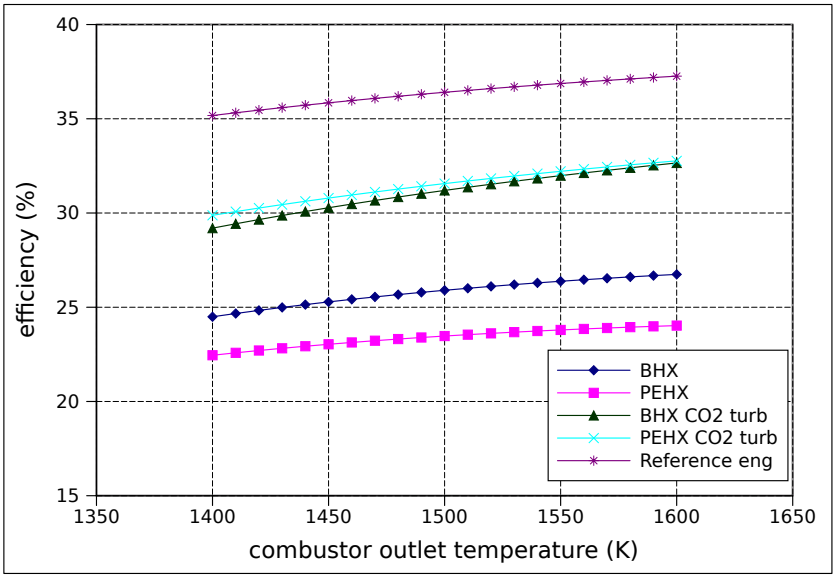

Figure 4.9. AZEP overall thermal efficiencies as a function of the combustor outlet temperature, with the reference engine performance.

pressure case, since the fraction of the oxygen extracted is kept high enough[1] (0.5) to be always higher than the stoichiometric quantity.

Must be remembered, anyway, that in the AZEP cycle the combustor outlet temperature can not be too low since the combustive mixture at the inlet of the combustion chamber is quite different from the conventional compressed air case (see Section 3.1.2).

Permeate side pressure equal to the compressor outlet pressure

The results concerning the efficiency (Figure 4.9) and the output work (Figure 4.10) show that the main performance trends of the AZEP cycles follow pretty accurately the reference power plant behaviour. The gap, for what concerns both the quantities studied, is not dependent on the COT but just on the plant layout. The charts confirm how the PEHX with the flue gas turbine arrangement is the best choice (especially in the regards of the power output) and that with the adoption of the additional turbine, the BHX and the PEHX layout efficiencies approach to very similar values. On the other hand, there is an important difference on the power output between the two layouts with the flue gas turbine included.

About the flue gas exhaust temperature (Figure 4.11) there is nothing

[1]Thanks to the high oxygen partial pressure ratio over the membrane, that resulted in reasonable permeate areas of the membrane.

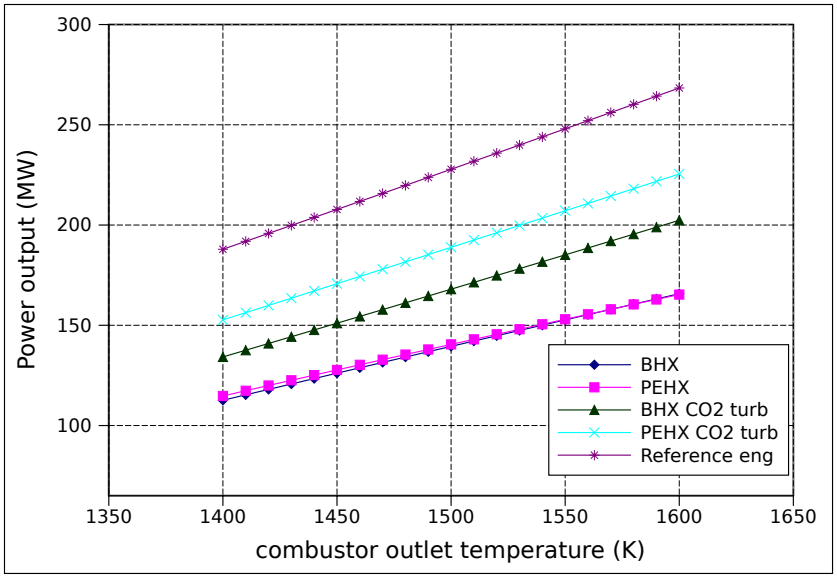

Figure 4.10. Power output of the eAZEP layouts for different values of the combustor outlet temperature, compared with the reference case data.

new to observe excluding the observations already expressed in the previous section: the two PEHX layouts are the most suitable options. Analysing the average Mixed Conductive Membrane temperature chart (Figure 4.12) the flue gas turbine insertion in the layout is confirmed to not affect the studied variable behaviour. In every case there is a good safety margin between the limit and the figured temperature of the membrane; again, it results confirmed that the BHX layouts show higher MCM temperatures than the PEHX ones.

The results showed in Figures 4.9, 4.10, 4.11, and 4.12 were obtained considering a flue gas recirculated mass flow of 448 $^{kg}/_{s}$ and the extraction of the oxygen mass flow spanning from 30% to the 38% of the theoretical removable quantity for the BHX layout and up to the 40% for the PEHX option. As explained above, the percentage was required to increase in accordance with the increase of the combustor outlet temperature.

Low constant permeate side pressure

The results concerning the near atmospheric pressure on the flue gas side of the power plant, confirm clearly the behaviour of the corresponding "high" pressure study. This is especially true for the temperature at the inlet of the HRSG — flue gas side — (Figure 4.15) and the one of the membrane (Figure 4.16) that show also a *quantitative* agreement with the previous study. The only small difference to describe regards only the BHX layout that shows

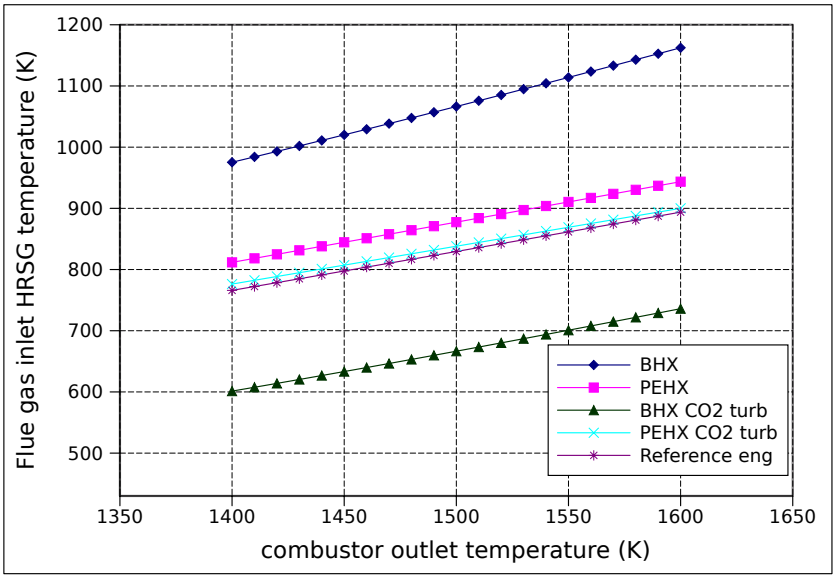

Figure 4.11. Flue gas HRSG inlet temperature for the AZEP cycles and the reference engine as a function of the combustor outlet temperature.

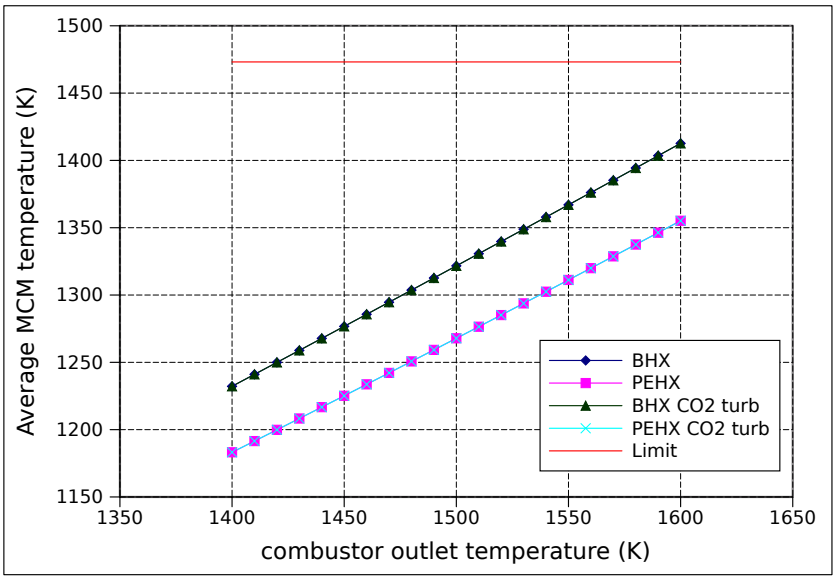

Figure 4.12. Average temperature of the MCM compared to its limit of 1200 °C [5, 6, 7], with the variation of the combustor outlet temperature.

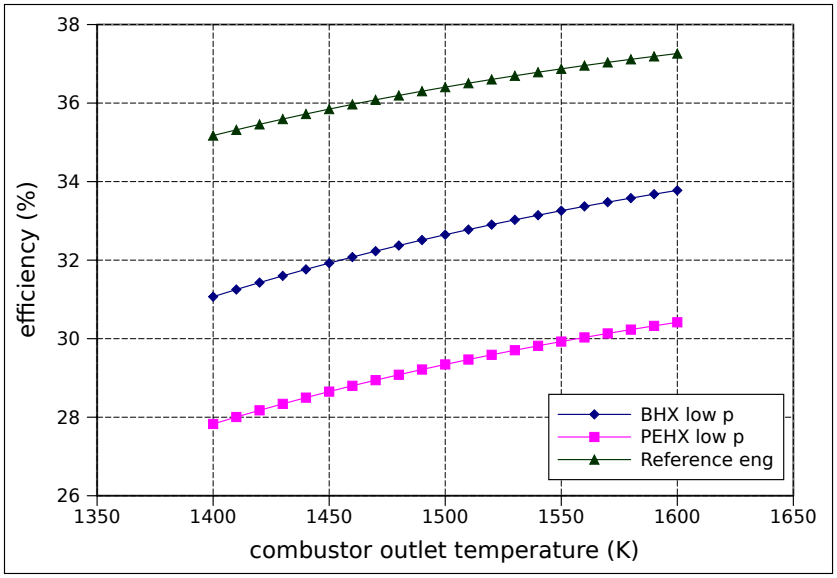

Figure 4.13. AZEP overall thermal efficiencies as a function of the combustor outlet temperature, with the reference engine data, keeping the permeate side pressure almost atmospheric.

a slightly higher temperature for the exhaust and a slightly lower one for the membrane.

The efficiencies (Figure 4.13) increase, as expected, their values but the trend remains completely consistent with the higher pressure permeate side study. In the power output results (Figure 4.14) the remarkable reduction of the gap in the regards of the reference case is clearly visible.

This part of the study has been carried out with the same value of the flue gas recirculated mass flow of the previous series of calculations ($448\,^{kg}/_{s}$) and transferring the 50% of the theoretical removable quantity of oxygen.

As a general comment, also in this case the increase of the combustion outlet temperature improve greatly the performance of the AZEP cycles following the results of the classic gas turbine theory (represented by the reference engine).

4.2.3 Recirculation flue gas mass flow effect

The mass flow of flue gas recirculated in the power plant is another "degree of freedom" available for the designer of an AZEP cycle and, of course, has an effect on its performance. For the sake of generality, eAZEP adopts an non-dimensional parameter to describe the amount of flue gas recirculated in the power plant (W_{17} in the eAZEP process flow diagram, Figure 3.1). The

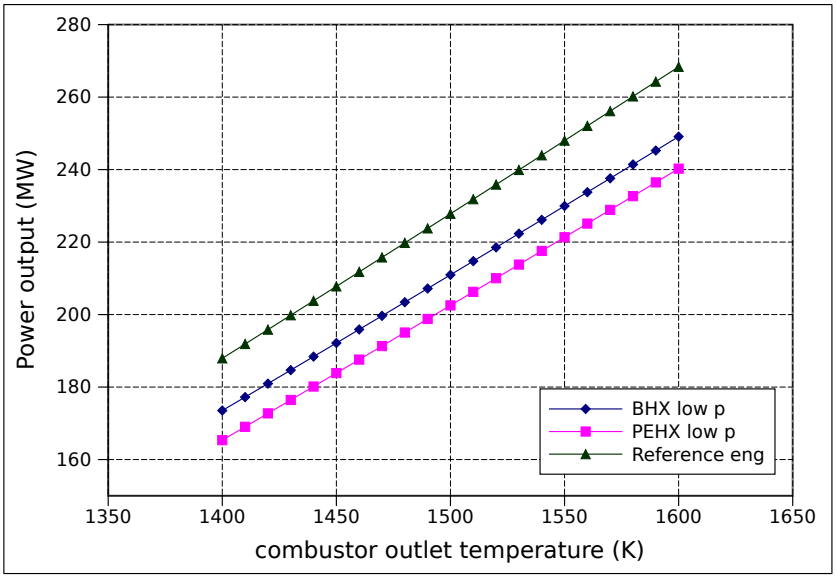

Figure 4.14. Power output of the eAZEP layouts for increasing values of the combustor outlet temperature and at constant atmospheric pressure on the permeate side. The results are compared with the reference case data.

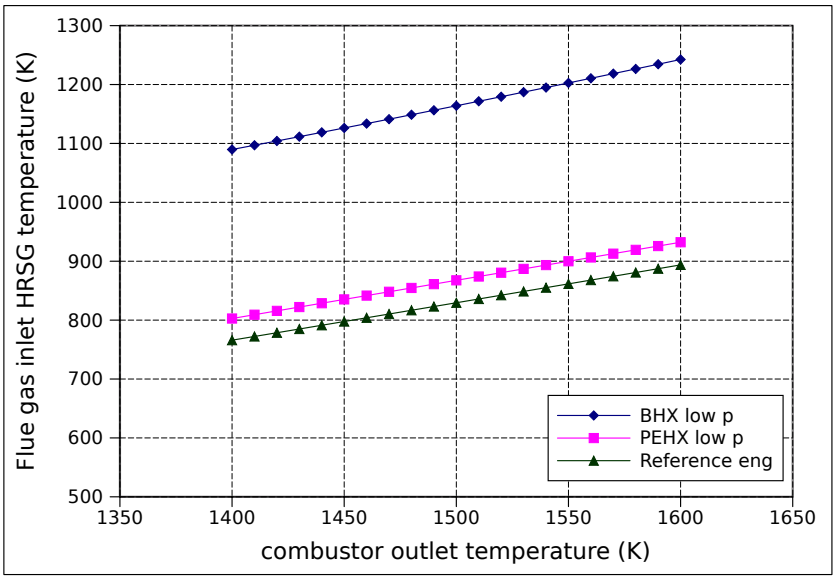

Figure 4.15. Flue gas HRSG inlet temperature for the AZEP cycles and the reference power plant as a function of the combustor outlet temperature. The pressure on the permeate side is kept constant at almost ambient pressure.

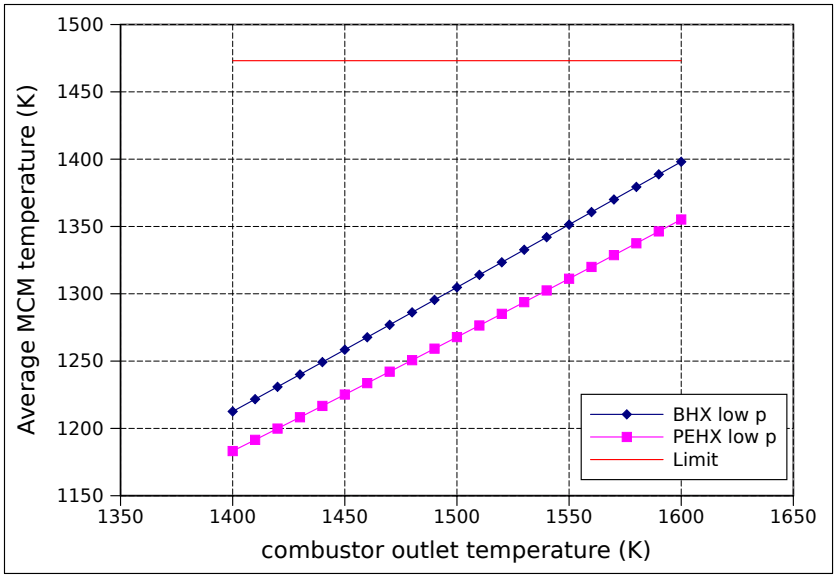

Figure 4.16. Average temperature of the MCM compared to its limit of 1200 °C [5, 6, 7], when the combustor outlet temperature is increasing and the permeate side pressure of the power plant is constant equal to the atmospheric pressure.

mass flow conveyed towards the HTHX is referred to the engine inlet one $W_{\text{in,eng}}$, giving the desired non-dimensional parameter ρ

$$\rho = \frac{W_{17}}{W_{\text{in,eng}}} \tag{4.1}$$

In this study the ρ value is varying from 0.5 to 0.95 when the pressure on the permeate side is equal to the compressor outlet pressure, while its lower limit is moved to 0.3 in the case of the ambient pressure permeate side simulation. The choice to pick different bounds is basically influenced by the convergence limitations of the solving process; the consequent inference is that the power plant at higher pressure on the permeate side has a restricted operating range. Moreover, both the PEHX layouts, do not converge with ρ lower than 0.6, this should be taken into account in the flexibility assessment of the power plant.

Because of the diluting effect of the recirculation mass flow, while ρ is increasing, the oxygen fraction of the gas at the combustor inlet is reducing and it could become lower than stoichiometric. For this reason the fraction of the oxygen depleted from the feed flow has been increased from the 32% to the 38.3% for the BHX layout and from 38% to the 42.9% for the PEHX

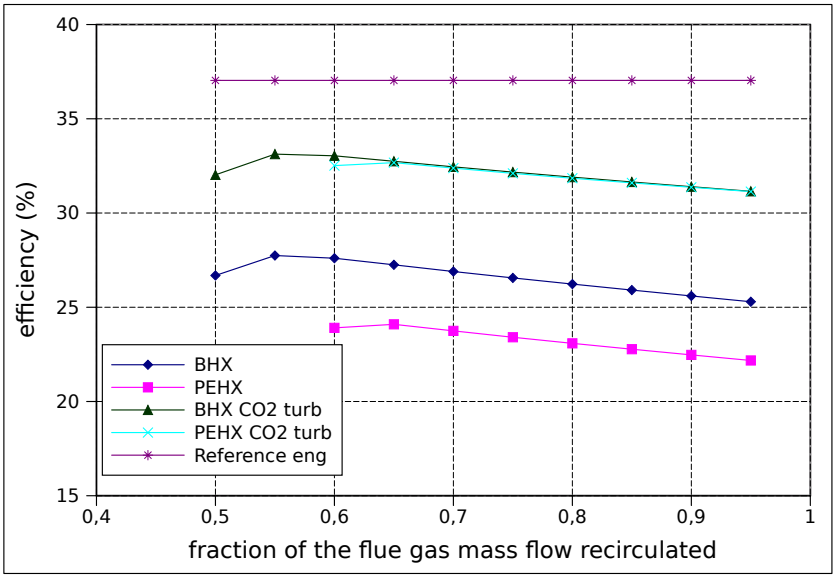

Figure 4.17. AZEP overall thermal efficiencies as a function of the recirculated flue gas mass flow expressed as a fraction over the inlet engine mass flow. The reference engine value is reported.

option. As usual, the low pressure permeate side arrangement worked without showing any problem at constant rate (50%).

Permeate side pressure equal to the compressor outlet pressure

The effect of the flue gas recirculated mass flow on the efficiency (Figure 4.17) shows a mild effect almost of the same type for all the eAZEP layouts. All the trends show an optimal ρ more or less close to the same values (around 0.6, higher for the PEHX arrangement, lower for the BHX option), and independent from the addition of the flue gas turbine. Considering instead the values of the efficiencies, the presence of the second turbine cancels the difference between the two layouts.

This last observation is no more valid analysing the results for the power output (Figure 4.18) where the simple BHX and PEHX plants deliver similar results and there is an important difference between the two layouts featured with the additional turbine. Also in this case there is an optimal recirculated mass flow for the variable being analysed; interestingly the optimal ρ is the same for the efficiencies and for the overall power output.

The exhaust flue gas temperature (Figure 4.19) is not affected by the variation of the recirculated mass flow, mainly because it is driven by the devices that are outside the flue gas recirculation path, devices whose behaviour is

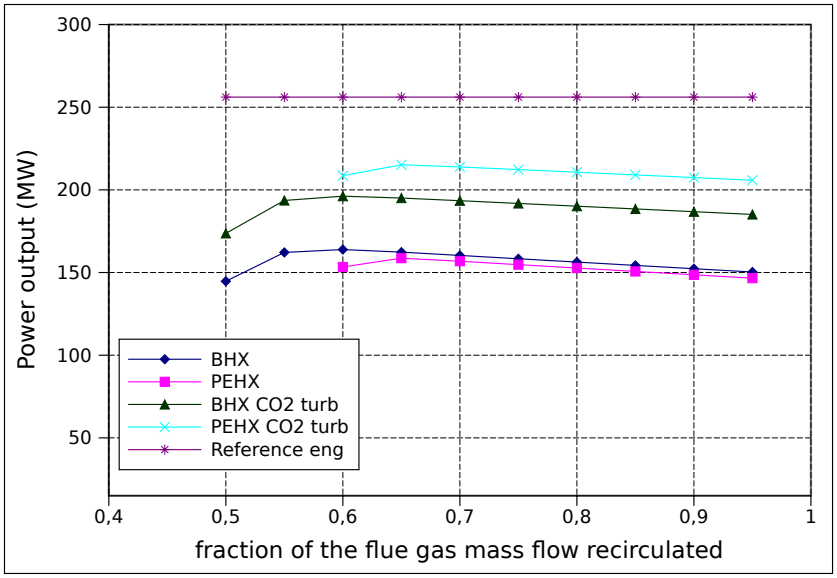

Figure 4.18. Power output of the eAZEP layouts for different fractions of the recirculated mass flow over the inlet engine mass flow. The value for reference engine case is reported.

actually not influenced by the increase or decrease of ρ. In particular the PEHX layouts are basically not sensitive to it. On the quantitative side, the characteristic "footprint" of each layout is reproduced also in this case, confirming the AZEP featured with the PEHX as the best option on this point of view.

The average temperature of the Mixed Conductive Membrane, instead, is hugely dependent on the flue gas recirculated mass flow (Figure 4.20), increasing its temperature more and more. With higher ρ, in fact, the heat capacity rate of the hot gas at the inlet of the membrane increase, determining the rapid approach to the limit temperature of 1473 K. Again the turbines do not influence the variation of the temperature and the BHX option shows higher temperatures than the PEHX.

It is useful to observe as the proportionality between the two quantities (ρ and the average MCM temperature) is not linear but pseudo-logarithmic and how the BHX and the PEHX layouts reduce their difference at higher ρ. Both the observations could be explained by the increase of the aforementioned heat capacity rate of flue gases (the hot stream for every heat exchanger) that determines higher temperatures throughout the power plant and, in particular, also in the Mixed Conductive Membrane.

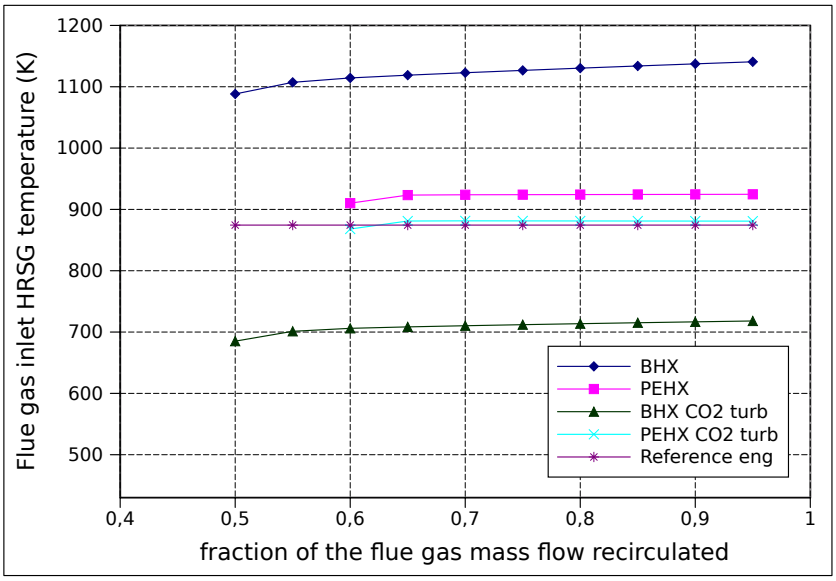

Figure 4.19. Flue gas HRSG inlet temperature for the AZEP cycles as a function of the fraction of the recirculated mass flow over the inlet engine mass flow. The corresponding reference engine value is reported.

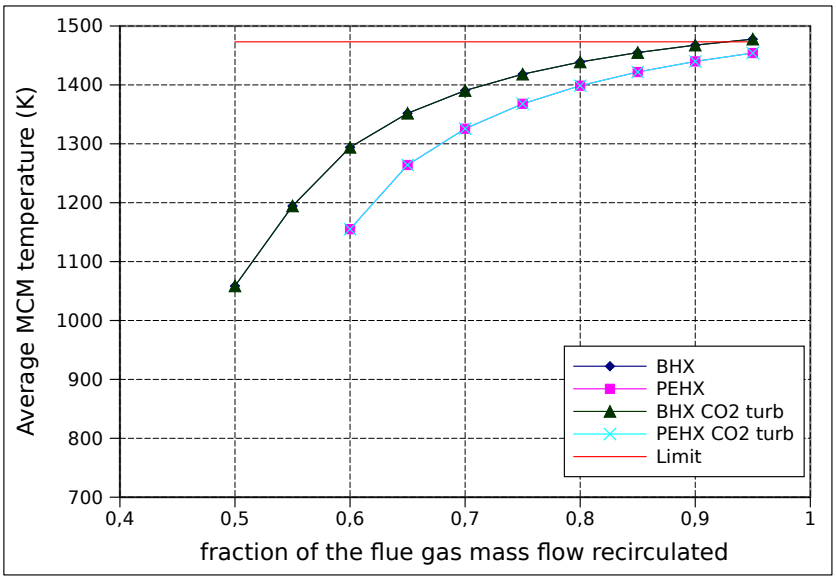

Figure 4.20. Average temperature of the MCM compared to its limit of 1200 °C [5, 6, 7], when the fraction of the recirculated mass flow over the inlet engine mass flow is increasing.

Low constant permeate side pressure

The analysis of the results obtained for the atmospheric pressure on the permeate side of the power plant, shows again a very interesting trend for the overall efficiency (Figure 4.21). The AZEP layouts, keeping roughly constant the same gap between them, approach rapidly the reference engine efficiency with the increase of ρ; in particular the BHX scheme (as usual, the better performing on this aspect) achieves an efficiency just 0.3% lower than the base case ($\rho = 0.95$).

This behaviour is easily explained observing that the increased oxygen partial pressure ratio across the Mixed Conductive Membrane, moves the optimal ρ described in the previous study to higher values. Since an high *optimal* value of ρ implies a larger heat capacity rate of the hot streams in the heat exchangers, it determines higher temperatures in the power plant and, in turn, also an higher temperature at the inlet of the air turbine. This last achievement explains why the family of power plants with the permeate side at nearly ambient pressure could reach higher efficiencies.

The AZEP cycles power output show an even stronger improvement (Figure 4.22) achieving better performance than the reference case for the highest values of ρ. Must be observed that the difference between the two layouts is reducing with the increase of the flue mass flow recirculated.

The dependence of the flue gas exhaust temperature (Figure 4.23) shows an initial rapid increase (at low values of ρ) and then a stabilization at the typical layout values: over the 1200 K for the BHX option, and slightly higher than the reference values (more than 900 K) for the PEHX one. In both cases, even in the range of their typical values, the temperatures are higher than the average obtained in all the studies.

The temperature of the Mixed Conductive Membrane (Figure 4.24) resembles the same trend of the previous study undertook for the plant with the pressure on the permeate side as high as the compressor outlet one but, since the range where ρ is varying is wider, it gives a more complete picture. In fact can be observed as at high and low values of ρ the difference in the membrane temperature for the two layouts reduces remarkably while during the "approach" to the limit temperature, they respond with different readiness (the BHX layout quicker than the PEHX one).

4.2.4 Compressor bleed mass flow effect

When considering the effect of the mass flow bled from the compressor outlet and addressed to be heated up (or, equally, to cool down the flue gas), can obviously be considered just the BHX layout. Also in this case, in agreement

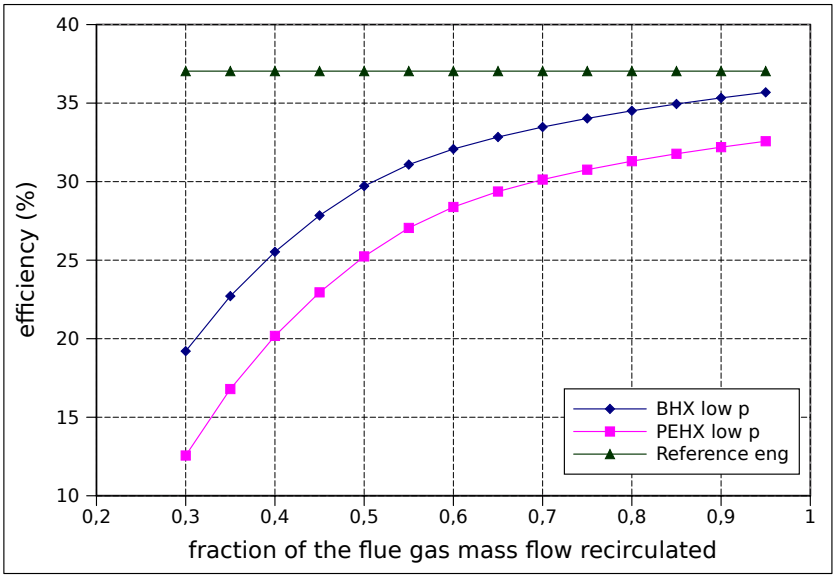

Figure 4.21. AZEP overall thermal efficiencies as a function of the recirculated flue gas mass flow expressed as a fraction over the inlet engine mass flow. The permeate side pressure is constant and almost atmospheric. The reference engine corresponding value is represented.

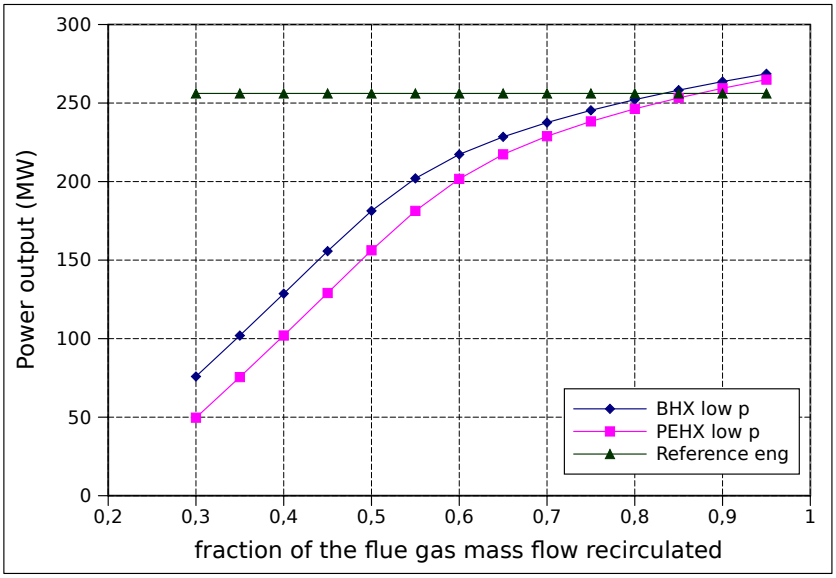

Figure 4.22. Power output of the eAZEP layouts for increasing values of the recirculated flue gas mass flow expressed as a fraction over the inlet engine mass flow. The results suppose a constant atmospheric pressure on the permeate side and are compared with the reference case value.

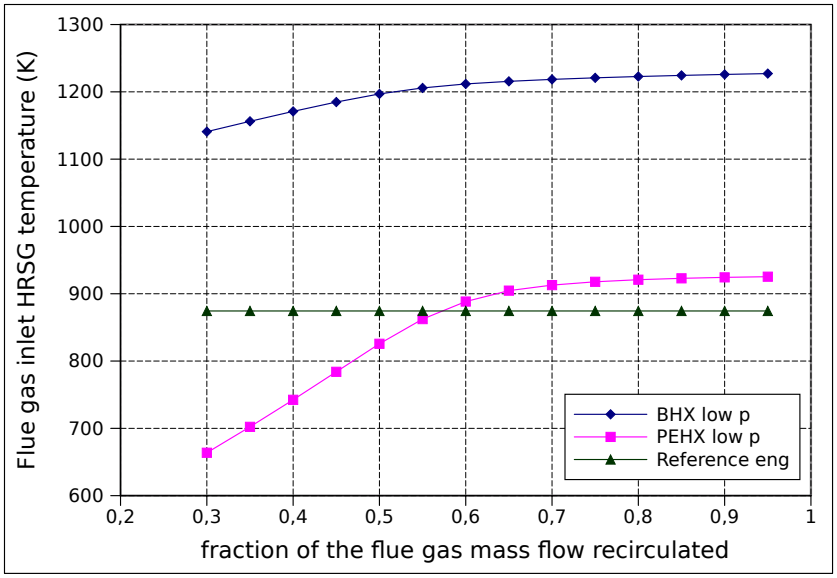

Figure 4.23. Flue gas HRSG inlet temperature for the AZEP cycles as a function of the recirculated flue gas mass flow expressed as a fraction over the inlet engine mass flow. The pressure on the permeate side is kept constant and almost at ambient pressure. The reference power plant value is included for comparison purposes.

with the internal representation of the quantity in eAZEP, the bleed mass flow (W_{20} in the Process Flow Diagram of Figure 3.1) has been expressed with an non-dimensional fraction β where the reference mass flow is the engine inlet one:

$$\beta = \frac{W_{20}}{W_{\text{in,eng}}} \tag{4.2}$$

The fraction of the bled mass flow has been changed from 0.01 to 0.2. All the results presented in this section are obtained with a recirculated flue gas mass flow of 448 $^{\text{kg}}/_{\text{s}}$ and a constant oxygen removal rate of 50% for the ambient pressure permeate side case.

In the first study (with the pressure on the permeate side equal to the value at the outlet of the compressor) since the air mass flow is reducing more and more with the increase of β, the average oxygen partial pressure on the feed side is reducing accordingly. This last conclusion is true if the removal rate of the oxygen is kept constant. So, under these assumptions, at high β can happen that the average oxygen partial pressure on the feed side become so close to the permeate partial pressure to require an area too large to be acceptable — Equation (3.56). This is why is necessary to gradually reduce the percentage of the oxygen removed over the theoretical amount while the

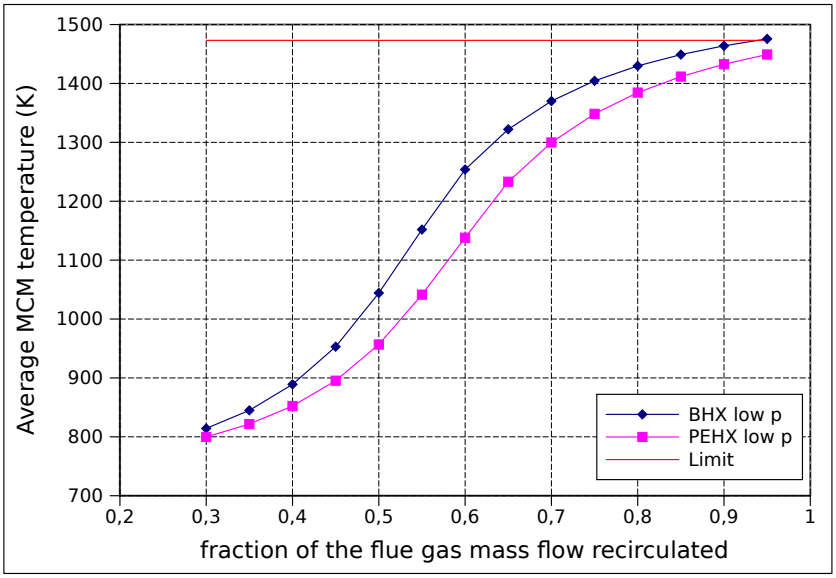

Figure 4.24. Average temperature of the MCM compared to its limit of 1200 °C [5, 6, 7], when the recirculated flue gas mass flow (expressed as a fraction over the inlet engine mass flow) is increasing. The permeate side pressure of the power plant is constant and equal to the atmospheric pressure.

bleed mass flow is increasing. Quantitatively the aforementioned percentage is reduced from the 40% for the smallest β to 32.4% for $\beta = 0.2$.

Permeate side pressure equal to the compressor outlet pressure

The efficiency trends of the BHX layouts in this case (Figure 4.25) are easily predictable. The base AZEP cycle shows an optimal value of the bled mass flow, around the 15%, where the other important result is the remarkable reduction of the exhaust flue gas temperature (Figure 4.27). So, for combined cycle applications, the β fine tuning can make the *simple* BHX layout a close competitor of the *simple* PEHX option. Unfortunately, the power output shows (Figure 4.26) a drop very important also where the efficiency is still quite high ($\beta > 0.16$).

As predictable, the increase of the bleed mass flow has a detrimental effect on the layout with the additional turbine because the flue gas become cooler and cooler, reducing the entry temperature of the flue gas expander. Then the efficiency shows a slight reduction, more sensitive at higher β, while the power output drops constantly and definitely. There are no different effects on the flue gas exhaust temperature than usual: the trend of the scheme with

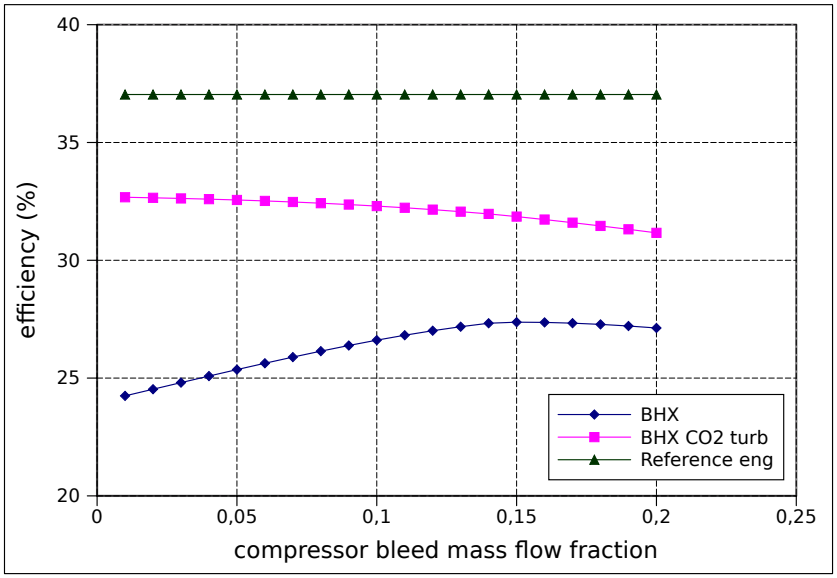

Figure 4.25. AZEP overall thermal efficiencies as a function of the mass flow bled from the compressor expressed as a fraction of the inlet engine mass flow. The reference engine value is also reported.

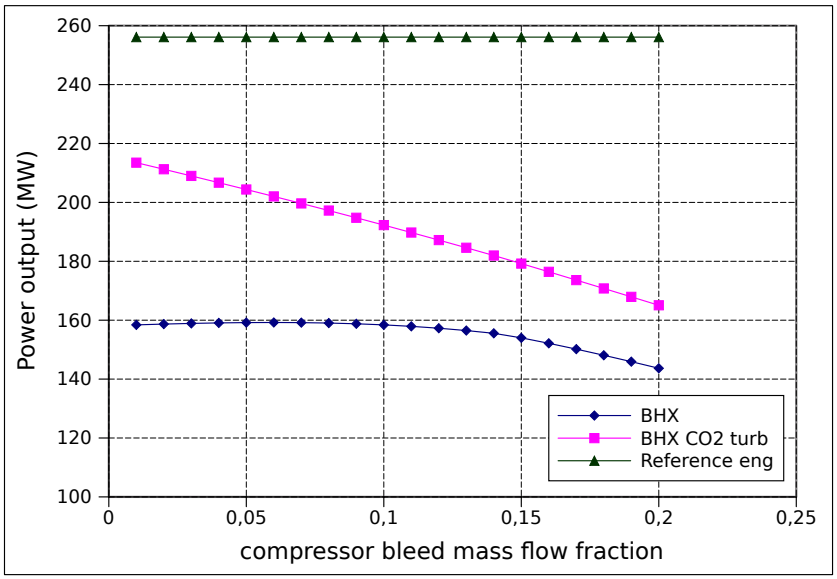

Figure 4.26. Power output of the eAZEP layouts for different fractions of the mass flow bled from the compressor over the inlet engine mass flow. The reference case value is reported.

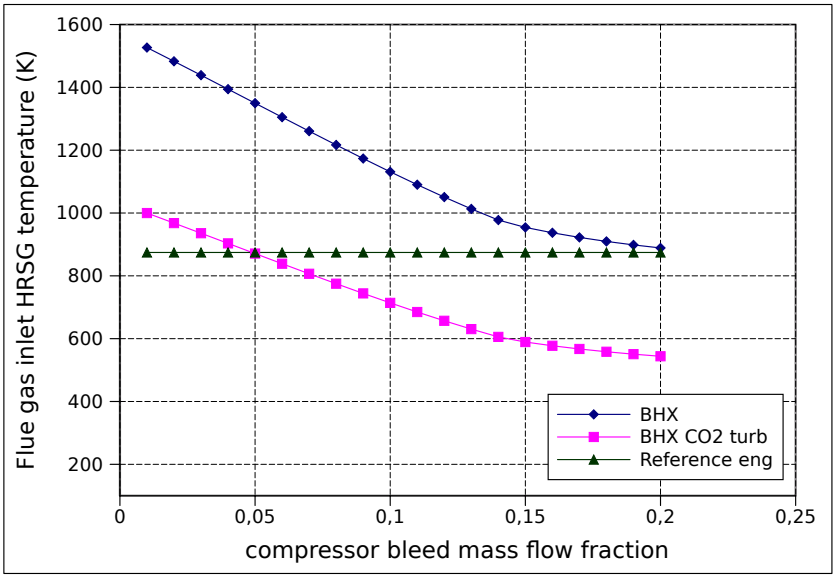

Figure 4.27. Flue gas HRSG inlet temperature for the AZEP cycles as a function of the fraction of the bled mass flow from the compressor over the inlet engine mass flow. The corresponding reference engine value is reported.

the additional turbine is the same of the simple BHX but it is shifted lower on the temperature axis of about 500 K.

As usual, the Mixed Conductive Membrane is not affected at all by the insertion of the additional turbine and its average temperature (Figure 4.28) study shows on the chart no difference for the two layouts. It is interesting to notice how the prescribed limit of the MCM temperature is approached rapidly while the bleed mass flow increase. This effect is due to the reduced heat capacity rate of the air stream (the cold flow) that gives way to the heating effect of the hot stream.

Low constant permeate side pressure

When considering the pressure on the permeate side very low (slightly higher than the ambient pressure), as often happens, it is possible to have a more complete picture of the trends and the response of the power plant when the parameter object of the study is varying. In fact, observing the results for the efficiency (Figure 4.29), it is undisguised that the optimal β is moved at higher values giving the possibility to the AZEP cycle to achieve an higher efficiency than its counterpart in the higher pressure permeate side study.

Anyway the most interesting results chart of this series is surely the power

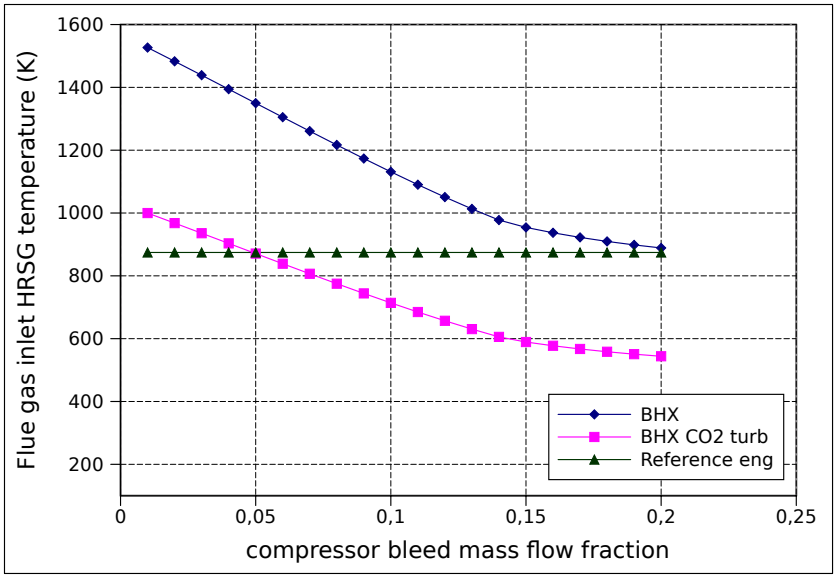

Figure 4.28. Average temperature of the MCM compared to its limit of 1200 °C [5, 6, 7], when the fraction of the mass flow bled from the compressor outlet over the inlet engine mass flow is increasing.

output one (Figure 4.30) where is clear how there is an optimal β also for the output work of the power plant. Since this optimal value is lower compared with its counterpart for the efficiency study, it was less marked in the higher pressure permeate side study. The reasons for this results are mainly related with the effect of the BHX on the inlet temperature of the air turbine which is influenced also by the outlet temperature of the air stream in the HTHX.

Very interesting is also to notice how the exhaust flue gas temperature can be effectively reduced very remarkably with the increase of just a few percentage points of the bleed mass flow fraction (Figure 4.31). Unfortunately, should be also pointed out that in order to bring the exhaust temperature below 1000 K ($\beta > 0.18$) must be accepted a penalty on the power output; altogether it results, anyhow, a good compromise.

Also in this case the average temperature of the Mixed Conductive Membrane increase rapidly with the increase of the mass flow bled from the compressor (Figure 4.32). The trend also in this case is explainable with the reduction of the heat capacity rate of the cold stream through the membrane.

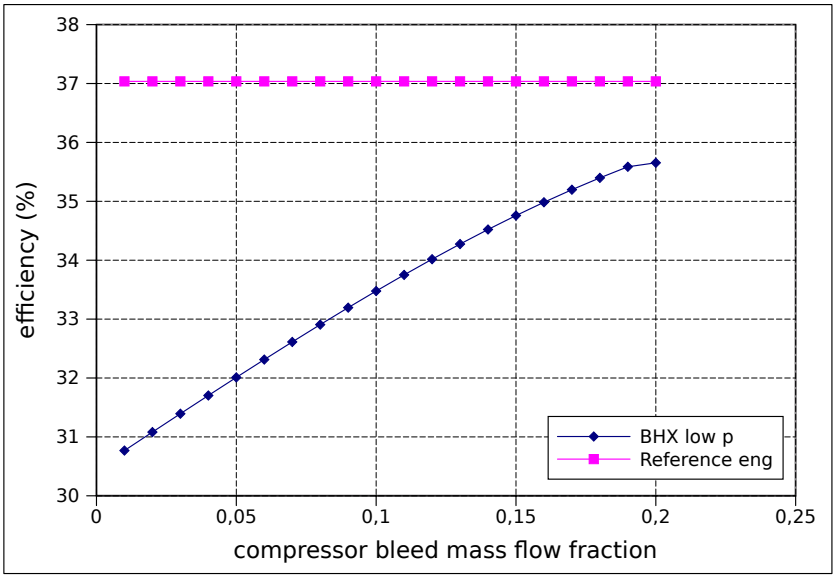

Figure 4.29. AZEP overall thermal efficiencies as a function of the mass flow bled from the compressor expressed as a fraction over the inlet engine mass flow. The permeate side pressure is constant and almost atmospheric. The reference engine corresponding value is represented.

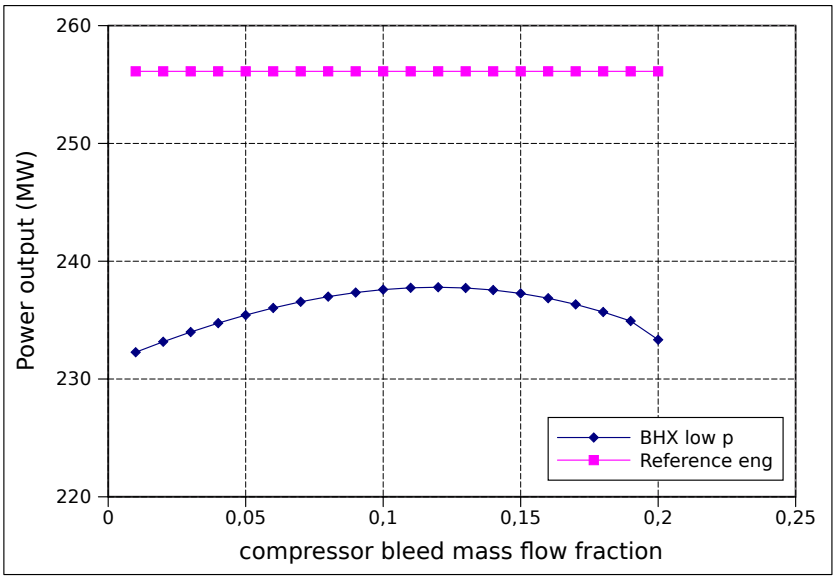

Figure 4.30. Power output of the eAZEP layouts for increasing values of the mass flow bled from the compressor as a fraction over the inlet engine mass flow. The results suppose a constant atmospheric pressure on the permeate side and are compared with the reference case value.

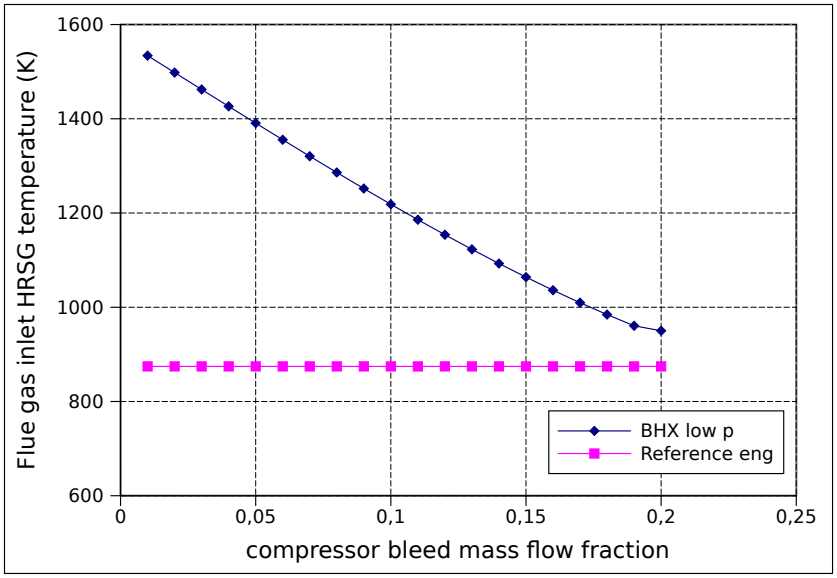

Figure 4.31. Flue gas HRSG inlet temperature for the AZEP cycles as a function of the mass flow bled from the compressor expressed as a fraction over the inlet engine mass flow. The pressure on the permeate side is kept constant and almost at ambient pressure. The reference power plant value is included for comparison purposes.

4.3 Conclusions

Carrying out a comparison based on the results highlighted in the singular studies, among the layouts available in eAZEP, the best choice is undoubtedly the PEHX option with the flue gas additional turbine. In fact, not only it shows the best performance as a stand alone thermodynamic cycle, but it also provides the flue gas stream at the optimal conditions for its exploitation in a combined cycle plant featured with an HRSG.

Discarding, instead, the expensive implementation of the additional turbine, the choice between the BHX and the PEHX layout is not straightforward. If on one hand the BHX option shows better efficiencies and higher power output for a fixed set of conditions, on the other it always suffers from too high exhaust temperature on the flue gas side and from a similar tendency for the membrane temperature. Has been showed in the last section that with the tuning of the mass flow bled from the compressor, is possible to soothe this trouble but, for a fixed exhaust temperature, the PEHX layout could be better performing.

From a rational point of view, the PEHX scheme suits better the combined cycle arrangement since it equalizes the temperature of the depleted air stream

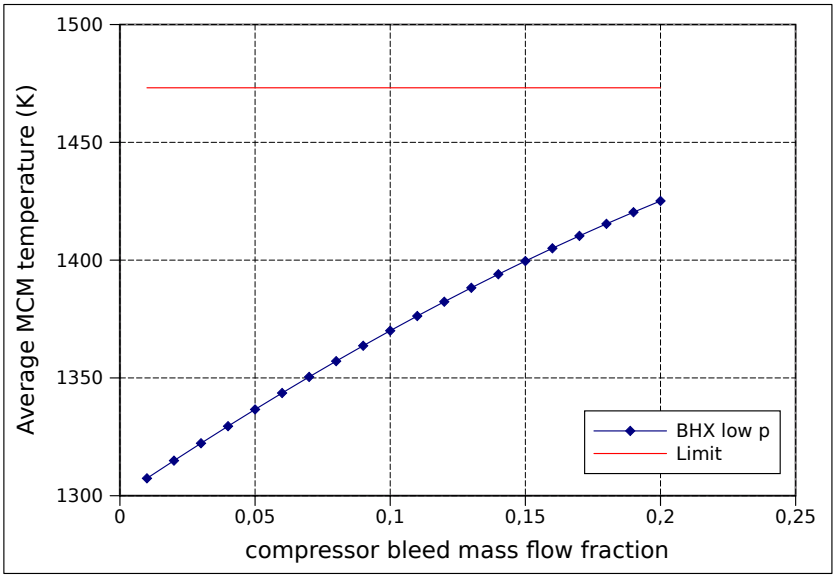

Figure 4.32. Average temperature of the MCM compared to its limit of 1200 °C [5, 6, 7], when the mass flow bled from the compressor outlet (expressed as a fraction over the inlet engine mass flow) is increasing. The permeate side pressure of the power plant is constant and equal to the atmospheric value.

and the flue gas stream optimising their thermal energy available in the HRSG. This advantage is just partially perceptible in the results reported; in fact, the exhaust temperature on the *air side* is not presented being usually closer to the conventional exhaust temperatures. It is likely that the lower efficiency and power output obtained by the stand-alone AZEP with PEHX layout, would be paid back by the better performance of the bottoming cycle.

One last conclusion can be pointed out from the series of the results obtained. Every effort spent in the enhancement of the mechanical and thermal properties of the Mixed Conductive Membrane materials are profusely repaid on the thermodynamic point of view allowing the reduction of the permeate side pressure and, then, boosting the performance of the power plant. Unfortunately this technological breakthrough is to be hoped in the best case scenario for the medium term view.

Summarizing, at the present technological state-of-the-art of the AZEP cycle components, the PEHX with the flue gas turbine arrangement is clearly the best option when investigating the complete sequestration of the carbon dioxide. Between the options without the additional turbine, the PEHX solution appears more suitable for the combined cycle integration, while the BHX arrangement seems more attractive for a stand alone power plant. Potential further studies surely would clarify especially this last point.

Chapter 5

Conclusions

A literature review was carried out to outline the basic aspects of the carbon capture techniques in the power generation sector. It showed that there are three main options in the topic:

- the pre-combustion capture;
- the oxy-fuel combustion;
- the post-combustion capture.

They were described briefly before to focus on the oxy-fuel cycles. Four concepts of this last category were considered:

- the semi-closed cycle;
- the Chemical Looping Combustion cycle;
- the electrochemical reactions in fuel cells;
- the AZEP cycle.

The last one is the object of this project, so was performed a broad literature survey on it and a detailed description of the cycle showing that

- there are no extensive studies dedicated *only* to the AZEP concept;
- most of the literature does not detail completely the computational assumptions;
- there is no evidence of a sensitivity analysis that investigates the potential of the cycle for different applications and highlights the key parameters that affect its performance.

Consequently, the objectives of this project are

- to provide a flexible, modular, modern computational tool (the eAZEP program) to investigate the AZEP cycle potential;
- to evaluate several AZEP layouts assessing their performance as a function of the cycle characteristic parameters and the technological level of the components (especially the Mixed Conductive Membrane);
- to provide a completely new off-design calculation routine for the bottoming steam plant to be used in the AZEP combined cycle arrangement.

All the efforts are strictly correlated to the main objective to contribute at the larger "Advanced Low Carbon Power Systems" project in order to provide computational tools and simulation results.

All the goals are achieved, mostly thanks to the development and use of eAZEP. The numerical results of the simulations show that

- the PEHX layout with the flue gas additional turbine is the best configuration of the AZEP cycle;
- between the simple layouts, without additional expander, the BHX option suits better stand-alone applications while the PEHX shows a better attitude for the combined cycle implementation;
- the improvement of the Mixed Conductive Membrane technological level can boost the overall plant performance at very competitive ranks, thanks to the reduction of the permeate side pressure.

Should be emphasized that this work contributed with original concepts to the knowledge about the topic. In particular, at the knowledge of the author, the following ideas are not present in the open literature

- the Post Expansion Heat exchanger layouts;
- the performance evaluation of the power plant for high values of the pressure ratio across the Mixed Conductive Membrane;
- a sensitivity analysis of the AZEP cycle.

Chapter 6

Future work

After the development of eAZEP, the most natural and easy step to carry out is to broaden the sensitivity analysis of the cycle considering

- more characteristic cycle parameters, also exploiting the results provided in this work which can suggest the quantities to investigate further;
- more layouts, as for instance the AZEP 85%, thanks to the modular structure of eAZEP that makes this task straightforward.

Can be also interesting to refine the membrane model improving the lumped approximation with the substitution of the Mixed Conductive Membrane with a series of devices which will bring more accurate results with the discretization of the process. In order to avoid an excessive increase of the computational effort for the membrane only, an appropriate numerical model in order to solve this particular application should be chosen and implemented; although eAZEP is able to provide its solver.

For the sake of accuracy, should be desirable to implement a precise model of the steam (at least in the flue gas mixture) in order to improve the reliability of the results. Must be observed, in fact, that especially in the flue gas of the AZEP cycle the oxygen fraction in the mixture is far higher than usual (even in comparison to the flue gas of a conventional gas turbine engine) and a model based just on the dependence from the temperature like the one implemented in eAZEP, could become not accurate enough for certain steam concentrations. The suggested model is the International Association for the Properties of Water and Steam (IAPWS) Industrial Formulation 1997 (IF-97)[1] that should provide a valuable model at a reasonable computational cost.

[1] http://www.iapws.org/relguide/IF97-Rev.pdf.

Without any doubt eAZEP should also be integrated with a combined cycle computational model in order to expand, correct and quantify the qualitative conclusions given in this work about the different layouts for combined cycle purposes, and also to compare the results with the few literature data.

It would be undoubtedly useful to carry out also a thermo-economic analysis of the cycle based on eAZEP in order to assess the profitability of the different industrial implementations of the alternative plant layouts.

Appendix A

Turbomachinery processes with real gas effect

In this chapter will be shown the derivation of the formula used to determine the output temperature of a turbomachinery. Since we are taking into account the variation of the specific heat at constant pressure with the temperature, it is necessary to correlate the polytropic efficiency with a thermodynamic function dependent from the temperature. Will be shown that it coincides with the entropy, considering the operating fluids model adopted in this work.

The proof will be carried out for a compression process, but it is applicable similarly for an expansion. Consider the first law of thermodynamics applied to the device (supposed adiabatic) both in the thermal and mechanical form

$$\mathcal{W} = h_2 - h_1 \tag{A.1}$$

$$\mathcal{W} = \int_1^2 v \, \mathrm{d}p + \mathcal{W}_\mathrm{w} \tag{A.2}$$

where $\mathcal{W}$ is the specific work and $\mathcal{W}_\mathrm{w}$ is the work lost in the process between the states 1 and 2. Considering the differential form of the previous expressions

$$\mathrm{d}\mathcal{W} = \mathrm{d}h_2 - \mathrm{d}h_1 = \mathrm{d}h \tag{A.3}$$

$$\mathrm{d}\mathcal{W} = v \, \mathrm{d}p + \mathrm{d}\mathcal{W}_\mathrm{w} \tag{A.4}$$

results that

$$\mathrm{d}h = \mathrm{d}\mathcal{W} = v \, \mathrm{d}p + \mathrm{d}\mathcal{W}_\mathrm{w} \tag{A.5}$$

but since

$$\mathrm{d}h = c_p \, \mathrm{d}T \tag{A.6}$$

results

$$c_p \, \mathrm{d}T = v \, \mathrm{d}p + \mathrm{d}\mathcal{W}_\mathrm{w} \tag{A.7}$$

For a compressor, the polytropic efficiency $\eta_{\mathrm{y,c}}$ is expressed as

$$\eta_{\mathrm{y,c}} = \frac{v\,\mathrm{d}p}{\mathrm{d}\mathcal{W}} \tag{A.8}$$

and substituting the Equation (A.4) gives

$$\eta_{\mathrm{y,c}} = \frac{v\,\mathrm{d}p}{v\,\mathrm{d}p + \mathrm{d}\mathcal{W}_{\mathrm{w}}} \tag{A.9}$$

After simple algebraic passages, results

$$\mathrm{d}\mathcal{W}_{\mathrm{w}} = \frac{v\,\mathrm{d}p}{\eta_{\mathrm{y,c}}} - v\,\mathrm{d}p \tag{A.10}$$

Substituting the last expression of $\mathrm{d}\mathcal{W}_{\mathrm{w}}$ in Equation (A.7)

$$c_p\,\mathrm{d}T = \cancel{v\,\mathrm{d}p} + \frac{v\,\mathrm{d}p}{\eta_{\mathrm{y,c}}} - \cancel{v\,\mathrm{d}p}$$

yelds to

$$\eta_{\mathrm{y,c}}\,c_p\,\mathrm{d}T = v\,\mathrm{d}p \tag{A.11}$$

Since the gas behaves according to the ideal gas law, the specific volume can be substituted

$$v = \frac{\mathcal{R}\,T}{p}$$

thus

$$\eta_{\mathrm{y,c}}\,c_p\,\mathrm{d}T = \frac{\mathcal{R}\,T}{p}\,\mathrm{d}p \tag{A.12}$$

that results in

$$\eta_{\mathrm{y,c}}\,c_p\,\frac{\mathrm{d}T}{T} = \mathcal{R}\,\frac{\mathrm{d}p}{p} \tag{A.13}$$

Integrating the previous equality between the states 1 and 2

$$\int_1^2 \eta_{\mathrm{y,c}}\,c_p\,\frac{\mathrm{d}T}{T} = \int_1^2 \mathcal{R}\,\frac{\mathrm{d}p}{p} \tag{A.14}$$

$$\eta_{\mathrm{y,c}}\int_1^2 c_p\,\frac{\mathrm{d}T}{T} = \mathcal{R}\int_1^2 \frac{\mathrm{d}p}{p} \tag{A.15}$$

it is possible to obtain the final formula starting from the definition of the entropy for an ideal gas

$$s_2 - s_1 = \int_1^2 c_p\,\frac{\mathrm{d}T}{T} - \mathcal{R}\int_1^2 \frac{\mathrm{d}p}{p} \tag{A.16}$$

So, since *in this work*[1] the model of the thermodynamic functions for the working fluid is not dependent on the pressure, the second addend must be cancelled

$$s_2 - s_1 = \int_1^2 c_p \frac{\mathrm{d}T}{T}$$

and the previous equality could be directly substituted in the Equation (A.15)

$$\eta_{\mathrm{y,c}} \left(s_2 - s_1\right) = \mathcal{R} \ln\left(\frac{p_2}{p_1}\right) \tag{A.17}$$

The proof is very similar for a turbine, the only difference is the definition of the polytropic efficiency $\eta_{\mathrm{y,t}}$ in the case of an expansion

$$\eta_{\mathrm{y,t}} = \frac{v\,\mathrm{d}p + \mathrm{d}\mathcal{W}_{\mathrm{w}}}{v\,\mathrm{d}p} \tag{A.18}$$

The final result for a turbine reads:

$$\frac{(s_1 - s_2)}{\eta_{\mathrm{y,t}}} = \mathcal{R} \ln\left(\frac{p_1}{p_2}\right) \tag{A.19}$$

[1] Please note that the subsequent derivations are *no more valid* if it is adopted a different model where the entropy is function of the pressure, too.

Appendix B

Combustor outlet composition for a gas-methane reaction

In this chapter will be showed analytically how to obtain the final composition vector at the end of the combustion phase in a generic reactor (Figure B.1) that has no losses for imperfect combustion and for heat leakage. The inlet fluid is supposed to be a mixture comprised of argon, carbon dioxide, oxygen, nitrogen, and steam, while the fuel is a mixture of methane and nitrogen.

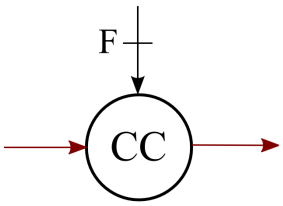

Figure B.1. The process flow diagram for a generic combustor.

The chemical reaction of the active species is the following

$$CH_4 + 2\,O_2 \longrightarrow 2\,H_2O + CO_2 \tag{B.1}$$

and the final result that will be proofed is

$$\begin{cases} f_{\mathrm{Ar}}^{\mathrm{out}} = f_{\mathrm{Ar}}^{\mathrm{in}} \dfrac{\alpha}{\alpha+1} \\ f_{\mathrm{CO_2}}^{\mathrm{out}} = f_{\mathrm{CO_2}}^{\mathrm{in}} \dfrac{\alpha}{\alpha+1} + \dfrac{\mathcal{M}_{\mathrm{CO_2}}}{\mathcal{M}_{\mathrm{CH_4}}} \dfrac{f_{\mathrm{CH_4}}^{\mathrm{f}}}{\alpha+1} \\ f_{\mathrm{O_2}}^{\mathrm{out}} = f_{\mathrm{O_2}}^{\mathrm{in}} \dfrac{\alpha-\alpha_s}{\alpha+1} \\ f_{\mathrm{N_2}}^{\mathrm{out}} = f_{\mathrm{N_2}}^{\mathrm{in}} \dfrac{\alpha}{\alpha+1} + \dfrac{f_{\mathrm{N_2}}^{\mathrm{f}}}{\alpha+1} \\ f_{\mathrm{H_2O}}^{\mathrm{out}} = f_{\mathrm{H_2O}}^{\mathrm{in}} \dfrac{\alpha}{\alpha+1} + \dfrac{\mathcal{M}_{\mathrm{H_2O}}}{\mathcal{M}_{\mathrm{CH_4}}} \dfrac{2\, f_{\mathrm{CH_4}}^{\mathrm{f}}}{\alpha+1} \end{cases} \tag{B.2}$$

The starting point is from the mass balance of the device

$$W_{\mathrm{in}} + W_{\mathrm{f}} = W_{\mathrm{out}} \tag{B.3}$$

and combines it with the definition of the gas-fuel-ratio α

$$\alpha = \frac{W_{\mathrm{in}}}{W_{\mathrm{f}}} \tag{B.4}$$

so that

$$W_{\mathrm{out}} = W_{\mathrm{in}} \frac{\alpha+1}{\alpha} \tag{B.5}$$

Since the component is supposed to work at steady state, the same formula could be re-written referred to the unit of time

$$m_{\mathrm{out}} = m_{\mathrm{in}} \frac{\alpha+1}{\alpha} \tag{B.6}$$

where m is the mass. Taking the reciprocal of both sides of the equality, it is obtained

$$\frac{1}{m_{\mathrm{out}}} = \frac{1}{m_{\mathrm{in}}} \frac{\alpha}{\alpha+1} \tag{B.7}$$

From this equation follows a different proof for each of the gas components.

B.1 Argon and other inert gas

Multiplying both the sides of Equation (B.7) by the mass of the argon m_{Ar} that is an inert gas and then remains constant before and after the reaction ($m_{\mathrm{Ar}} = m_{\mathrm{Ar}}^{in} = m_{\mathrm{Ar}}^{out}$), results

$$\frac{m_{\mathrm{Ar}}}{m_{\mathrm{out}}} = \frac{m_{\mathrm{Ar}}}{m_{\mathrm{in}}} \frac{\alpha}{\alpha+1} \tag{B.8}$$

Remembering the definition of the mass fraction $f_i = {}^{m_i}/_{m_{\text{tot}}}$, the final formula is obtained

$$f_{\text{Ar}}^{\text{out}} = f_{\text{Ar}}^{\text{in}} \frac{\alpha}{\alpha + 1} \tag{B.9}$$

The same procedure can be followed for the *inlet* quantities of the carbon dioxide and steam: they actually behave passively in the regards of the reaction. In fact this model does not include *any* chemical equilibrium effect that would be affected by a potential high concentration of CO_2 or H_2O.

B.2 Nitrogen

Although the nitrogen is an inert gas, the proof in the previous section can not be applied exactly for it because in the fuel is present an additional fraction of nitrogen $f_{\text{N}_2}^{\text{f}}$.

Thus multiplying both the sides of Equation (B.7) by the final mass of nitrogen $m_{\text{N}_2}^{\text{out}}$

$$\frac{m_{\text{N}_2}^{\text{out}}}{m_{\text{out}}} = \frac{m_{\text{N}_2}^{\text{out}}}{m_{\text{in}}} \frac{\alpha}{\alpha + 1} \tag{B.10}$$

and simply observing that $m_{\text{N}_2}^{\text{out}} = m_{\text{N}_2}^{\text{in}} + m_{\text{N}_2}^{\text{f}}$ results

$$f_{\text{N}_2}^{\text{out}} = \frac{m_{\text{N}_2}^{\text{in}} + m_{\text{N}_2}^{\text{f}}}{m_{\text{in}}} \frac{\alpha}{\alpha + 1} \tag{B.11}$$

Multiplying and dividing by the total fuel mass m_{f} the right-hand side of the previous expression rearranged

$$f_{\text{N}_2}^{\text{out}} = f_{\text{N}_2}^{\text{in}} \frac{\alpha}{\alpha + 1} + \frac{m_{\text{N}_2}^{\text{f}}}{m_{\text{f}}} \frac{m_{\text{f}}}{m_{\text{in}}} \frac{\alpha}{\alpha + 1} \tag{B.12}$$

and remembering that $\alpha = {}^{m_{\text{in}}}/_{m_{\text{f}}}$

$$f_{\text{N}_2}^{\text{out}} = f_{\text{N}_2}^{\text{in}} \frac{\alpha}{\alpha + 1} + f_{\text{N}_2}^{\text{f}} \frac{1}{\alpha} \frac{\alpha}{\alpha + 1} \tag{B.13}$$

it is possible to write the final formula

$$f_{\text{N}_2}^{\text{out}} = f_{\text{N}_2}^{\text{in}} \frac{\alpha}{\alpha + 1} + \frac{f_{\text{N}_2}^{\text{f}}}{\alpha + 1} \tag{B.14}$$

B.3 Carbon dioxide

As usual, the first step is to multiply Equation (B.7) by the final mass of carbon dioxide $m^{\text{out}}_{\text{CO}_2}$

$$\frac{m^{\text{out}}_{\text{CO}_2}}{m_{\text{out}}} = \frac{m^{\text{out}}_{\text{CO}_2}}{m_{\text{in}}} \frac{\alpha}{\alpha+1} \tag{B.15}$$

Observing that the final CO_2 mass is the sum of the inlet quantity plus its stoichiometric mass $m^{\text{s}}_{\text{CO}_2}$ derived from the complete chemical reaction (B.1), results

$$\frac{m^{\text{out}}_{\text{CO}_2}}{m_{\text{out}}} = \frac{m^{\text{in}}_{\text{CO}_2} + m^{\text{s}}_{\text{CO}_2}}{m_{\text{in}}} \frac{\alpha}{\alpha+1} \tag{B.16}$$

that rearranged gives

$$f^{\text{out}}_{\text{CO}_2} = \left(f^{\text{in}}_{\text{CO}_2} + \frac{m^{\text{s}}_{\text{CO}_2}}{m_{\text{in}}} \right) \frac{\alpha}{\alpha+1} \tag{B.17}$$

Expanding the expression and substituting α in the last term at the right-hand side

$$f^{\text{out}}_{\text{CO}_2} = f^{\text{in}}_{\text{CO}_2} \frac{\alpha}{\alpha+1} + \frac{m^{\text{s}}_{\text{CO}_2}}{m_{\text{in}}} \frac{m_{\text{in}}}{m_{\text{f}}} \frac{1}{\alpha+1} \tag{B.18}$$

remembering that $m_{\text{f}} = {}^{m_{\text{CH}_4}}/_{f^{\text{f}}_{\text{CH}_4}}$ results

$$f^{\text{out}}_{\text{CO}_2} = f^{\text{in}}_{\text{CO}_2} \frac{\alpha}{\alpha+1} + \frac{m^{\text{s}}_{\text{CO}_2}}{m_{\text{in}}} \frac{m_{\text{in}}}{m_{\text{CH}_4}} \frac{f^{\text{f}}_{\text{CH}_4}}{\alpha+1} \tag{B.19}$$

Cancelling and using the molar expression of the mass $m = n \cdot \mathcal{M}$ it is obtained

$$f^{\text{out}}_{\text{CO}_2} = f^{\text{in}}_{\text{CO}_2} \frac{\alpha}{\alpha+1} + \frac{n^{\text{s}}_{\text{CO}_2} \mathcal{M}_{\text{CO}_2}}{n_{\text{CH}_4} \mathcal{M}_{\text{CH}_4}} \frac{f^{\text{f}}_{\text{CH}_4}}{\alpha+1} \tag{B.20}$$

and since in the stoichiometric reaction one mole of carbon dioxide and one mole of methane are involved, it is possible to derive the final expression present in (B.2)

$$f^{\text{out}}_{\text{CO}_2} = f^{\text{in}}_{\text{CO}_2} \frac{\alpha}{\alpha+1} + \frac{\mathcal{M}_{\text{CO}_2}}{\mathcal{M}_{\text{CH}_4}} \frac{f^{\text{f}}_{\text{CH}_4}}{\alpha+1} \tag{B.21}$$

B.4 Oxygen

In order to make the proof easier, it is better to derive the stoichiometric gas-fuel-ratio α_{s} for the combustion reaction first. Starting from its definition

it is possible to carry out same simple derivations

$$\alpha_{\mathrm{s}} = \frac{m^{\mathrm{s}}_{\mathrm{in}}}{m^{\mathrm{s}}_{\mathrm{f}}} = \frac{m^{\mathrm{s}}_{\mathrm{in}}}{m^{\mathrm{s}}_{\mathrm{CH_4}}} f^{\mathrm{f}}_{\mathrm{CH_4}} = \frac{n^{\mathrm{s}}_{\mathrm{in}} \mathcal{M}^{\mathrm{in}}_{\mathrm{gas}}}{n^{\mathrm{s}}_{\mathrm{CH_4}} \mathcal{M}_{\mathrm{CH_4}}} f^{\mathrm{f}}_{\mathrm{CH_4}} \tag{B.22}$$

Remembering the molar fraction definition for the oxygen $\chi_{\mathrm{O_2}} = {}^{n_{\mathrm{O_2}}}/_{n_{\mathrm{gas}}}$ and that the stoichiometric molar ratio between the oxygen and the methane is ${}^{2}/_{1}$ — Reaction (B.1) — results

$$\alpha_{\mathrm{s}} = \frac{2\, f^{\mathrm{f}}_{\mathrm{CH_4}}}{\chi_{\mathrm{O_2}}} \frac{\mathcal{M}_{\mathrm{gas}}}{\mathcal{M}_{\mathrm{CH_4}}} \tag{B.23}$$

that, after a bit of algebra, turns out in the desired final expression of the stoichiometric gas-fuel-ratio

$$\alpha_{\mathrm{s}} = \frac{2\, f^{\mathrm{f}}_{\mathrm{CH_4}}}{f^{\mathrm{in}}_{\mathrm{O_2}}} \frac{\mathcal{M}_{\mathrm{O_2}}}{\mathcal{M}_{\mathrm{CH_4}}} \tag{B.24}$$

Returning back to the main proof, it is necessary to multiply Equation (B.7) by the final mass of oxygen $m^{\mathrm{out}}_{\mathrm{O_2}}$

$$\frac{m^{\mathrm{out}}_{\mathrm{O_2}}}{m_{\mathrm{out}}} = \frac{m^{\mathrm{out}}_{\mathrm{O_2}}}{m_{\mathrm{in}}} \frac{\alpha}{\alpha + 1} \tag{B.25}$$

since the final amount of oxygen is the excess of the stoichiometric quantity $m^{\mathrm{out}}_{\mathrm{O_2}} = m^{\mathrm{in}}_{\mathrm{O_2}} - m^{\mathrm{s}}_{\mathrm{O_2}}$, results

$$f^{\mathrm{out}}_{\mathrm{O_2}} = \frac{m^{\mathrm{in}}_{\mathrm{O_2}} - m^{\mathrm{s}}_{\mathrm{O_2}}}{m_{\mathrm{in}}} \frac{\alpha}{\alpha + 1} \tag{B.26}$$

that becomes

$$f^{\mathrm{out}}_{\mathrm{O_2}} = \frac{1}{\alpha + 1} \left(\alpha\, f^{\mathrm{in}}_{\mathrm{O_2}} - \alpha \frac{m^{\mathrm{s}}_{\mathrm{O_2}}}{m_{\mathrm{in}}} \right) \tag{B.27}$$

and finally making $f^{\mathrm{in}}_{\mathrm{O_2}}$ explicit on the right-hand side, results

$$f^{\mathrm{out}}_{\mathrm{O_2}} = \frac{f^{\mathrm{in}}_{\mathrm{O_2}}}{\alpha + 1} \left(\alpha - \alpha \frac{m^{\mathrm{s}}_{\mathrm{O_2}}}{m_{\mathrm{in}}} \frac{1}{f^{\mathrm{in}}_{\mathrm{O_2}}} \right) \tag{B.28}$$

Considering now just the last addend between the parentheses

$$\alpha \frac{m^{\mathrm{s}}_{\mathrm{O_2}}}{m_{\mathrm{in}}} \frac{1}{f^{\mathrm{in}}_{\mathrm{O_2}}}$$

it is possible to substitute $f^{\text{in}}_{\text{O}_2}$ and α

$$\frac{m_{\text{in}}}{m_{\text{f}}}\frac{m^{\text{s}}_{\text{O}_2}}{m_{\text{in}}}\frac{m_{\text{in}}}{m^{\text{in}}_{\text{O}_2}} = \frac{m_{\text{in}}}{m_{\text{CH}_4}} f^{\text{f}}_{\text{CH}_4}\frac{m^{\text{s}}_{\text{O}_2}}{m^{\text{in}}_{\text{O}_2}} \tag{B.29}$$

substituting the mass as a product of the number of moles times the molecular weight, results

$$\frac{n^{\text{in}}_{\text{gas}}\,\mathcal{M}_{\text{gas}}}{n^{\text{s}}_{\text{CH}_4}\,\mathcal{M}_{\text{CH}_4}}\frac{n^{\text{s}}_{\text{O}_2}\,\mathcal{M}_{\text{O}_2}}{n^{\text{in}}_{\text{O}_2}\,\mathcal{M}_{\text{O}_2}} f^{\text{f}}_{\text{CH}_4} \tag{B.30}$$

In the last expression is possible to substitute the definition of χ_{O_2} and the stoichiometric oxygen-methane molar ratio (equal to 2)

$$\frac{2\, f^{\text{f}}_{\text{CH}_4}}{\chi_{\text{O}_2}}\frac{\mathcal{M}_{\text{gas}}}{\mathcal{M}_{\text{CH}_4}} \tag{B.31}$$

This is the stoichiometric gas-fuel-ratio as shown in Equation (B.23). So

$$\alpha\frac{m^{\text{s}}_{\text{O}_2}}{m_{\text{in}}}\frac{1}{f^{\text{in}}_{\text{O}_2}} = \alpha_{\text{s}} \tag{B.32}$$

that substituted in the formula (B.28) gives the final expression

$$f^{\text{out}}_{\text{O}_2} = f^{\text{in}}_{\text{O}_2}\frac{\alpha-\alpha_s}{\alpha+1} \tag{B.33}$$

B.5 Water vapour

The proof is very similar to the carbon dioxide one (must be used just the corresponding notation), so they will not be commented. The starting point

is, as always, Equation (B.7).

$$\frac{m^{\text{out}}_{\text{H}_2\text{O}}}{m_{\text{out}}} = \frac{m^{\text{out}}_{\text{H}_2\text{O}}}{m_{\text{in}}} \frac{\alpha}{\alpha+1} \tag{B.34}$$

$$\frac{m^{\text{out}}_{\text{H}_2\text{O}}}{m_{\text{out}}} = \frac{m^{\text{in}}_{\text{H}_2\text{O}} + m^{\text{s}}_{\text{H}_2\text{O}}}{m_{\text{in}}} \frac{\alpha}{\alpha+1} \tag{B.35}$$

$$f^{\text{out}}_{\text{H}_2\text{O}} = \left(f^{\text{in}}_{\text{H}_2\text{O}} + \frac{m^{\text{s}}_{\text{H}_2\text{O}}}{m_{\text{in}}} \right) \frac{\alpha}{\alpha+1} \tag{B.36}$$

$$f^{\text{out}}_{\text{H}_2\text{O}} = f^{\text{in}}_{\text{H}_2\text{O}} \frac{\alpha}{\alpha+1} + \frac{m^{\text{s}}_{\text{H}_2\text{O}}}{m_{\text{in}}} \frac{m_{\text{in}}}{m_{\text{f}}} \frac{1}{\alpha+1} \tag{B.37}$$

$$f^{\text{out}}_{\text{H}_2\text{O}} = f^{\text{in}}_{\text{H}_2\text{O}} \frac{\alpha}{\alpha+1} + \frac{m^{\text{s}}_{\text{H}_2\text{O}}}{m_{\text{in}}} \frac{m_{\text{in}}}{m_{\text{CH}_4}} \frac{f^{\text{f}}_{\text{CH}_4}}{\alpha+1} \tag{B.38}$$

$$f^{\text{out}}_{\text{H}_2\text{O}} = f^{\text{in}}_{\text{H}_2\text{O}} \frac{\alpha}{\alpha+1} + \frac{n^{\text{s}}_{\text{H}_2\text{O}} \mathcal{M}_{\text{H}_2\text{O}}}{n_{\text{CH}_4} \mathcal{M}_{\text{CH}_4}} \frac{f^{\text{f}}_{\text{CH}_4}}{\alpha+1} \tag{B.39}$$

Before to derive the final expression, must be noticed that the steam-methane molar fration in Reaction (B.1) is 2; thus

$$f^{\text{out}}_{\text{H}_2\text{O}} = f^{\text{in}}_{\text{H}_2\text{O}} \frac{\alpha}{\alpha+1} + \frac{\mathcal{M}_{\text{H}_2\text{O}}}{\mathcal{M}_{\text{CH}_4}} \frac{2\, f^{\text{f}}_{\text{CH}_4}}{\alpha+1} \tag{B.40}$$

References

[1] Hanne Marie Kvamsdal, Kristin Jordal, and Olav Bolland. A quantitative comparison of gas turbine cycles with CO_2 capture. *Energy*, 32(1):10–24, 2007.

[2] Sven Gunnar Sundkvist, Stein Julsrud, Bent Vigeland, Tyke Naas, Michael Budd, Hans Leistner, and Dieter Winkler. Development and testing of AZEP reactor components. *International Journal of Greenhouse Gas Control*, 1(2):180–187, 2007.

[3] Björn Fredriksson Möller, Tord Torisson, Mohsen Assadi, Sven Gunnar Sundkvist, Mats Sjödin, Åke Klang, Knut Ingvar Åsen, and Kjersti Wilhelmsen. AZEP gas turbine combined cycle power plants — Thermoeconomic analysis. *International Journal of Thermodynamics*, 9(1):21–28, 2006.

[4] William H Press, Saul A Teukolsky, William T Vetterling, and Brian P Flannery. *Numerical Recipes in Fortran 77 — The Art of Scientific Computing*. Cambridge University Press, Cambridge, United Kingdom, second edition, 2001.

[5] Kirsten Foy and Evgeny Yantovski. History and state-of-the-art of fuel fired zero emission power cycles. *International Journal of Thermodynamics*, 9(2):37–63, 2006.

[6] Kay Damen, Martijn van Troost, André Faaij, and Wim Turkenburg. A comparison of electricity and hydrogen production systems with CO_2 capture and storage. Part A: Review and selection of promising conversion and capture technologies. *Progress in Energy and Combustion Science*, 32(2):215–246, 2006.

[7] Timothy Griffin, Dominikus Bücker, and Allen Pfeffer. Technology options for gas turbine power generation with reduced CO_2 emission. *Journal of Engineering for Gas Turbines and Power*, 130(4):041801–1–041801–8, 2008.

[8] European Environment Agency. Energy and environment report 2008. Technical Report 6/2008, European Environment Agency, Kongens Nytorv 6 1050 Copenhagen K Denmark, 2008.

[9] Rune Bredesen, Kristin Jordal, and Olav Bolland. High-temperature membranes in power generation with CO_2 capture. *Chemical Engineering and Processing: Process Intensification*, 43(9):1129–1158, 2004.

[10] Timothy Griffin, Sven Gunnar Sundkvist, Knut Ingvar Åsen, and Tor Bruun. Advanced zero emissions gas turbine power plant. *Journal of Engineering for Gas Turbines and Power*, 127(1):81–85, 2005.

[11] Lars Ingolf Eide, Marie Anheden, Anders Lyngfelt, Juan Carlos Abanades, Mourad Younes, Denis Clodic, Alain A. Bill, Paul H M Feron, Alexandre Rojey, and Fabrice Giroudière. Novel capture processes. *Oil and Gas Science and Technology*, 60(3):497–508, 2005.

[12] J.-Ch. Haag, A Hildebrandt, Herwart Hönen, Mohsen Assadi, and Reinhold Kneer. Turbomachinery simulation in design point and part-load operation for advanced CO_2 capture power plant cycles. In *Conference of 2007 ASME Turbo Expo*, volume 3, pages 239–250, Montreal, Que., 2007. Conference Date: 14 May 2007 through 17 May 2007; Conference Code: 70222.

[13] Erik G Lindfeldt and Mats O J Westermark. An integrated gasification zero emission plant using oxygen produced in a mixed conducting membrane reactor. In *Conference of 2006 ASME 51st Turbo Expo*, volume 4, pages 33–40, Barcelona, 2006. Conference Date: 6 May 2006 through 11 May 2006; Conference Code: 68506.

[14] Ramesh K Shah and Dusan P Sekulić. *Fundamentals of heat exchanger design*. John Wiley & Sons, Hoboken, New Jersey, USA, 2003.

[15] Michael J. Zehe, Sanford Gordon, and Bonnie J. McBride. CAP: A Computer Code for Generating Tabular Thermodynamic Functions from NASA Lewis Coefficients. Technical Paper NASA TP-2001-210959-REV1, NASA, National Aeronautics and Space Administration John H. Glenn Research Center at Lewis Field Cleveland, Ohio 44135-3191, February 2002. 82 pages.

[16] Giovanni Lozza. *Turbine a gas e cicli combinati*. Progetto Leonardo, Bologna, Italy, 1996. In Italian.

[17] John H Lienhard IV and John H Lienhard IV. *A Heat Transfer Textbook*. Phlogiston Press, Cambridge, Massachusetts, USA, version 1.31 edition, January 2008.

[18] Sadik Kakaç and Hongtan Liu. *Heat exchangers: selection, rating and thermal design*. CRC Press, Boca Raton, Florida, USA, second edition, 2002.

[19] Jaka Sunarso, S Baumann, J M R Serra, Wilhelm A Meulenberg, S Liu, Yaosheng S Lin, and João Carlos Diniz da Costa. Mixed Ionic-Electronic Conducting (MIEC) ceramic-based membranes for oxygen separation. *Journal of Membrane Science*, 320(1–2):13–41, 2008.

[20] Anthonie J Burggraaf and Louis Cot. *Fundamentals of inorganic membrane science and technology*. Elsevier Science, 1996.

[21] Yutie Liu, Xiaoyao Tan, and K Li. Mixed conducting ceramics for catalytic membrane processing. *Catalysis Reviews — Science and Engineering*, 48(2):145–198, 2006.

[22] S Eriksson, Magali Boutonnet, and Sven G Järås. Catalytic combustion of methane in steam and carbon dioxide-diluted reaction mixtures. *Applied Catalysis A: General*, 312(1–2):95–101, 2006.

[23] Cleve Moler. *Numerical Computing with MATLAB*. Society for Industrial and Applied Mathematics (SIAM), Philadelphia, Pennsylvania, USA, 2004.

[24] Pierre J Dechamps, N Pirard, and Philippe J Mathieu. Part load operation of combined cycle plants with and without supplementary firing. In *Proceedings of the 8th Congress and Exposition on Gas Turbines in Cogeneration and Utility, Industrial and Independent Power Generation*, volume 9, pages 371–380, Portland, OR, USA, 1994. ASME, New York, NY, United States. Conference Date: 25 October 1994 through 27 October 1994; Conference Code: 42263.

[25] Meherwan P Boyce. *Handbook for cogeneration and combined cycle power plants*. ASME (American Society of Mechanical Engineers) Press, New York, New York, USA, 2002.

[26] Konrad Eichhorn Colombo, Lars Imsland, Olav Bolland, and Svein Hovland. Dynamic modelling of an oxygen mixed conducting membrane and model reduction for control. *Journal of Membrane Science*, 336(1-2):50–60, 2009.

[27] Marie Laure Fontaine, Truls Norby, Yngve Larring, Tor Grande, and Rune Bredesen. Oxygen and Hydrogen Separation Membranes Based on Dense Ceramic Conductors. *Membrane Science and Technology*, 13:401–458, 2008. cited By (since 1996) 0.

Bibliography

[28] Pierre Brandt. An Evaluation of the Advanced Zero Emissions Power Plant Cycle. Master of Science in Thermal Power Thesis, Cranfield University — School of Engineering, 2007.

[29] Ravi Prasad, Christian Friedrich Gottzmann, and Raymond Francis Drnevich. Method for Producing Oxygen and Generating Power Using a Solide Electrolyte Membrane Integrated with a Gas Turbine. Patent, December 1998. US Patent Number 5 852 925.

[30] Giancarlo Ruggieri. Advanced low carbon power systems: Evaluation of auto thermal reformer combined cycle. Master of Science in Thermal Power Thesis, Cranfield University — School of Engineering, 2008.

[31] DTI (Department of Trade and Industry) UK. Review of the Feasibility of Carbon Dioxide Capture and Storage in the UK, 2003.

[32] Desmond E Winterbone. *Advanced Thermodynamics for Engineers.* Butterworth-Heinemann, 1996.

[33] Adrian Bejan and Allan D Kraus. *Heat transfer handbook.* John Wiley & Sons, Hoboken, New Jersey, USA, 2003.

[34] Bengt Sunden and Mohammad Faghri. *Computer simulations in compact heat exchangers*, volume 1. Computational Mechanics Publications, Southampton, United Kingdom, 1998.

[35] Bartow K Hodge. *Analysis and design of energy systems.* Prentice-Hall, Englewood Cliffs, New Jersey, USA, second edition, 1990.

[36] Sadik Kakaç, A E Bergles, and F Mayinger. *Heat exchangers: thermal-hydraulic fundamentals and design.* McGraw-Hill International Book, first edition, 1981. Papers from the NATO Advanced Study Institute on "Heat Exchangers — Thermal-Hydraulic Fundamentals and Design." held in Istanbul, Turkey, Aug. 4–15, 1980.

[37] Sherman J Xu and William J Thomson. Oxygen permeation rates through ion-conducting perovskite membranes. *Chemical Engineering Science*, 54(17):3839–3850, 1999.

[38] Xianfeng Chang, Chun Zhang, Xueliang Dong, Chao Yang, Wanqin Jin, and Nanping Xu. Experimental and modeling study of oxygen permeation modes for asymmetric mixed-conducting membranes. *Journal of Membrane Science*, 322(2):429–435, 2008.

[39] Qing Zeng, Yan-bo Zuo, Chuan-gang Fan, and Chu-sheng Chen. CO_2-tolerant oxygen separation membranes targeting CO_2 capture application. *Journal of Membrane Science*, 335(1–2):140–144, 2009.

[40] Jens B Smith and Truls Norby. On the steady-state oxygen permeation through $La_2NiO_{4+\delta}$ membranes. *Journal of the Electrochemical Society*, 153(2):A233–A238, 2006.

[41] Stephen J Chapman. *Fortran 90/95 for Scientists and Engineers*. WCB/McGraw-Hill, Boston, Massachusetts, USA, 1998.

[42] Jeanne C Adams, Walter S Brainerd, Jeanne T Martin, Brian T Smith, and Jerrold L Wagener. *Fortran 90 Handbook — Complete ANSI/ISO Reference*. McGraw-Hill, New York, New York, USA, 1992.

[43] John Reid. The New Features of Fortran 2003. Technical Report N1579, ISO/IEC/JTC1/SC22/WG5 (International Fortran Standards Committee), Benson, United Kingdom, 2003.

Colophon

The work presented in this thesis was developed using exclusively open source software. The code was developed with the Photran plug-in for the Eclipse Platform IDE (Integrated Development Environment), the GNU compilers g95 and gfortran, and the GNU utility make. A few re-compilations were performed using the Microsoft Visual Studio package but *not* for development purposes. This thesis was typeset in LaTeX 2_ε while the pictures were partly produced with OpenOffice Draw, partly with Inkscape, and also using LaTeX 2_ε itself. The charts in the "Results and discussion" chapter were produced with Gnumeric. The bibliographic database was managed by JabRef which was interfaced to LaTeX with BibTeX. The thesis presentation was created using LaTeX 2_ε, too. All the aforementioned programs (except Microsoft Visual Studio) were running on a GNU/Linux Ubuntu operating system.

Note: The LaTeX 2_ε document class chosen for this work is the standard `book`. Just a few variations were implemented to comply with the "Prescribed Form for the presentation of theses at Cranfield University" but the main typographic parameters (as, for instance, the fonts) remained the standard ones. The bibliographic style required to be adopted is `unsrt`.

Final version: October 5, 2009.